FLAMINIA CORNAGGIA

# Role of marine sediments mineralogy in the study of magnetotactic bacteria

São Paulo
2020

FLAMINIA CORNAGGIA

# Role of marine sediments mineralogy in the study of magnetotactic bacteria

Tese apresentada ao Instituto Oceanográfico da Universidade de São Paulo, como parte dos requisitos para obtenção do título de Doutor em Ciências, Programa de Oceanografia, área de Oceanografia Geológica.

Orientador: Prof. Dr. Luigi Jovane

São Paulo

2020

CORNAGGIA, Flaminia. **Role of marine sediments mineralogy in the study of magnetotactic bacteria**. Tese de Doutorado apresentada ao Instituto Oceanográfico da Universidade de São Paulo para obtenção do título de Doutor em Ciências, Programa de Oceanografia, área de Oceanografia Geológica.

Aprovado em: ___/___/_____

Versão Corrigida

Banca Examinadora

Prof. Dr. _____ Instituição_____

Presidente Assinatura_____

Prof. Dr. _____ Instituição_____

Conceito_____ Assinatura_____

Prof. Dr. _____ Instituição_____

Conceito_____ Assinatura_____

Prof. Dr. _____ Instituição_____

Conceito_____ Assinatura_____

Dedico essa trabalho à minha família: a meus pais, que me ensinaram a importância dos estudos, a meu marido, que é um estudioso apaixonado, e às minhas filhas, ainda no início de suas vidas estudantis.

AGRADECIMENTOS

Agradeço a todos aqueles que me ajudaram a chegar até aqui:

Minha família, que nunca desistiu de mim: meus pais e os irmãos que eles me deram, meu marido e a grande família que ele me deu, e os irmãos que a vida me trouxe. Eles são a rocha em que me apoio e deles vem minha força para viver a vida com alegria.

A minha irmã Flavia Brandão Bezerra, anjo da guarda e revisora do meu português.

Os professores que me guiaram nesse caminho e que, agora, permanecem na vida como amigos e mestres, colegas no caminho do conhecimento, especialmente Daniel Bowen e Paolo Lamagna. E para aqueles que permanecem no meu coração: Br. Lawrence Bradford O.S.B., Felice Cesana e Jack Davis.

Padre Benedetto Tempellini O.P., o guia de uma vida.

Os colegas do laboratório CORE, para a ajuda, moral e material, eles conseguiram manter a minha saude mental nesse caminho.

O Prof. Dr. Luigi Jovane, pela disponibilidade, o carinho e a amizade que foram fundamentais para realizar e prosseguir este estudo.

O Instituto Oceanográfico, pela oportunidade de realização do curso.

O presente trabalho foi realizado com apoio da Coordenação de Aperfeiçoamento de Pessoal de Nível Superior – Brasil (CAPES) – Código de Financiamento 001.

# RESUMO

CORNAGGIA, Flaminia. **Role of marine sediments mineralogy in the study of magnetotactic bacteria**. 2020. 113 f. Tese (Doutorado) – Instituto Oceanográfico, Universidade de São Paulo, São Paulo, 2020.

Os minerais sedimentares marinhos respondem a alterações do ambiente sedimentar e, portanto, podem ser indicativos de condições ambientais e climáticas específicas. O uso da composição mineralógica do sedimento marinho para reconstruir condições ambientais passadas e presentes possui grande potencial, se utilizado com os devidos cuidados. Neste trabalho, amostras de sedimentos marinhos foram analisadas com Difração de Raios-X de Pó (XRPD) para caracterizar a composição mineralógicas com foco em reconstruções paleoceanográficas e compreender as condições ambientais em que as bactérias magnetotáticas (MTB) se encontram. O MTB é um grupo heterogêneo de procariontes gram-negativos que biomineralizam internamente cristais magnéticos chamados magnetossomos, encontrados em ambientes aquáticos de todo mundo, . A presença dos MTB tem sido associada a eventos passados de aquecimento global e alta produtividade primária, tendo, portanto, um potencial uso como proxies paleoceanográficos. Portanto, compreender os processos que vinculam o MTB ao ambiente é fundamental para restringir sua ecologia e usá-los de modo adequato como proxies paleoambientais. Em particular, apresentamos três estudos de caso nos quais os dados mineralógicos foram complementados com estudos de propriedades magnéticas, dados geoquímicos e análises estatísticas. O primeiro apresenta um cenário abissal (planície abissal da Tasmânia) com modificações induzidas pelo clima na escala de 100 mil anos durante o evento do clima médio do Eoceno Médio (MECO); o segundo trata de um ambiente estuarino-lagunar (Cananéia, BR) com interferência antrópica na escala de 100 anos; o terceiro enfoca um ambiente ria recente (Mamanguá, BR) que pode ser considerado estável nas escalas de tempo anual a milenar. Nos dois primeiros casos, as principais modificações ambientais são reconhecidas através das variações das composições mineralógicas, enquanto no último MTB prosperam e não ocorrem variações consideráveis na composição mineralógica. O estudo da composição mineralógica dos sedimentos da Planície Abissal da Tasmânia nos permitiu confirmar a ocorrência de acidificação do oceano durante o MECO e mostrar que chegou a profundidades abissais. Além disso, esse arquivo pode produzir a primeira evidência de

magnetossomos dopados com Mn em ambientes naturais. O estudo de caso de Cananéia reconstruiu um ambiente estuarino-lagunar, mostrando a resposta de minerais sedimentares a modificações antrópicas. Embora nos três estudos de caso a presença de MTB seja concomitante com um aumento na fração mineral da argila, os dados não são suficientes para confirmar claramente uma ligação entre a presença de MTB e a composição mineralógica. Os MTB são um grupo polifilético e são encontrados em todos os ambientes aquáticos, o que implica que seja necessário o máximo cuidado ao correlacionar o termo geral MTB a uma característica específica ou preferência ecológica. Muitos fatores devem ser considerados paralelamente à composição mineralógica do ambiente, especialmente a taxonomia específica das bactérias estudadas, o que não foi possível neste estudo. Como o MTB consiste em diferentes táxons com diferentes modos de vida, é necessário um estudo mais extenso em colaboração com biólogos para selecionar comunidades MTB bem definidas do ponto de vista taxonômico, a fim de determinar o papel da mineralogia nos fatores ecológicos.

Palavras-chave: Mineralogia. Difração de raios-X. Sedimentos marinhos. Bactérias magnetotáticas. Paleoceanografia. Reconstrução paleoambiental.

# ABSTRACT

CORNAGGIA, Flaminia. **Role of marine sediments mineralogy in the study of magnetotactic bacteria**. 113 p. 2020. Tese (Doutorado) – Instituto Oceanográfico, Universidade de São Paulo, São Paulo, 2020.

Marine sedimentary minerals respond to modifications in the sedimentary environment, and thus can be representative of specific environmental and climatic conditions. The use of sedimentary mineralogical composition to reconstruct past and present environmental conditions has great potential, if used with the appropriate care. In this work, samples of marine sediments were analysed with X-Ray Powder Diffraction (XRPD) to characterize the mineralogical assemblages with focus on paleoceanographic reconstructions and characterization of environments in which magnetotactic bacteria (MTB) live. MTB are a heterogeneous group of gram-negative prokaryotes found in aquatic environments worldwide that internally biomineralize magnetic crystals called magnetosomes. Their presence has been linked to past events of global warming and high primary productivity, thus have a potential use as paleoceanographic proxies. Therefore, understanding the processes that link MTB to their environment is fundamental to constrain their ecology and use them efficiently as paleoenvironmental proxies. In particular, we present three case studies in which mineralogical data are integrated with magnetic properties, geochemical data, and statistical analyses. The first presents an abyssal setting (Tasman Abyssal Plain) with climate induced modifications at the 100ky scale during the Middle Eocene Climatic Optimum (MECO) event; the second addresses a lagoonal-estuarine environment (Cananeia, BR) with anthropic interference at the 100y scale; the third focuses on a recent ría environment (Mamanguá, BR) that can be considered stable at the annual to millennial time scales. In the former two cases, main environmental modification are recognized through the variations of mineralogical assemblages, whereas in the latter MTB thrive and no appreciable variations in the mineralogical composition occur. The study of the mineralogical composition of the sediments on the Tasman Abyssal Plain allowed us to confirm the occurrence of ocean acidification during the MECO and show that it even reached abyssal depths. Besides, this archive may yield the first evidence of Mn-doped magnetosomes in natural environments. The Cananeia case study reconstructed a lagoonal-estuarine environment, showing the response of sedimentary minerals to anthropic

modifications. Although in all three case studies the presence of MTB is concomitant with an increase in the clay mineral fraction, data are not sufficient to clearly confirm a link between the presence of MTB and the mineralogical composition. MTB are a polyphyletic group and are found ubiquitous in aquatic environments, this implies that utmost care has to be used when correlating the general term MTB to a specific characteristic or ecologic preference. Many factors should be considered alongside the mineralogical composition of the environment, especially the specific taxonomy of the studied bacteria, which has not been possible to do in this study. As MTB consist of different taxa with different modes of life, a more extensive study in collaboration with biologists is necessary to select MTB communities well-defined form the taxonomical point of view, in order to determine the role of mineralogy in the ecological factors.

Keywords: Mineralogy. X-ray diffraction. Marine sediment. Magnetotactic bacteria. Paleoceanography. Paleoenvironmental reconstruction.

# SUMMARY

# 1 - INTRODUCTION

Unravelling the Earth climate history is one of the most intriguing challenges for Earth scientists. Paleoceanographic proxies provide information for reconstructing climate changes, global and regional oceanography, and biogeochemical cycles in the ocean. These proxies are measurable descriptors of environmental variables that are not directly measurable in the past, such as temperature, salinity, primary productivity, nutrient content, and surface-water carbon dioxide concentrations.

MTB are a heterogeneous group of gram-negative prokaryotes that live in aquatic environments worldwide and internally biomineralize magnetic crystals of magnetite ($Fe_3O_4$) or greigite ($Fe_3S_4$) wrapped in a lipid membrane, called magnetosomes. Magnetosomes crystals can be preserved through geologic time as magnetofossils; however, only few pre-Quaternary records of bacterial magnetite have been reported, as burial into anoxic diagenetic environments causes its dissolution (DELONG; FRANKEL; BAZYLINSKI, 1993; SCHÜLER; BAEUERLEIN, 1998; SAKAGUCHI; ARAKAKI; MATSUNAGA, 2002; REITNER et al. 2005; PÓSFAI; KASAMA; DUNIN-BORKOWSKI, 2006; VASILIEV et al., 2008; ROBERTS et. al., 2011).

MTB and their magnetofossils have been found and studied in sediments of acqueous environments worldwide, and often have been found to be the major remanence carrier in marine sediments (HESSE, 1994).

The presence of MTB has been linked to events of global warming and high primary productivity in the geological past (SCHUMANN et al., 2008; ROBERTS et. al., 2011; CHANG et al., 2012; ROBERTS et al., 2012; LARRASOAÑA et al., 2012; SAVIAN et al., 2014 and 2016). The use of MTB as paleoclimatic and paleoenvironmental indicators is a rather new methodology and work still needs to be done to utilize it in various contexts. Especially, there are still significant uncertainties about the ecological conditions in which they dwell and about the mechanisms that may stimulate and sustain their production (PETERSEN; VON DOBENECK; VALI, 1986; YAMAZAKI, 1998; JOVANE et al., 2012).

The original aim of this research project was to characterize by X-Ray powder diffraction (XRPD) the mineralogical composition of sediments in which MTB, or their magnetofossils, were recovered, for paleoenvironmental reconstructions and to investigate a possible link between the mineralogical composition of the sediment and the MTB production. Since MTB live within the sediment, the mineralogical composition of the sedimentary environment probably has an influence on their behaviour and mode of life. The presence of MTB in marine environments is linked to the presence of specific elements, especially iron, and conditions that

are still quite unknown. The characterization of the sedimentary environment, therefore, could constrain some of the key environmental parameters for MTB.

The characterization of sedimentary minerals in different marine settings was here used to reconstruct, with the support of other oceanographic proxies, the environmental conditions where the MTB or the magnetofossils were found, in the attempt to clarify such unknowns and create paleoceanographic reconstructions.

The study of marine sediments through their composition and provenance, and its application as paleoceanographic proxy, has been more and more recognized over the years. Sedimentary minerals form directly in the depositional basin by authigenesis or biogenically induced precipitation, or come from the alteration, erosion, and runoff of pre-existing rocks on land. All these processes are linked to specific environmental and climatic conditions, on land and at the sea bottom; consequently, the mineralogical composition of the sediments can be used as proxy for characterizing the respective depositional environment (SINGER, 1984).

Therefore, marine sedimentary minerals can bear the signature of specific environmental and climatic conditions. For example, the occurrence of chlorite, illite, palygosrkite, and quartz can indicate dry conditions on land, whereas kaolinite is typical of humid conditions with more intensive weathering (SINGER, 1984). Another important mineral is aragonite, which increases in carbonate oozes respect to calcite under cooler conditions (DROXLER et al., 1984).

Clay minerals in marine sediments are particularly important for paleoclimatic and paleoenvironmental studies, as they are the main constituents of deep marine sediments (SINGER, 1984) and may also influence the preservation of organic matter in the sediments, and therefore play a significant role in carbon cycling (KENNEDY and WAGNER, 2011). Clay minerals in modern marine sediments are mainly detrital, they form after weathering on land, and then are transported for long distances as detrital grains until deposition onto the sea bottom. Therefore, they bear a signal related to the respective source area and to the processes that controlled the transport (ESLINGER and PEVEAR, 1985). The distribution of detrital clays in modern ocean sediments depends mainly on latitude, as consequence of the different climatic and respective continental weathering conditions (GRIFFIN; WINDOM; GOLDBERG, 1968; RATEEV et al., 1969; ESLINGER AND PEVEAR, 1985, CHAMLEY, 1989). Illite is the most common detrital mineral in the oceans and is more abundant in the northern hemisphere, because of the higher abundance of mica rich metamorphic rocks (SINGER, 1984). Detrital chlorite is concentrated at higher latitudes because it is unstable under warm climatic conditions and it is transported mainly by glaciers. Kaolinite, on the other hand, forms in tropical soils and

therefore is dominant in the equatorial regions, where leaching and chemical weathering are more intense (BISCAYE, 1965; ZIMMERMAN, 1977).

In modern marine environments, authigenic clays are less common but locally important. These minerals originate directly in the sedimentary basin either by precipitation from solutions onto the sediment (neoformed clays), or by alteration of pre-existing phyllosilicates. Therefore, authigenic minerals might be indicators of specific conditions in the depositional environment. The term authigenic must not be confused with diagenetic, as authigenic minerals precipitate from the water column at the sediment-water interface, whereas diagenetic clays grow within the sediment significantly after deposition. Therefore, the formers can be indicative of the conditions at the bottom of the depositional basin, whereas the latters depend on the sediment pore waters (ESLINGER and PEVEAR, 1985). The discrimination between these two types of minerals is not always easy. The most common authigenic clay in modern oceans is smectite that comes mainly from the alteration of volcanic material. It is more abundant in the southern hemisphere, especially in the South Pacific Ocean, where there is a larger input of volcanic respect to detrital material (SINGER, 1984, ESLINGER and PEVEAR, 1985). Consequently, variations in clay-minerals distribution throughout a stratigraphic section can be interpreted as shifts through time in the prevailing conditions in the continental source areas or at the sea bottom, depending on whether the occurring minerals are detrital or authigenic (SINGER, 1984; ESLINGER and PEVEAR, 1985).

Mineral assemblages are especially sensitive to modifications in the sedimentary environment conditions, and thus respond to climatic changes, type and intensity of erosional processes, variation of endogenous activity, and changes in oceanic and atmospheric circulation (CHAMLEY, 1979 and 1989; ROBERT and CHAMLEY, 1990). However, the relationship between climatic and environmental parameters and sedimentary minerals is not always straightforward. The formation and variation of sedimentary minerals, especially clays, depend also on factors such as topography, geomorphology, parent-rock lithology, selection during transport, and post-depositional and diagenetic alteration. The contribution of each of these factors is not easy to identify, but must be carefully considered and evaluated in order to make paleoclimatic and paleoenvironmental interpretations of a sedimentary mineralogical assemblage. The most important factors to consider are:

- The distinction between authigenic and detrital minerals as they bear different kinds of information. For example, smectite is a common detrital clay mineral that comes from regions with highly contrasting seasons and a pronounced dry season (SINGER, 1984). However, it is also the most important authigenic marine clay, forming primarily by

halmyrolysis of basalts and pyroclastic material on the seafloor (IACOVIELLO et al., 2012). Therefore, it is fundamental to identify the origin of smectite (whether detrital or authigenic) in a specific environment before using it as paleoclimatic or paleoenvironmental indicator. Frequently, sedimentary mineral assemblages include both authigenic and detrital minerals, and the distinction between the two is not always easy.

- Diagenetic processes can also modify the original composition of mineral assemblages in the sediments. The likelihood for diagenetic alteration increases with the burial depth of the sediment, and clays can be indicative of the burial and thermal history that a succession underwent. Therefore, information about the burial history of the sediments must be always considered alongside minerals characterization and abundance, in order to accurately target the primary signal.
- Detrital minerals are not always representative of the original assemblage formed by weathering in a specific area, as it can be altered during transport through selective erosion of the source soils, grain size sorting, and differential flocculation. Different types of transport preferentially mobilize and accumulate different grain size, and even mineral fractions. Besides, detrital grains can be transported and reworked by multiple agents before reaching the sea floor and their effect can change in magnitude or direction through time (SINGER, 1984). Consequently, sedimentary minerals must be characterized also according to the respective provenance and transport processes.

To avoid complications and a correct characterization of a mineral assemblage, the primary concern should be the careful selection of location and setting, with conditions suitable for the type of signal intended to target. Moreover, mineralogical data should be integrated with other parameters, such as microfossils, trace elements, or stable isotopes, in a multi-proxy approach, in order to make a robust paleoclimatic reconstruction (SINGER, 1984, ESLINGER and PEVEAR, 1985).

In this project the mineralogical characterization of sedimentary rocks through XRPD from a large arrays of contexts has been integrated with magnetic and geochemical studies performed by collaborators. Magnetosomes crystals are nanometric and their abundance is generally too low to be detectable by XRPD analysis and XRPD is not able to distinguish between detrital and biogenic magnetite. For these reasons, the study of the magnetic properties of the sediment done by colleagues is necessary to discriminate between biogenic and non-biogenic magnetite crystals, and therefore identify the biogenic crystals produced by bacteria. The goal is to obtain complete paleoenvironmental and paleoclimatic reconstructions and to enlighten the role of the

sediment composition on the ecology of MTB. Special attention has been given to clay minerals, as studies showed a possible relationship between the presence of magnetotactic bacteria and clay minerals concentration (SAVIAN et al., 2014).

Statistical analyses have also been particularly helpful in this work, for identifying mineralogical and elemental variations throughout the analysed stratigraphic records, in particular the Hierarchical Cluster Analysis (HAC). HAC is a preliminary analytical tool to identify significant variations within the XRPD results. This method creates a hierarchy of clusters based on distance metrics, which means considering how much the results are similar of different from each other. The software analyses the diffractograms profiles and peaks produced by XRPD, and then creates groups, or clusters, of samples on the base of their similarity.

In this work, mineralogical analyses were conducted in a variety of contexts and settings were MTB were encountered. Three case studies were chosen among them as the most representatives and valuable: one on the Tasman abyssal plain and two from the South-Eastearn brazilian coast:

*1) TASMAN ABYSSAL PLAIN:* in this study we observe significant changes indicating the response to the Middle Eocene Climatic Optimum (MECO) perturbation in the magnetic, mineralogical, and chemical parameters of a Core from the Tasman Abyssal Plain (IODP Site U1511). Our results suggest more acid bottom water over the Tasman abyssal plain during the MECO, and an abrupt end of these conditions. This work provides the first evidence of MECO at abyssal depths and shows that acidification affected the entire oceanic water column during this event. In this setting, the signal of magnetofossils from MTB is very strong within the MECO interval, and in another interval characterised by a prominent increase in Mn, just above the MECO interval. Mineralogical data indicate an increase in clay content in these two intervals. The high abundance of Mn in this environment is of particular interest, as some of this element might have been incorporated within the magnetosomes. If this is confirmed, this may be the first occurrence of Mn-doped magnetosomes observed in a natural environment. This work has been published in the journal *Scientific Reports*, with the title: *Abyssal oceanic circulation and acidification during the Middle Eocene Climatic Optimum (MECO).* DOI:10.1038/s41598-020-63525-3

*2) CANANEIA-IGUAPÉ ESTUARINE LAGOONAL SYSTEM:* The Cananéia-Iguapé system is a combined estuarine-lagoonal sedimentary system, located along the SE coast of Brazil. It consists of a network of channels and islands oriented mainly parallel to the coast. About 165 years ago, an artificial channel, the Valo Grande, was opened in the northern part of this system

to connect the Ribeira River to the estuarine-lagoon complex, and underwent various phases of opening and closure that strongly influenced the surrounding environment. In this study, we present mineralogical, chemical, magnetic, and geochronological data from a sediment core collected at the southern end of the lagoonal system showing how the phases of the opening and closure of the channel are expressed in the sedimentary record. This work represents an example of how anthropogenic modifications in a lagoonal-estuarine sedimentary system influence the sediment composition. In this environment, the signal of MTB, given by living bacteria, is weak and limited to a few centimetres depth, meaning that the conditions for their survival are not optimal. The clay content throughout the core is very low, but there is a small increase in total clay content in the interval where the MTB where encountered. This work has been published in the journal *Frontiers in Earth Sciences*, as *Cornaggia et al. (2018) Diversions of the Ribeira River Flow and Their Influence on Sediment Supply in the Cananeia-Iguapé Estuarine-Lagoonal System (SE Brazil).*

*3) SACO DE MAMANGUÁ:* The Mamanguá ría (RJ, Brazil) is an elongate coastal inlet formed by the partial submergence of a river valley, characterised by restricted water circulation and weak tidal action. Surface sediments are predominantly composed of clay and silt. Core 9M was collected within the inner part of the ría. This site, chosen in opposition to the Cananeia site, represents an environment in which the MTB thrive (magnetic properties register MTB signal within the uppermost 35 cm of the core), representing therefore optimal conditions for their production. XRPD analysis in the core identifies a homogenous mineralogical composition, with constant high clay content. This work contributed to an article published in *Journal of Geophysical Research: Solid Earth,* as *Rodelli et Al. (2019) Diagenetic fate of biogenic soft and hard magnetite in chemically stratified sedimentary environments of Mamanguá Ría, Brazil.*

The first two case studies, discussed in chapter 4 and 5 of this work, are examples where the variation in mineralogical composition of marine sediments reflected important environmental changes, and thus it has been used to reconstruct the evolution of these conditions through time: they represent an abyssal setting with climate induced modifications at the 100kyr scale and a lagoonal-estuarine environment with anthropic interference at 100yr. Both these environments were successfully reconstructed through the characterization of the sedimentary mineral assemblage in a multidisciplinary approach.

The third case study, the Saco do Mamanguá setting, represent a stable environment where mineralogical variations throughout the sediment core are minimal and the clay content is relatively high. This case study was chosen as it represents an environment similar to the

Mamanguá setting but with high MTB production. The idea was to use it as a *"control setting"* to understand the importance of the sediment composition, especially clay minerals, in the ecology of MTB.

During this PhD work the obstacles encountered were related directly to the nature of the MTB, which represent a polyphyletic group. MTB are ubiquitous in aquatic environments, and recently a number of extremophiles MTB have been described and include halophilic, alkaliphilic, cryophilic, and thermophilic taxa (LEFÈVRE; FRANKEL; A BAZYLINSKI, 2011; BAZYLINSKI and LEFÈVRE, 2013; ABREU and ACOSTA-AVALOS, 2018). This implies that it is not possible to relate the general term MTB to a specific preference or behaviour without falling intoextreme generalization. Although in all our case studies the presence of MTB is concomitant with an increase in the clay mineral fraction, it was beyond the scope of this study to characterize the MTB species or magnetite type for each case study. Even if MTB seem to prefer to live in clay-rich sediments, it was not possible to define how much this factor is important, as the variables influencing their survival are many and a more extensive study should be done, including a more accurate characterization of the bacterial taxonomy and mode of life.

# 2 - MAGNETOTACTIC BACTERIA

The first record of MTB bacteria appeared in 1963 in a publication written by Salvatore Bellini of the Institute of Microbiology at the University of Pavia (Italy). Looking at swamp mud samples at the microscope, he noticed a group of bacteria that oriented themselves in a unique direction on the slide. When he realized that the bacteria were following the lines of the Earth's magnetic field, from south to north, he named them “magnetosensitive" (JOGLER and SCHÜLER, 2009).

The first scientific publication on MTB was published by Richard Blakemore, a microbiologist at the Woods Hole Oceanographic Institution, in 1975. He independently observed bacteria capable of orienting themselves in the direction of Earth's magnetic field. Thus, he coined the term magnetotaxis for the phenomena and Magnetotactic for the bacteria (BLAKEMORE, 1975).

The term “Magnetotactic Bacteria” is of no taxonomic significance and defines a heterogeneous group of gram-negative prokaryotes, not necessarily phylogenetically related. Regardless of their morphology (they display a numerous cellular morphologies including multicellular, see fig. 1) or taxonomic classification, MTB have flagella and possess specific intracellular structures called magnetosomes (SPRING and BAZYLINSKI, 2006), which allow them to passively align and actively swim along the geomagnetic field (BLAKEMORE, 1975; BAZYLINSKI AND FRANKEL, 2004; BAZYLINSKI and WILLIAMS, 2007). Most MTB can swim at speeds nearly twice that of Escherichia coli in spite of being larger in size and of having less flagellar proteins (SHARMA et al., 2008).

Magnetosomes consist of a permanently magnetic nano-sized crystals of magnetite ($Fe_3O_4$) or greigite ($Fe_3S_4$) (GORBY et al., 1988; BAZYLINSKI et al., 1995; BAZYLINSKI and FRANKEL, 2004) bound to a lipidic bilayer membrane. Most MTB present the magnetosomes organized in chains that increase the effect of each magnetosome, causing the bacteria cell to align to the magnetic field lines and behave like a miniature compass needle. The magnetic dipole moment of the cell is often large enough that its interaction with Earth’s magnetic field overcomes the thermal forces that tend to randomize the orientation of the cell in its aqueous surroundings. MTB are sensitive to oxygen concentrations and use aerotaxis to swim towards a zone of optimal oxygen concentration (BLAKEMORE, 1975 and 1982; LOWENSTAM, 1981; GORBY, BEVERIDGE and BLAKEMORE, 1988; PETERSEN; WEISS; VALI, 1989; MATSUNAGA and OKAMURA, 2003; BAZYLINSKI and FRANKEL, 2004; KOMEILI, 2006; KOPP and KIRSCHVINK, 2008). Since water oxygen concentration in natural settings

is commonly depth-dependent, and the Earth's magnetic field has a downward inclination, the orientation along field lines aids in the search for the optimal concentration.

Although they display different crystalline morphology and structure, depending on the bacterial species and the environmental conditions, magnetosomes crystals are crystallographically perfect (GORBY, BEVERIDGE and BLAKEMORE, 1988; BAZYLINSKI et al., 1995; KEIM et al., 2009, BAZYLINSKI and FRANKEL 2004; KOMEILI, 2006; CHANG et al., 2012; JOVANE et al., 2012; SHARMA and BALOMAJUMDER, 2011; TANAKA et al., 2012; PROZOROV et al. 2014).

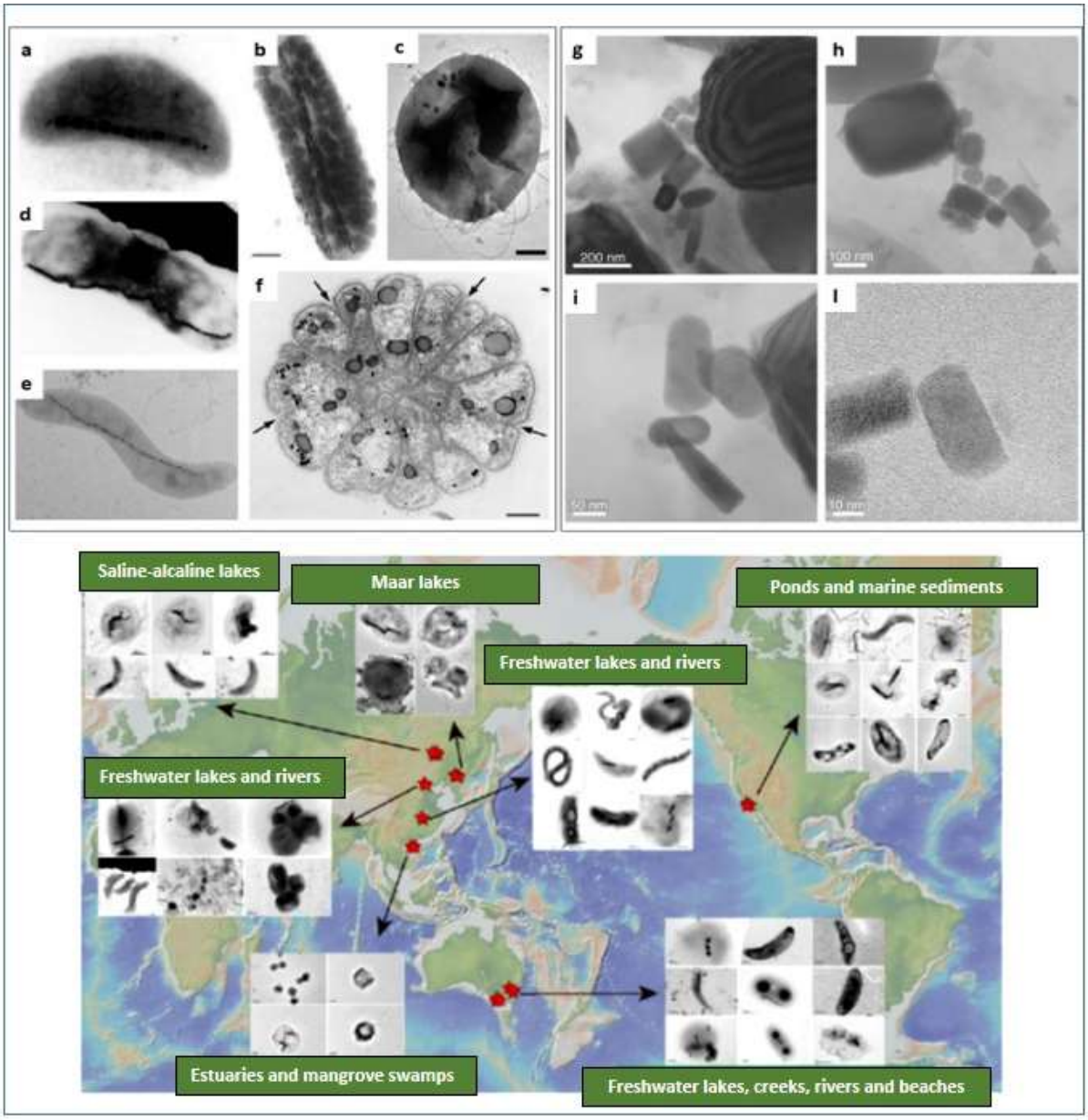


**Fig. 1: On top the left various morphology of MTB: a) vibrios; b) and d) rods (Bar = 1.0 µm); c) coccoid (Bar = 200 nm); e) spirilla; f) multicellular organism (Bar = 1.0 µm). (from YAN et al., 2012). On the top right (g,h,i,l): TEM images of magnetosomes crystals (from Roberts et al., 2012). On the bottom: Spacial distribution of some species of MTB and their relative habitats (from LIN et al., 2017).**

At the death of the bacterial cell, the inorganic magnetosome crystals can be preserved in sediment and act as magnetofossils with the potential to provide paleoenvironmental information. However, due to their small size, magnetosomes tend to dissolve when buried under anoxic diagenetic environments (e.g., ROBERTS et al., 2011; FAIVRE AND SCHÜLER, 2008, KOPP and KIRSCHVINK, 2008, TARDUNO, 1994) and have therefore only been reported in a few pre-Quaternary locations (KOPP and KIRSCHVINK, 2008). Since magnetosome crystals are Single Domain (SD) particles, they are ideal palaeomagnetic recorders and have been found to be responsible a great contriubution in the paleomagnetic signals in sedimentary records worldwide (e.g., PETERSEN et al., 1986; KIRSCHVINK, 1982). MTB have been commonly considered microaerophilic to anaerobic, as they prevalently live at and below the oxic-anoxic transition zone of aquatic environments worldwide (e.g. BLAKEMORE et al., 1985). The first aerobic MTB was cultured by MATSUNAGA et al. (1990), while, more recently, YAMAZAKI and SHIMONO (2013) demonstrated that the main contribution to the magnetic signal in a red clay interval of the Integrated Ocean Drilling Program Site U1365 in the South Pacific Gyre, is given by magnetofossils of MTB. This interval contained abundant dissolved oxygen and no oxic-anoxic transition zone. Other laboratory studies have confirmed strains of strictly anaerobic (non-obligatory) nitrous oxide reducing and obligatory sulphate reducing (HESSE, 1994) MTB. These observations refute the common thought that all MTB require low levels of oxygen to grow and produce magnetite.

Dissolved iron and oxygen contents in local environments are known to be limiting factors for the production and preservation of biogenic magnetite, but also influence the morphology and crystallinity of the magnetosomes (YAMAZAKI and SHIMONO, 2013; RODELLI et al., 2019). Studies have suggested that more elongated magnetosomes morphologies are present in less oxygenated waters while more equant morphologies are present in more oxygenated ones (RODELLI et al., 2019). This seem to confirm what already proposed by YAMAZAKI and SHIMONO (2013) which reported that aerophilic MTB in red clays have cubo-octahedral morphology and that magnetofossil morphology could be used as a paleoenvironmental indicator; as the proportion of elongated magnetofossils increases in less oxic environments.

MTB are considered of high ecological significance as have been reported to be the dominant species of the bacterial population in some environments (SPRING et al., 1993). Moreover, they are widespread in the aquatic environments of the world, even in extreme environments like the Mono Lake (a saline and alkaline lake in California) which is iron limited due to the low solubility of this metal at high pH (FAIVRE and SCHÜLER, 2008).

During the las decades, scientific studies on MTB, their magnetofossils and the attempt to use biogenic magnetite signal as proxy have proliferated, Some authors have linked their presence to increased aeolian dust flux and surface water eutrophication (ROBERTS et al., 2011). Others link the distribution of giant magnetofossils in the geological record with hyperthermal events as the enhanced global weathering and expanded suboxic diagenetic environments during these events would provided more bioavailable iron for MTB.

Since the discovery of the variety of habitats in which MTB dwell, the focus of many scientists has shifted from the sediment oxygen content to magnetite preservation in sediments. In fact, when suitable conditions exist, the magnetosomes crystals are preserved in the sediment as magnetofossils can carry important paleomagnetic information and relevant contribution to the overall paleomagnetic record (TARDUNO et al., 1998; EGLI, 2004; ROBERTS et al., 2012). Therefore it is important to understand the natural variability of the biogenic magnetite produced by different MTB species in defferent context. Magnetofossils identification nowadays is mostly achieved through the recognition of discrete biogenic components with different coercivity (e.g. Egli, 2004; RODELLI, 2019).

Despite the ubiquitous occurrence of MTB, their cultivation has been difficult because of the restricted ecological conditions in which they live. The progress made in biotechnology and magneto-technology is gradually enlightening the process of biomineralization, ecology of MTB, magnetisms of MTB and magnetosomes, and identification of MTB magnetofossils in sediments (POSTEC et al., 2012). The study of MTB proved to have a serious impact in a number of diverse research fields including microbiology, geology, mineralogy and biomineralization, crystallography, chemistry, biochemistry, physics, limnology and oceanography, astrobiology and even in many medical fields (e.g.: BAZYLINSKI and SCHÜBBE, 2007; ALPHANDÉRY, 2014; MATHURIYA, 2016). Understanding the processes that link MTB to their living environments is fundamental to reconstructing past chemical variations in the water column and sediment, and for using the magnetic properties of biogenic magnetite as environmental proxy indicators.

# 3 - METHODOLOGIES

In this chapter are described the main techniques utilized in this PhD work: primarily X-ray diffraction (XRD), secondarily, Hyerarchical Cluster Analysis (HAC) and magnetic properties. XRD is the main technique used in this PhD work to identify the mineralogical components of the sediment containing the signature of MTB to understand the sedimentary environment in which they live. A secondary technique used in this work is HAC: this technique allows the grouping of XRD results (diffractograms) on the base of similarities of their profiles and peaks, allowing a better understanding of the sedimentary successions. Various types of magnetic analyses done by colleagues and described below, were used to identify the magnetic signature of MTB (living or fossils).

These methodologies have been integrated for each case study with other techniques depending on the specific goals of each case study. All the techniques with the relative sample choice, number and treatment, are described in the methods sections of each case study for a better understanding of each specific case study.

## *3.1. X-Ray Diffraction*

X-ray Diffraction (XRD) crystallography has been fundamental in the development of many scientific fields as it permits to determine the atomic and molecular structure of any type of crystalline material. This technique has not been important only in mineralogical studies, but it has been vital to other sciences as, for example, it was the main method that was used to determine the structure of the DNA and is still very important in the pharmacy industry. XRD is, indeed, the main method for characterizing the atomic structure of new materials.

In this work, XRD was used to characterize the mineralogical composition of marine sediments in which the MTB were found to create paleoenvironmental reconstructions.

### *3.1.1. Physics of XRD*

Bragg diffraction (also known as the Bragg formulation of X-ray diffraction) was first proposed by Lawrence and William Henry Bragg in 1913. They found that crystals hit by X-rays, at certain specific wavelengths and incident angles, produced intense peaks of reflected radiation. By measuring the angles and intensities of the diffracted beams, a three-dimensional picture of the electron density within the crystal is produced, allowing the determination of the mean positions of the atoms in the crystal.

X-ray crystallography is a form of elastic scattering: the X-rays generated by the scattering have the same energy and wavelength as the incoming X-rays, only with altered direction. In figure

2 is presented a schematic representation of the diffraction process: the incoming beam causes each scatterer (atom hit by X-ray) to re-radiate a small portion of its intensity as a spherical wave. If scatterers are arranged symmetrically with a separation *d*, these spherical waves will interfere constructively only in directions where their path-length difference *2d sin θ* equals an integer multiple of the wavelength *λ* creating a peak in the diffractogram at that determined angle. If the path length difference is not a multiple of the wavelength, the waves will not be in phase; therefore, they will not produce constructive interference and will not produce any reflection spot in the diffraction pattern.

The effect of the constructive or destructive interference intensifies because of the cumulative effect of reflection in successive crystallographic planes of the crystalline lattice (as described by Miller notation). The specific directions of diffracted X-rays that obey Bragg´s Law and produce constructive interference appear as spots on the diffraction pattern.

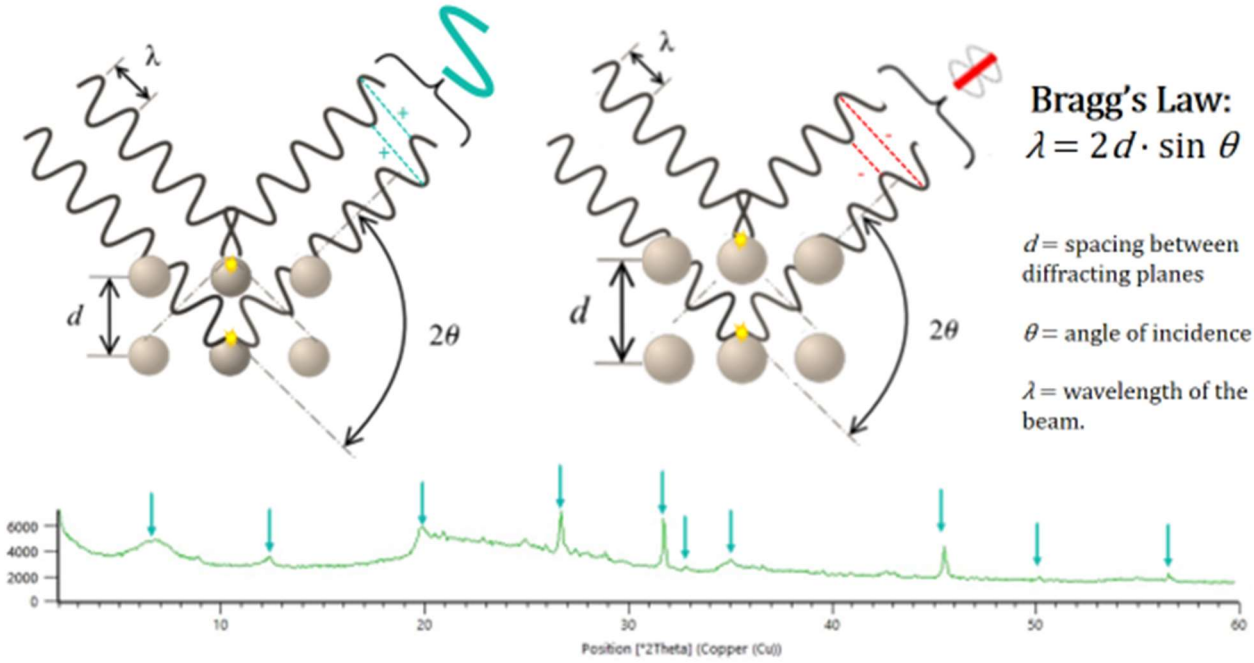


**Fig.2: Schematic representation of Bragg's Law and interference. Two beams with identical wavelength and phase approach a crystalline solid and are scattered off two different atoms within it. The lower beam traverses an extra length of 2dsinθ. Constructive interference occurs when this length is equal to an integer multiple of the wavelength of the radiation. On the left constructive interference that produces a reflection peak; on the right destructive interference that does not produce reflection peak. At the bottom an example of diffractogram, blue arrows indicate the main peaks.**

The Bragg's equation explains very well why X-rays and not other types of electromagnetic radiations are used for crystallography: in principle, any wave impinging on a regular array of scatterers produces diffraction, but to produce significant diffraction, the spacing between the scatterers and the wavelength of the incident wave should be similar in size. X-ray wavelength λ is typically the same order of magnitude (1–100 angstroms) as the spacing *d* between planes

in the crystal allowing the best diffraction pattern. Radiations with longer wavelength would not have sufficient resolution to determine the atomic positions, while shorter-wavelength radiations, such as gamma rays, interact too strongly with matter, producing particle-antiparticle pairs.

*3.1.2. Short history of crystallography and X-ray diffraction*

The first scientific work on crystals was done by Kepler in 1611, in his work *Strena seu de Nive Sexangula* (A New Year's Gift of Hexagonal Snow) he hypothesized that spherical water particles where packed regularly creating the hexagonal symmetry of snowflake crystals. Nicolas Steno conducted the first actual experimental investigation on crystal symmetry in 1669 concluding that the angles between faces of a crystal remain constant in every crystal of the same type. In 1784, Haüy discovered that every face of a crystal could be described as a stack of identical 3D patterns, leading to the idea of a unit cell that repeats indefinitely along three not necessarily perpendicular axes. In the second half of the 1800, Hessel, Bravais, Fedorov, Schönflies and Barlow compiled a complete catalogue of the possible symmetries of crystals, but some of these structures could not be validated until the discovery of X-ray crystallography. Just as this studies where being concluded, Wilhelm Roentgen discovered X-rays (1895). Physicists were initially uncertain of the nature of X-rays, but soon they came to the conclusion that X-rays were waves of electromagnetic radiation. It was only in 1905 that Albert Einstein introduced the concept of photon and therefore the idea of the dualistic essence of X-rays, as they display particle-like properties, leading William Henry Bragg to argue in 1907 that X-rays were not electromagnetic radiation. In 1912, the first experiments of X-ray diffraction were conducted: Max von Laue confirmed that X-rays were a form of electromagnetic radiation and Arnold Sommerfeld, using very thin wedge-shaped slits experiments, estimated the wavelength of X-rays around $4 \times 10^{-9}$ cm (ROBOTTI 2013). The scientific community at that time supported mostly the idea that X-rays were electromagnetic waves, it was only in 1922 with the work of Arthur Compton about the scattering of X-rays from electrons that the concept of photon and of the dualistic particle-wave essence of X-rays was accepted.

Since the 1920s, X-ray diffraction has been the principal method for determining the arrangement of atoms in minerals and metals. Since then the application of X-ray crystallography was implemented in many scientific fields as a tool for a better understanding of complex molecules not only inorganic but also organic. In many cases X-ray diffraction studies were a breakthrough. Dorothy Crowfoot Hodgkin was the first scientist that successfully used X-ray crystallography to study and identify structures of different proteins and biological

molecules, this lead to further studies on biological molecules that eventually brought to the discovery through an XRD image of DNA by Rosalind Franklin, Watson and Crick of the double helices structure of DNA.
In biochemistry and pharmaceutics XRD is still widely used to identify the structure and purity of molecules as well as some processes: for example Halasz et al. (2013) were able to monitor in real time and in situ by powder X-ray diffraction, with a non-invasive method, the synthesis of porous metal–organic frameworks from ZnO.
XRD was also used to study the soil of Mars when in the October of 2012, the Curiosity rover analyzer revealed the presence of several minerals, including feldspar, pyroxenes and olivine, and suggested that the Martian soil in the sample was similar to the "weathered basaltic soils" of Hawaiian volcanoes.

*3.1.3. Analytical Procedures:*

XRPD analyses were performed with an Olympus BTX II with a Co anode ($\lambda = 1.789$ Å) in the Centro Oceanográfico de Registros Estratigráficos (CORE) laboratory of the Oceanographic Institute of the University of São Paulo. About 1 $cm^3$ of sediment was gently pulverized in a jade mortar by hand and sieved through a 63µm sieve. Then, about 15 mg of powder were analysed at 30 kV and 0.326 mA, over a range 5–55° 2θ, with a step size of 0.05°, and 100 exposures over 22 minutes. Mineral identification was done using the PANalytical High Score Plus software equipped with the Crystal Structure Database (DOWNS and HALL-WALLACE, 2003), the Crystallography Open Database, and the collection from the International Centre for Diffraction Data (Newtown Square, PA).

### *3.2. Hierarchical Agglomerative Clustering (HAC):*

Statistical analyses were applied to mineralogical and chemical data throughout this work as a tool to identify mineralogical and elemental variations and correlations. Especially important for this work was cluster analysis: clustering is a type of machine learning algorithm where data objects are grouped on the base of similarity with each other. There are various types of cluster analysis, one such type is Hierarchical Agglomerative Clustering (HAC).
Agglomerative hierarchical clustering algorithms are among the oldest and most used methods of cluster analysis. The HAC algorithm checks for the pair of data points with the smallest distance and groups them into cluster with an iterative procedure until all the data points are brought under one single big cluster.

The result of this algorithm is a tree-based structured called Dendrogram (see fig.3). The order of pairwise coupling of the objects in the data set is shown, and the value of the similarity function (level) at which each fusion occurred (RASMUSSEN, 1992).

For HAC diffractograms collected with the Olympus BTX benchtop were analysed with the PANalytical High Score Plus software. The software analyses the diffractograms profiles and peaks and groups the samples on the base of their similarity and for each cluster identifies the most representative sample.

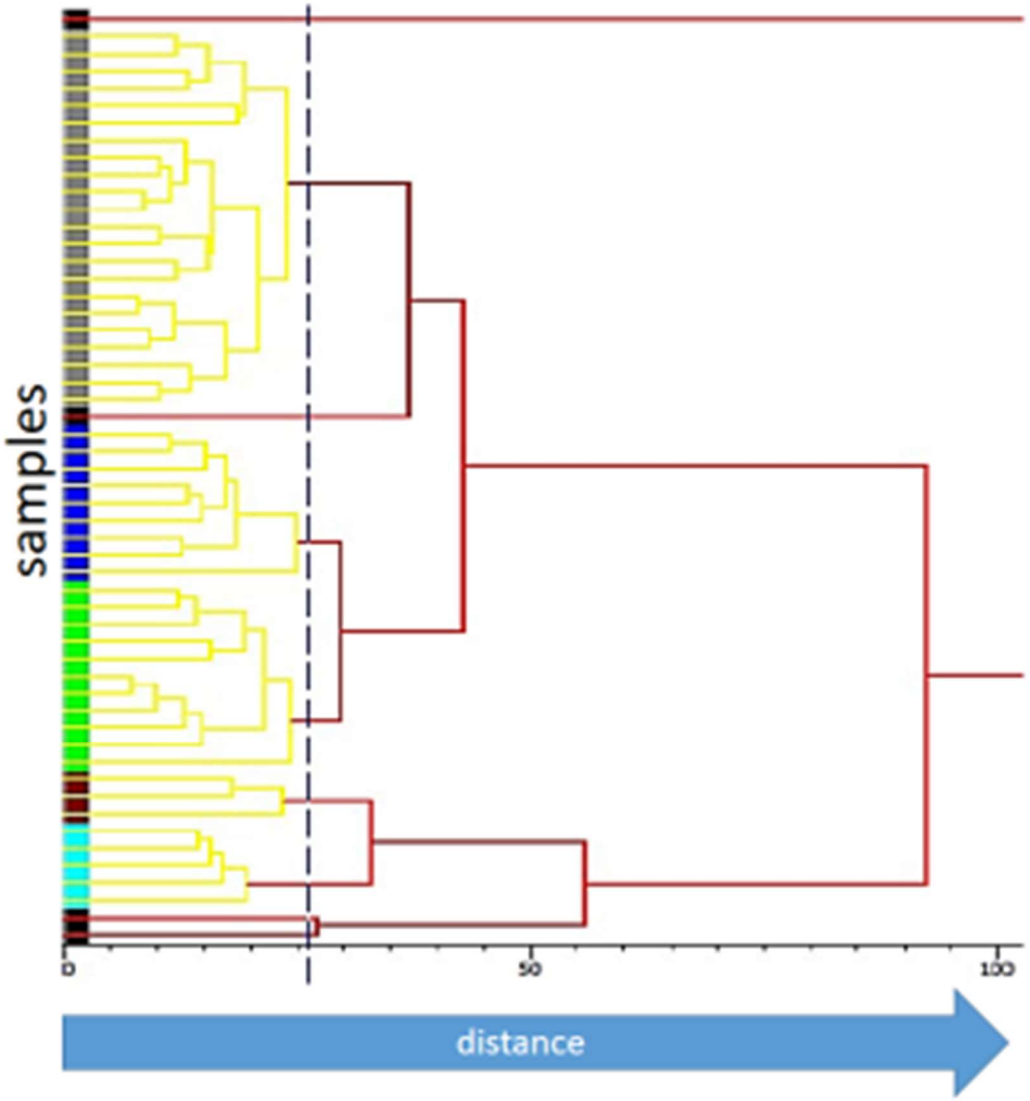


**Fig. 3: Example of HAC of XRPD data from Cananeia (RJ) (see chapter 4). Clusters are formed by pairing samples on the base of similarity, iteratively, until one single big cluster is obtained.**

### *3.3. Magnetic properties:*

In this work the results of magnetic properties analyses of marine sediments were used to determine the presence of MTB (as living bacteria or magnetofossils). MTB produce magnetic crystals to keep themselves aligned with the N-S direction of the earth magnetic field and swim actively along its lines. These magnetic crystals can display different morphologies, but all are nanometric, crystallographically perfect and possess permanent magnetization (e.g.: GORBY et al., 1988; BAZYLINSKI et al., 1995; BAZYLINSKI and FRANKEL 2004; KOMEILI et al., 2006; CHANG et al., 2012; JOVANE et al., 2012). Four techniques were used in this PhD work to discriminate between biogenic and non-biogenic magnetic crystals in sediments and therefore identify the biogenic crystals produced by the MTB within the sediment:

*3.3.1. Magnetic Susceptibility (MS):*

MS is a measure of how much a material is prone to magnetization when a magnetic field is applied.

Volume specific susceptibility, denoted by "κ", is dimensionless and is given as:

$$\kappa = M/H$$

*where: M = Induced Magnetization, and H = applied magnetic field*

The mass specific susceptibility "χ" is defined as:

$$\chi = \kappa/\rho \ [m3\ kg{-}1\ ]$$

*where ρ = density of the substance.*

There are two possible responses of a material to an applied magnetic field:

- Paramagnetic / Superparamagnetic and Ferromagnetic particles will align with the magnetic field ($\chi>0$), in this case the magnetic field in the material would be strengthened by the induced magnetization.
- Diamagnetic particles will align against the field ($\chi<0$), in this case, the magnetic field in the material would be weakened by the induced magnetization.

Generally, nonmagnetic materials are classified as para- or diamagnetic because they do not possess permanent magnetization without an external magnetic field. Ferrimagnetic materials, like biosynthesized magnetite and greigite, possess permanent magnetization even without external magnetic field and do not have a well-defined zero-field susceptibility. In the case of MTB and its magnetosomes, it has been proved in laboratory experiments (e.g. HARASKO et al., 1993) that the MS can be used to calculate the concentration of MTB in a medium.

*3.3.2. Anhysterethic Remanent Magnetization (ARM):*

ARM is a magnetic mineral analysis technique that involves the measurement of the effects of small (usually 0.5 mT) biased artificial magnetic fields on bulk natural samples. The measurement is performed on a demagnetized sample that is magnetized along one axis with a known artificial magnetic field and has its resultant magnetic moment measured. ARM response is generally controlled by the presence of micrometer or sub-micrometer sized magnetite (Fe3O4) in the sediment, such as magnetite of biogenic origin produced by magnetotactic bacteria (BLOEMENTAL et al., 1992, LARASSOAÑA et al., 2012).

*3.3.3. Isothermal Remanent Magnetization (IRM):*

IRM is laboratory induced technique which gives the response of the relative abundance of magnetic minerals in a sample. An isothermal remanent magnetisation (IRM) is applied to a sample by exposing it to the large applied magnetic field (Commonly 0.9mT). The magnetization increases with the increase in applied field until the sample gets saturated, which is called SIRM. After measuring acquired SIRM a backfield (BIRM) of 300 mT is applied in opposite direction to reverse the lower coercivity mineral components. This external field reorients the magnetic moments of specific minerals in the sample, especially, those with a magnetic coercivity lower than the applied field. A value of 0.9T is typically used to find the signal of MTB as it influences very fine magnetite, and can be used as an indicator of relative variation of biogenic magnetite along a core (BLOEMENTAL et al., 1992, EVANS and HELLER, 2003).

*3.3.4. First Order Reversal Curve (FORC):*

FORC is an advanced technique for studying the magnetic mineral assemblages in a bulk sample. FORC diagrams are contour plots of the partial hysteresis curves plotted in a two dimensional distribution. The FORC is a 2D representation of the coercivity range versus the magnetostatic interactions among magnetic particles in a sample (ROBERTS et al., 2000 and 2017). In FORC diagrams, the horizontal axis represents the coercivity denoted by Hc while the vertical axis, Hu shows the magnetostatic interaction among magnetic particles. Biogenic magnetite is known to have a coercivity distribution centred around 20-40 mT (depending on the MTB species) and virtually no magnetic interaction. This is explained by the presence of small and pure magnetite crystals that form a long chain. These crystals are arranged in a way that act as a single crystal (ROBERTS et al., 2000; EGLI et al., 2010; ROBERTS et al., 2011; 2012 and 2013). For these reasons, biogenic magnetite has a distinct fingerprint in a FORC diagram, with a very narrow central ridge (fig. 4) and FORC analyses are an excellent method

for detecting signatures due to biogenic magnetite (EGLI et al., 2010; HESLOP et al., 2014; JOVANE et al., 2012; ROBERTS et al., 2012).

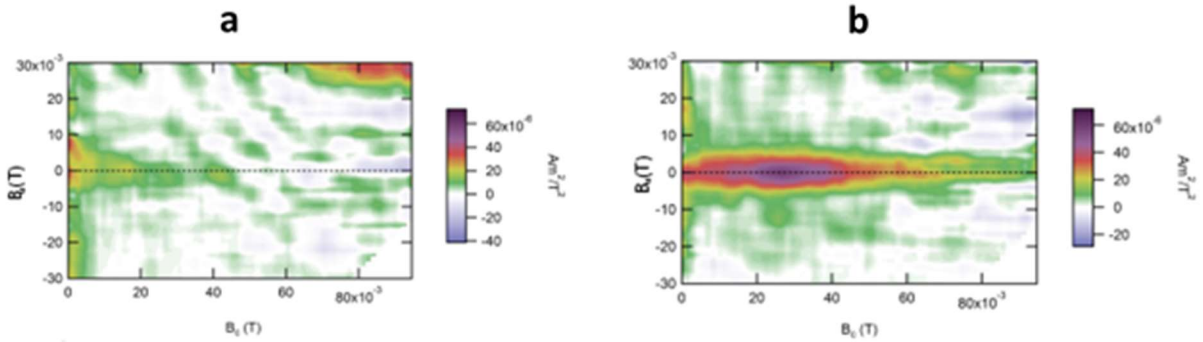


**Fig. 4: Two examples of FORCs results from Mamanguá (Rodelli et Al 2019). a) sample with no magnetic signature of bacteria; b) a very distinct signature of a sample rich in bacteria.**

*3.3.5. Analytical Procedures:*

Detailed magnetic measurements were made continuously throughout the core on U-channel samples with 2 × 2 cm cross section and length <1.5 m (WEEKS et al., 1993). Discrete oriented samples were collected in demagnetized plastic cylinders.

The Natural Remanent Magnetization (NRM) was analyzed with a 2-G Enterprises superconducting rock magnetometer located in a magnetically shielded room at the Paleomagnetism Laboratory, Instituto de Astronomia, Geofísica e Ciências Atmosféricas, Universidade de São Paulo, Brazil. To identify primary and secondary magnetic components, stepwise Alternating Field (AF) demagnetization was used, with steps of 0, 5, 10, 15, 20, 25, 30, 40, 50, 60, 70, 80, 90, and 100 mT. Data were analysed with the software of Xuan and Channell (2009) to isolate the characteristic remanent magnetization, using principal component analysis (Kirschvink, 1980), and deconvolution was applied. The magnetometer response functions were measured using an internal standard edge effect due to the half-width of the magnetometer response function requiring data removal from the first and last 5 cm of each U-channel to avoid artefacts during deconvolution.

Different rock magnetic measurements were performed to characterize the magnetic mineralogy of the core. Mass-dependent magnetic susceptibility was determined on discrete samples using an Agico KF1 Kappabridge.

Artificial magnetic fields of known characteristics were used in order to study the response of the samples in different conditions and the following parameters were determined:

- Anhysteretic remanent magnetization (ARM), which was measured first by imposing a 0.1 mT DC bias field while applying a 0.1 T demagnetizing alternating field, and then

by progressively demagnetizing via AF with fields of 5, 10, 15, 20, 25, 30, 40, 50, 60, 70, 80, 90, 100 mT;

- Isothermal remanent magnetization was imparted by applying a 1.0 T direct field (IRM@1.0), after measuring the magnetization Backfield IRM was imparted by applying a direct field of 0.1 (IRM@-0.1) and 0.3 mT (IRM@-0.3) in the opposite direction (e.g., KING and CHANNELL, 1991; VEROSUB and ROBERTS, 1995; JOVANE et al., 2013). From these parameters the S-ratios were calculated (S-Ratio300 as IRM@0.3/IRM@1.0; and S-Ratio100 as IRM@0.1/IRM@1.0), which measure the relative abundance of high coercivity (e.g., hematite, goethite) and low coercivity (e.g., magnetite) minerals. The hard isothermal remanent magnetization (HIRMs), which reflects the concentrations of high coercivity minerals, was calculated as (HIRM300 = (IRM@0.3+IRM@1.0)/2 and HIRM100 = (IRM@0.1+IRM@1.0)/2); the relative magnetic grain size variations were estimated as ARM/IRM@1.0 (Evans and Heller, 2003). In order to perform the measurements with the 2G Cryogenic Magnetometer we used the Laboratory of Paleomagnetism of the Institute of Astronomy, Geophysics and Atmospheric Sciences of the University of São Paulo, Brazil.

FORCs were analysed at the Centro Oceanográfico de Registros Estratigráficos (CORE) Laboratory, Instituto Oceanográfico, Universidade de São Paulo, Brazil using a Lake Shore Cryotronics Inc. vibrating sample magnetometer, and FORC diagrams were elaborated using the FORCINEL 3.0 software (HARRISON and FEINBERG, 2008).

# 4 – THE TASMAN ABYSSAL PLAIN: ABYSSAL OCEANIC CIRCULATION AND ACIDIFICATION DURING THE MIDDLE EOCENE CLIMATIC OPTIMUM (MECO)

**This case study produced an article which is currently under review in the journal *Scientific Reports* with the title *"Abyssal oceanic circulation and acidification during the Middle Eocene Climatic Optimum (MECO)"* by Flaminia Cornaggia, Simone Bernardini, Martino Giorgioni, Gabriel L. X. Silva, André Istvan M. Nagy, Luigi Jovane**

***Abstract***

The Middle Eocene Climatic Optimum (MECO) is a global warming event that occurred at around 40 Ma and lasted about 500 kyr. We study this event in an abyssal setting of the Tasman Sea, using the IODP Core U1511B-16R, collected during the expedition 371. We analyse magnetic, mineralogical, and chemical parameters to investigate the evolution of the sea bottom conditions at this site during the middle Eocene. We observe significant changes indicating the response to the MECO perturbation. Moreover, we identify a prominent Mn anomaly just above the MECO interval, which indicates a sudden precipitation of Mn oxides probably catalysed by MTB. Our results suggest more acid bottom water over the Tasman abyssal plain during the MECO, and an abrupt end of these conditions. This work provides the first evidence of MECO at abyssal depths and shows that acidification affected the entire oceanic water column during this event.

### *4.1. Introduction*

The Eocene (~56–34 Ma) was characterized by a gradual climatic cooling, accompanied by decreasing atmospheric $pCO_2$ and culminating with the onset of the Antarctic glaciation in the early Oligocene (33 Ma) (ZACHOS et al., 2008; INGLIS et al., 2015; ANAGNOSTOU et al., 2016; CRAMWINCKEL et al., 2018 and 2019). This trend was interrupted during the middle Eocene by a warm period known as Middle Eocene Climatic Optimum (MECO), with duration of ~500 kyr and a warmth peak at ~40 Ma (e.g. JOVANE et al., 2007; 2010). The MECO has been identified in several sedimentary records around the globe, including the South Pacific Ocean (BOHATY and ZACHOS, 2003; EDGAR et al., 2010). It is related to an increase in seawater temperature, from the surface to deep bathyal depths, and increasing $pCO_2$ in the atmosphere (BOHATY et al., 2009; BIJL et al., 2010). Moreover, significant changes in atmospheric and oceanic circulation dynamics and in the patterns of continental rainfall are recorded (e.g. MARVEL and BONFILS, 2013, REGO et al. 2018 and references therein). However, classic climatic models fail to explain how such conditions could persist for several hundreds of thousand years (e.g. SLUIJS et al., 2013).

Southern Ocean (SO) circulation is extremely important for understanding the climatic evolution during the Eocene, and particularly during the MECO. The separation of Australia from Antarctica during the middle-late Eocene profoundly affected the circulation and made this region particularly sensitive to paleoceanographic changes (RÖHL et al., 2004, CRAMWINCKEL et al., 2019).

The IODP Hole U1511B was collected during the Expedition 371 on the Tasman abyssal plain (TAP). Core U1511B-16R, considered in this study, belongs to the middle Eocene and the sections 16R-4 and 16R-5 contain the base of the magnetochron C18n, which is the magnetostratigraphic marker of the MECO (e.g. JOVANE et al., 2007; BOHATY et al., 2009; SAVIAN et al., 2014 and 2016; RODELLI et al., 2018). This interval is characterized by a more clayey lithology, and increasing magnetic susceptibility (MS) and Natural Gamma Radiation (SUTHERLAND et al., 2019). Thus, this record offers a unique opportunity to study how the SO system responded to the MECO at abyssal depths. Here we present chemical elements and mineralogical data, studied with various analytical and statistical methods. We give special attention to the mineralogical characterization of clay minerals and Mn-Fe oxides, which are strongly controlled by chemical conditions (e.g. pH, Eh, ionic strength), water circulation, and microbial activity. Therefore, a proper characterization of these minerals can provide valuable information about their crystallization environment. Our results show that a major change in deep-water circulation occurred over the TAP during the MECO.

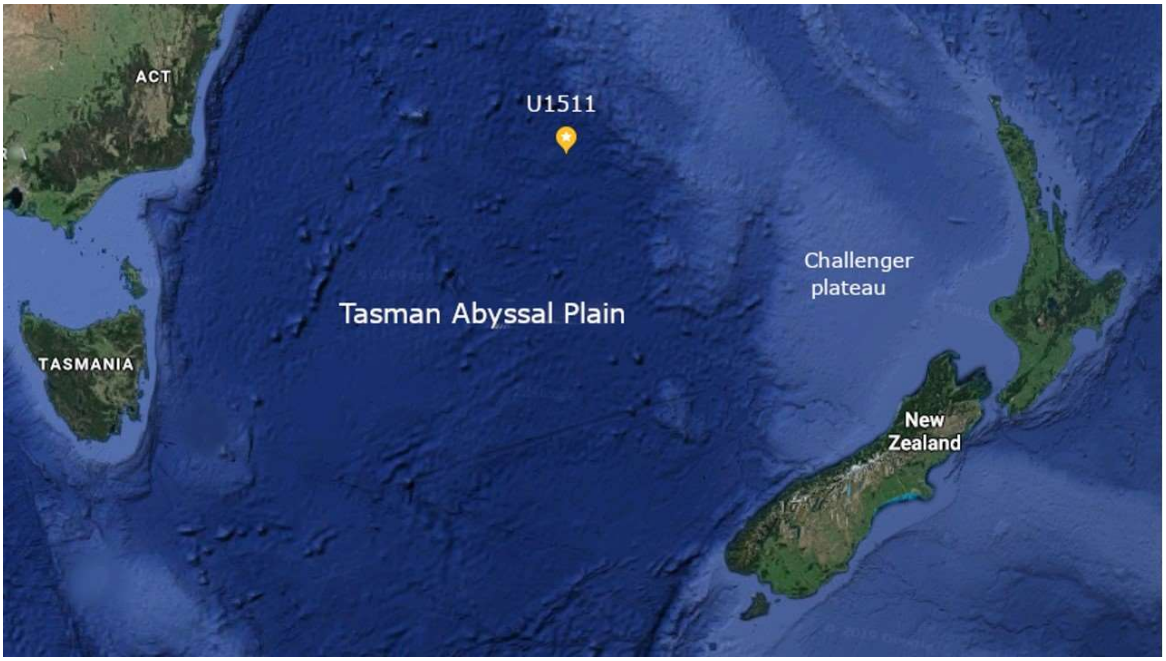


**Fig. 5: Geographical location of Site U1511B**

### *4.2. Geological and stratigraphic setting*

The IODP Hole U1511B was collected during the Expedition 371 on the TAP, at a water depth of 4858 m, ~945 km east of Australia and ~990 km northwest of New Zealand (Figure 5). The sedimentary succession is mainly of Cenozoic age and lies onto an oceanic crust that formed during the Late Cretaceous (GAINA et al., 1998; SUTHERLAND, 1999).

At this site, ~560 m of sediments were recovered, consisting of clays and diatoms, with radiolarians and other bio-siliceous components, and traces of nannofossils, detrital, and authigenic components. Radiolarian biostratigraphy allowed for calibrating a well-established succession of paleomagnetic reversals and date the succession from the Paleocene to the Quaternary (SUTHERLAND et al., 2019). The IODP Core U1511B-16R, considered in this study, belongs to the Bartonian stage, in the middle of Eocene.

The Core U1511B-16R (259,56 – 268,54 mbsf) consists mainly of ~9 m of diatomite, with sparse small bioturbations, with minor clays and other siliceous microfossils (i.e. radiolarians, sponge spicules and silicoflagellates). The absence of calcareous microfossils did not allow a precise estimate of the paleodepth, however, a lower bathyal to abyssal depth can be inferred by the lack of preserved carbonate, indicating conditions completely below the CCD (SUTHERLAND et al., 2019). Sections 16R-4 and 16R-5 of the Hole U1511B contain the base of the magnetochron C18n, which is the magnetostratigraphic marker of the MECO (e.g. JOVANE et al., 2007; BOHATY et al., 2009; SAVIAN et al., 2014, 2016; RODELLI et al., 2018). This corresponds to an interval characterized by a more clayey lithology, and increasing

magnetic susceptibility (MS) and Natural Gamma Radiation (NGR) (SUTHERLAND et al. 2019). The sedimentation rate estimated during the Expedition 371 provides a duration of ~170 kyr for the MECO at this site, which is about 330 kyr shorter than that observed elsewhere (SUTHERLAND et al., 2019; BOHATY et al., 2009).

### *4.3. Materials and methods*

Magnetic susceptibility, color variations, biostratigraphic data, and X-Ray Fluorescence (XRF) data been measured by the IODP 371 expedition crew and are publicly available at the online repository website (http://iodp.tamu.edu/LORE/).

A total of 37 samples were collected from the Core U1511B-16R. Part of the material was grounded and used for XRPD, XRF, and FT-IR analyses, whereas the rest, untreated, was used for optical microscope, SEM-EDS and Raman spectroscopy analyses.

#### *4.3.1. Scanning Electron Microscopy and Energy Dispersive Spectroscopy (SEM-EDS)*

The samples were coated in carbon and then analysed at the Scanning Electron Microscopy Laboratory of the Geosciences Institute of the University of São Paulo (LabMev - IGc – USP). The scanning electron microscope (SEM) used is a LEO 440, by LEO Electron Microscopy Ltd. Equipped with an X-ray Dispersive Energy Spectrometer (EDS) with a Si (Li) solid-state detector controlled by Inca 300 software from Oxford Ltd. The analyses were conducted at 20 kV of Acceleration Voltage, with working distance from 5 to 18 mm, and an EDS Live Quotation Time of 100s.

#### *4.3.2. X-Ray Powder Diffraction (XRPD)*

Two types of XRPD analyses were performed:

- Conventional XRPD analysis were performed on 7 samples at the X-Ray diffraction Laboratory of the Geoscience Institute of the University of Brasilia using a Rigaku Ultima IV with a copper anode ($\lambda = 1.5406$ Å), working at 35kV and 15 mA. The samples chosen were the closest to the most representative of each cluster identified with the HAC. Two samples were chosen from the pre-MECO, pre-MECO transition, and post-MECO intervals, respectively, and one sample from the MECO interval. As the sediments contain 90-99% of clay, measurements were taken in four steps, according to the standard procedure for clay treatment: bulk, clay fraction, clay fraction after vacuum solvation in ethylene glycol, and after 5 hours heating to 490 °C. Mineral identification was

done using the Jade 9 software with the ICDD PDF-2 (2010) and ICDD PDF-4 (2010) databases.

- Bench-top XRPD analyses were performed with an Olympus BTX II with a Co anode (λ = 1.789 Å) in the Centro Oceanográfico de Registros Estratigráficos (CORE) laboratory of the Oceanographic Institute of the University of São Paulo. Bulk mineralogy was analysed in all the 37 samples for statistical purposes. An aliquot of about 1 $cm^3$ of sediment was gently pulverized in a jade mortar by hand and sieved through a 63µm sieve. Then, about 15 mg of powder were analysed at 30 kV and 0.326 mA, over a range 5–55° 2θ, with a step size of 0.05°, and 100 exposures over 22 minutes. Mineral identification was done using the PANalytical High Score Plus software equipped with the Crystal Structure Database (DOWNS and HALL-WALLACE, 2003), the Crystallography Open Database, and the collection from the International Centre for Diffraction Data (Newtown Square, PA).

*4.3.3. Fourier-Transform Infrared Spectroscopy (FT-IR)*

Spectra were collected using a Nicolet iS50 FT-IR spectrometer at the Laboratorio di Spettroscopia Infrarossa, Dipartimento di Scienze (Università Roma Tre), equipped with a DTGS detector and a KBr beamsplitter. The nominal resolution was 4 $cm^{-1}$, and 64 scans were averaged for each sample and for the background. Samples were prepared as pellets containing about 1 mg of powdered sample in 200 mg of KBr.

*4.3.4. Raman spectroscopy*

For each sample, we performed several point analyses by Raman spectroscopy, in order to check for possible inhomogeneities. Raman measurements were performed with a progressively increasing laser power, in order to avoid degradation of the samples. The analyses were performed at room temperature using an inVia Renishaw Raman spectrometer at the Laboratorio di Spettroscopia Raman, Dipartimento di Scienze (Università Roma Tre). The spectrometer was equipped with a diode laser (532 nm, output power 50 mW), an edge filter to select the Raman scattering avoiding the elastic contribution, a 1800 lines/mm diffraction grating and a Peltier cooled 1024x256 pixel CCD detector. Samples were mounted on the manual stage of a Leica DM2700 M confocal microscope. Laser beam focusing and collection of Raman signals were realized with a 100x objective (with 2mW and 5 accumulations of 10s each, in the range of 200-900 $cm^{-1}$). The Raman spectrometer was calibrated prior to the

measurements using a Si wafer and by performing the automatic offset correction. The spectra acquisition and data analyses were performed using WiRE™ and Origin softwares. The peak positions are estimated to be accurate to at least ±2 $cm^{-1}$.

*4.3.5. X-Ray Fluorescence (XRF) scanning*

XRF scanner data of the Core U1511B-16R were obtained with an AVAATECH scanner XRF at the IODP base in College Station (Texas, USA) and are available in the IODP online data repository (http://iodp.tamu.edu/LORE/). Data have been normalized to minimize analytical errors by dividing each entry by the mean value of all the counts of the respective element (WELTJE and TJALLINGII, 2008).

*4.3.6. First-order reversal curve (FORC)*

FORCs were analysed using a Lake Shore Cryotronics Inc. vibrating sample magnetometer at the Centro Oceanográfico de Registros Estratigráficos (CORE) Laboratory, Instituto Oceanográfico, Universidade de São Paulo, Brazil. FORC diagrams were produced using the FORCINEL 3.0 software (HARRISON and FEINBERG, 2008).

*4.3.7. Statistical Analyses*

- Hierarchical cluster analysis (HAC):

  XRPD diffractograms collected with the Olympus BTX II Bench-top XRD were analysed with the PANalytical High Score Plus software for HAC.

- Partitioning Cluster Analysis (PCA):

  This method was applied to the XRF, magnetic susceptibility, and reflectance data of the Core U1511B-16R. The fuzzy *c*-means algorithm proposed by Bezdek et al., (1984) was used for the partitioning approach. This algorithm refers to a soft method of clustering, in which each sample of a dataset can belong to more than one cluster simultaneously. The clustering values are expressed in terms of a variable called pertinence, which fluctuates within a continuous interval [0, 1] (DEKKERS et al., 1994). A sample with pertinence values close to zero indicates a poor similarity with the cluster, whereas pertinence close to one represents high similarity.

- K-means cluster analysis:

  K-means clustering was applied to XRF and MS data. This is a method divides the number of observations in a defined number (K) of clusters. Each cluster is characterized by the

mean value of the data contained. Each observation belongs to the cluster with the closest mean, which represents the prototype of the respective cluster.

- Pearson correlation

The Pearson correlation coefficient was applied to the XRF and MS data to identify correlations among them. The Pearson correlation coefficient measures the linear correlation between two variables and is expressed with a value between +1 and −1. A value equal to 1 represents a direct correlation between the two variables, describable by a linear equation in which Y and X increase together. A value equal to −1 represents an inverse correlation, describable with a linear equation in which Y decreases as X increases. When the Pearson coefficient equals to 0 there is no linear correlation between the two variables. The Pearson correlation was applied to the series of the entire Core U1511B-16R, and also on individual stratigraphic intervals, identified by interpolating k-means clustering, PCA, and HAC.

### *4.4. Results*

At the optical microscope, all samples appear as light yellowish-brown grained mixture of different minerals, with micrometric black and red grains. In the interval between 264.9-266.7 mbsf, the red grains are more abundant, making the colour of the sediment reddish-brown.

#### *4.4.1. Physical Properties*

Physical properties: results for bulk density and grain density suggest a lithological change at the MECO depth (one single point was collected in the MECO interval), where density increase and porosity decrease indicate a higher clay content (SUTHERLAND et al, 2018). These observations are confirmed by P-wave velocity (PWC), shown in figure 6, which remains below 1600 m/s from the top of core 16R to the depth of ~264,8m (end of MECO), compatible with a diatomite sediment. Then it spikes up and remains high, although variable, above 1600 m/s until the depth of about 166,4 (beginning of the MECO) and then drop again until the end of the core. The decrease in diatoms content, sediments would have caused the clayey sediment to undergo compaction with an increase in bulk density, a decrease in porosity and a decrease in sedimentation rate.

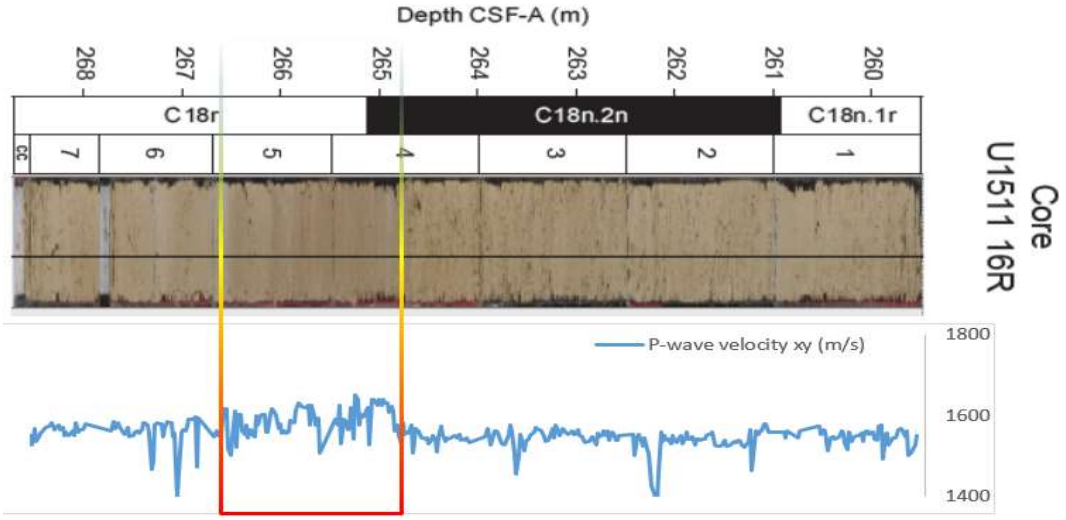


**Fig. 6: P-wave velocity results**

### *4.4.2. Magnetic properties*

Magnetic Susceptibility (MS) analysed by the IODP 371 expedition (fig. 7) clearly demonstrates an anomaly during the MECO interval and one high peak after it. Being a ferrimagnetic material, an increase in biogenic magnetite content in the sediment would cause an increase in MS (Harasko et al., 1993). FORCs measurements confirm the presence of MTB in the MECO interval (Fig.8).

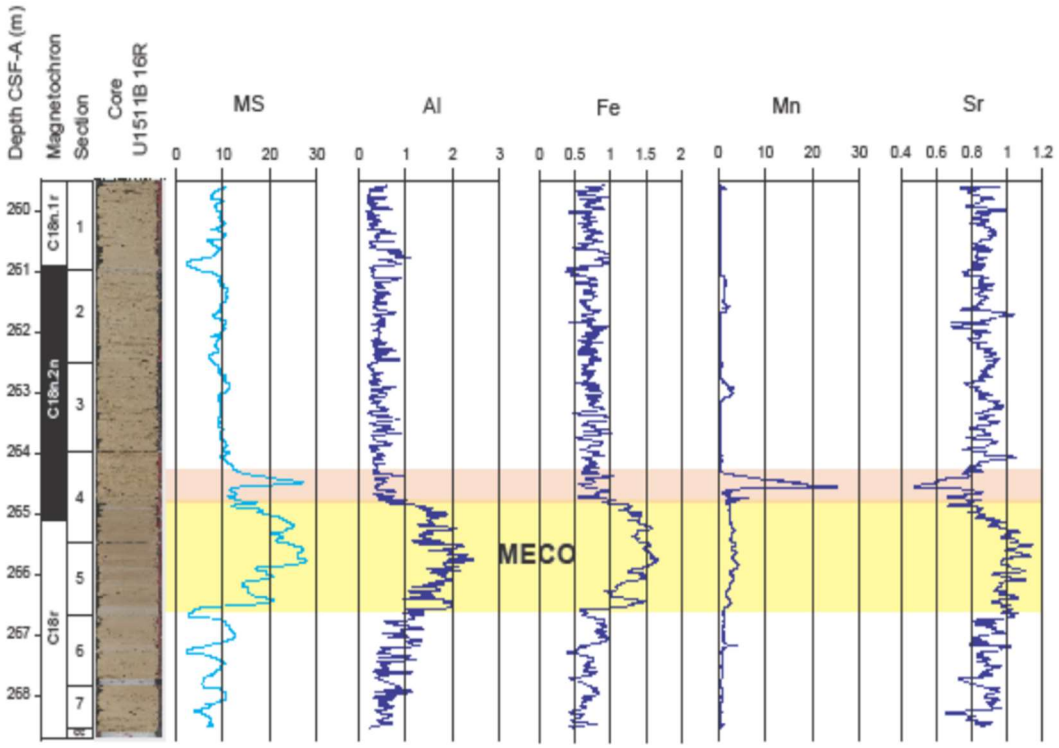


**Fig. 7: Litho- and magnetostratigraphy, Magnetic Susceptibility (MS), and main elements abundance analysed by XRF of core U1511B16R. The MECO interval is highlighted in yellow and the Mn anomaly just above it is highlighted in red. Litho- and magnetostratigraphy and MS from SUTHERLAND et al. (2019)**

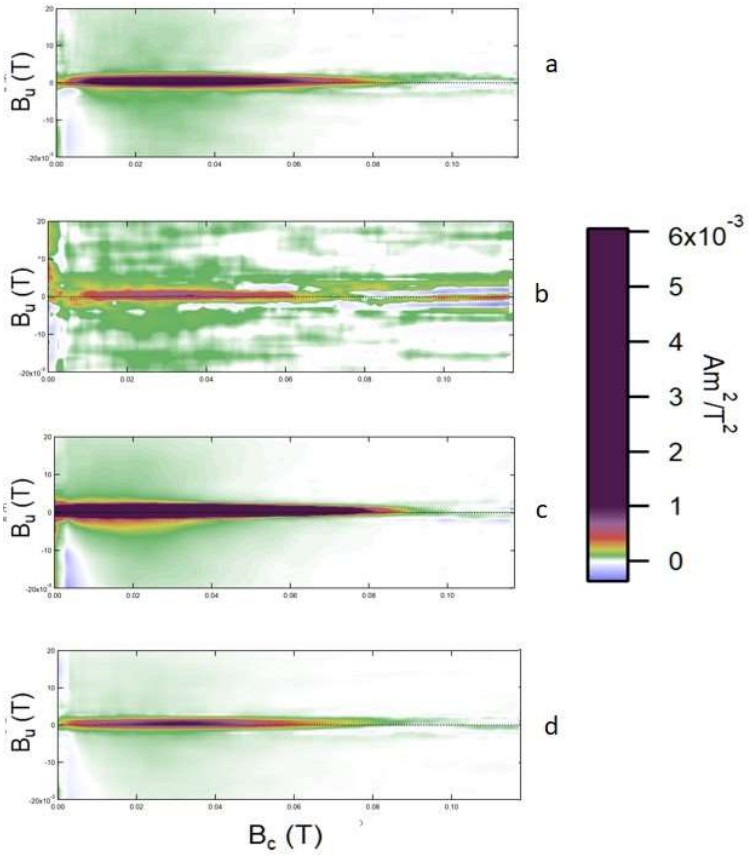


**Fig. 8: FORCs measurements for core U1511B-16: a) 262,4 mbsf; b) 262,6 mbsf; c) 265,66 mbsf; d) 267,66 mbsf.**

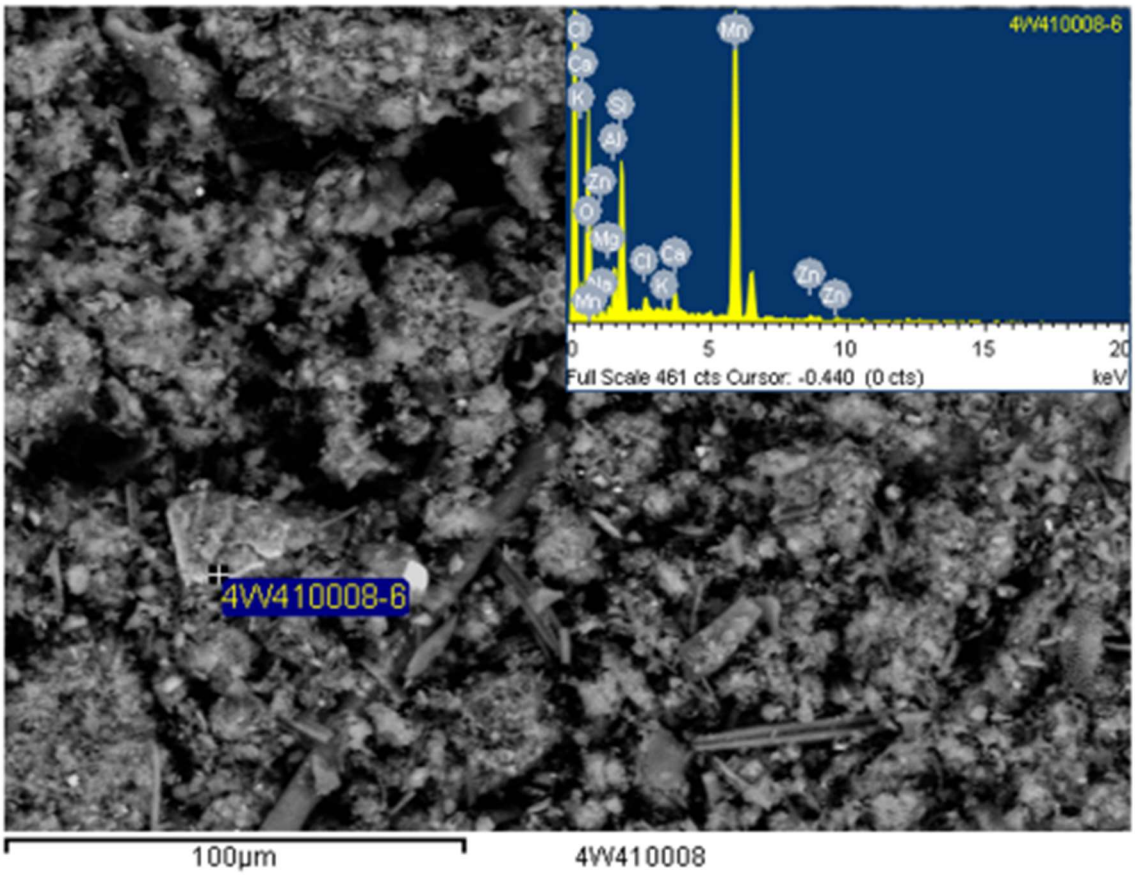


**Fig. 9: SEM-EDS results for Mn rich granules in sample 16R_4W_41-42 (264.4 mbsf).**

*4.4.3. SEM-EDS*

SEM-EDS analysis shows that the samples contain biogenic silica and clay minerals, rich in Si, Al, Na, and Cl. The red and black grains observed at optical microscope, result rich in Fe and Mn, respectively. Besides, the Mn-rich black grains contain also significant Ca and K (Fig. 9).

*4.4.4. XRF*

XRF-scanner data show a change in chemical composition in the 266.5-264.8 mbsf interval, which corresponds to the stratigraphic position of the MECO (fig. 9 and 10). All the detrital elements (Al, Ti, Fe, K, and Si) increase, whereas Cl decreases, and Ca and Sr display various fluctuations. Of particular interest is Mn, which shows a slight increase within this interval and a prominent peak just above it encompassing several cm. The detrital elements increase and the overlying peak of Mn are also concomitant with high values of MS (fig.10).

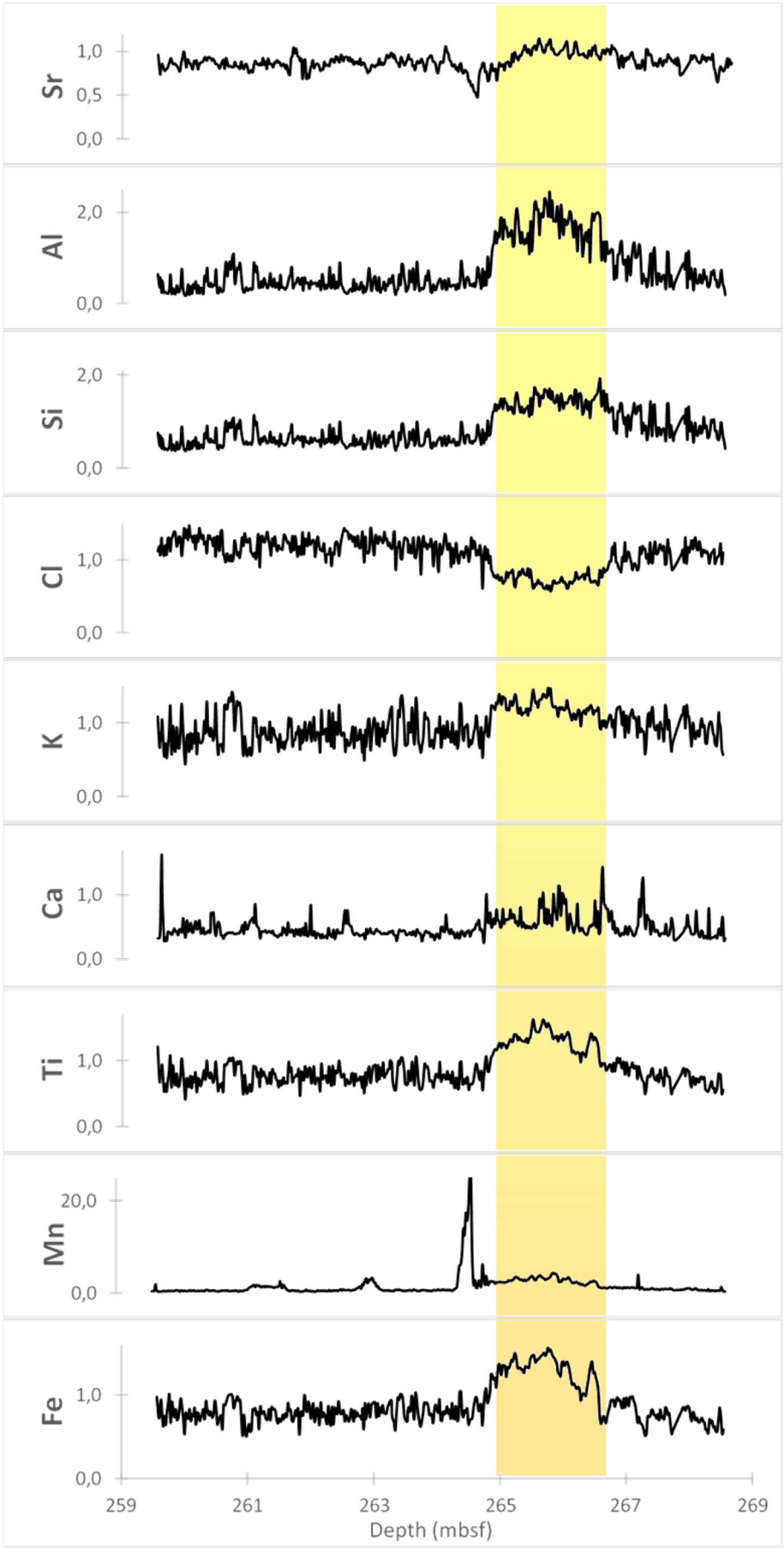


**Fig. 10: XRF results for the main elemental composition of core U1511B_16R. The abundance of each element has been normalized to the mean value of the same element for the whole core. The yellow band shows the MECO interval. XRF analyses show a general increase of all elements in the MECO interval but Sr and Cl. Sr abundance in this interval does not display an appreciable variation. Cl is related with halite at this site which precipitate from seawater in sediment pores. The decrease in sediment porosity observed in the MECO interval is caused by the decrease biogenic silica sedimentation rate in this interval this causes the sediment to trap less seawater. Note that the prominent Mn positive peak corresponds to a negative peak of Sr, whereas other elements have no significant variations. This indicates that this Mn anomaly is not due to an increase of hydrothermal activity, but to a change in the environmental conditions at the bottom.**

*4.4.5. XRPD*

Bulk XRPD patterns of all the investigated samples show very sharp Bragg peaks of quartz at d-spacing (Å)(hkl) of 4.26(100), 3.34(011), 2.13(200), 1.82(112),) (ICDD ID number 00-046-1045) and of halite at d-spacing (Å)(hkl) of 3.25(111), 2.82(200), 1.99(202), 1.63(222) (ICDD ID number 00-005-0628) and broad peaks due to clay minerals (fig. 11a). In order to better characterize the clay phases, XRPD was performed on the clay fraction (fig. 11b), after vacuum solvation in ethylene glycol (fig. 11 c), and after 5 hours heating to 763 K (fig. 11d). In the clay fraction Illite, (main peaks at d-spacing (Å)(hkl) of 10.02(001), 4.47(110), 3.57(-112), 3.34(022), 2.86(-113), 2.56(200) (ICDD ID number 00-043-0685)) and kaolinite (main peaks at d-spacing (Å)(hkl) of 7.16(001), 3.57 (002), 2.34(20-2) (ICDD ID number 00-029-1488)) were recognized (figure 11b). The ethylene glycol solvation does not affect the peaks position of illite and kaolinite while, the broad peak at a d-spacing around 15 Å shifts to ~17.3 Å (figure 11c). Finally, this peak shifts to 10.23 Å when the samples were heated to 490°C because of the loss of interlayer water (figure 11d). All these features allow to recognize a mineral from the smectite group. Despite EDS data show micrometric Mn/Fe-rich grains, no Bragg peaks related to Mn/Fe phases has been detected in the diffraction patterns.

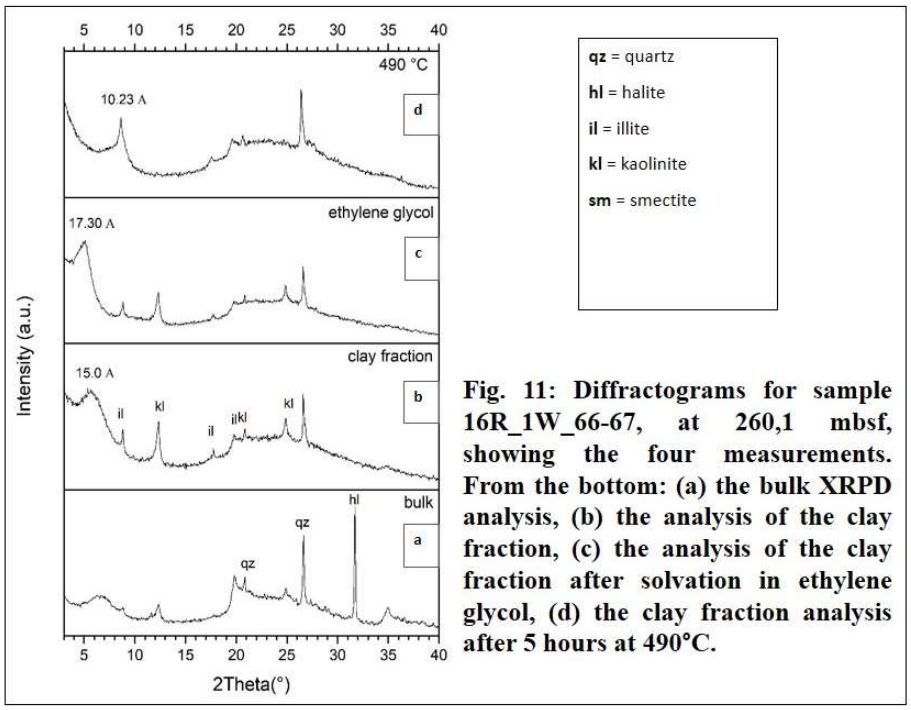


**Fig. 11: Diffractograms for sample 16R_1W_66-67, at 260,1 mbsf, showing the four measurements. From the bottom: (a) the bulk XRPD analysis, (b) the analysis of the clay fraction, (c) the analysis of the clay fraction after solvation in ethylene glycol, (d) the clay fraction analysis after 5 hours at 490°C.**

A distinct change in clay minerals assemblage occurs in the 266.57-264.85 mbsf interval, with a relative increase of the signal of smectite respect to the other minerals (see fig. 12)

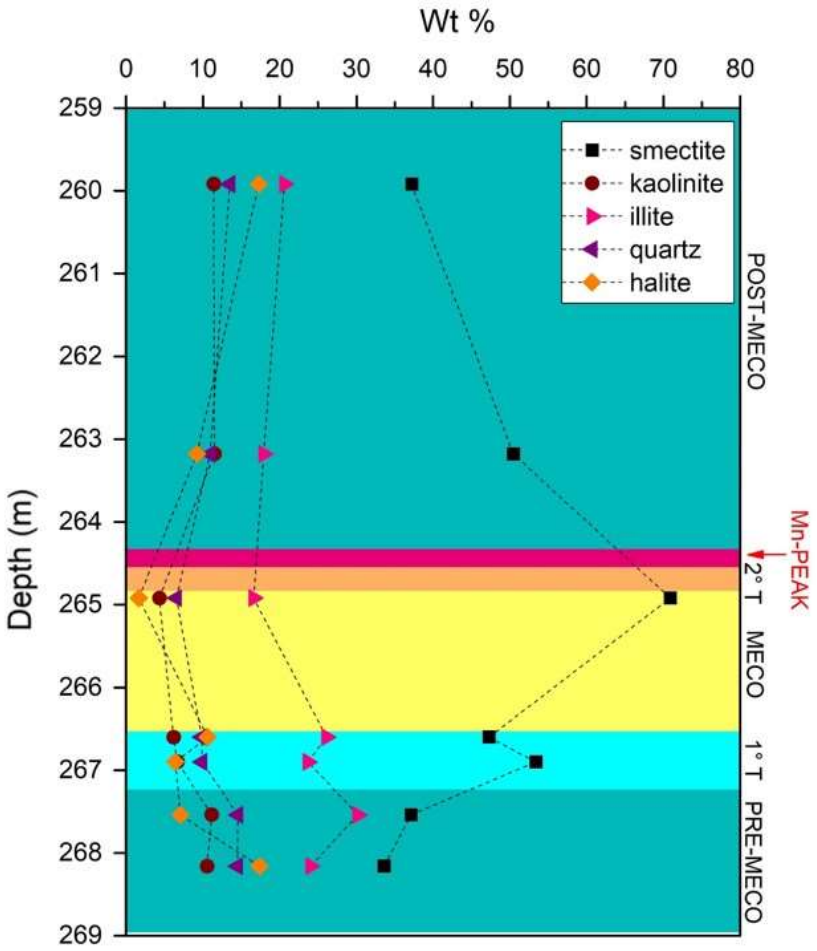


**Fig. 12: Conventional XRD results from the IODP Core U1511B_16R.**

*4.4.6. FT-IR*

FT-IR investigation further confirms the absence of carbonate minerals as recognized by XRPD. Indeed, no absorption bands were detected around 1450 $cm^{-1}$. All collected spectra show bands at 470, 536, 912, 1041, 1083, 1631, 3430, 3619 and 3698 $cm^{-1}$ and a shoulder at around 433 $cm^{-1}$ due to the presence of clay minerals (kaolinite and smectite) (CHUKANOV, 2014). Bands at 1083, 798 and 696 allow the detection of quartz (CHUKANOV, 2014). In the MECO samples red grains suggest the presence of poor-crystalline Fe-oxides not detectable by X-ray diffraction. The absorption band at 536 and the shoulder at 433 $cm^{-1}$ suggest the presence of hematite (CHUKANOV, 2014) (fig. 13).

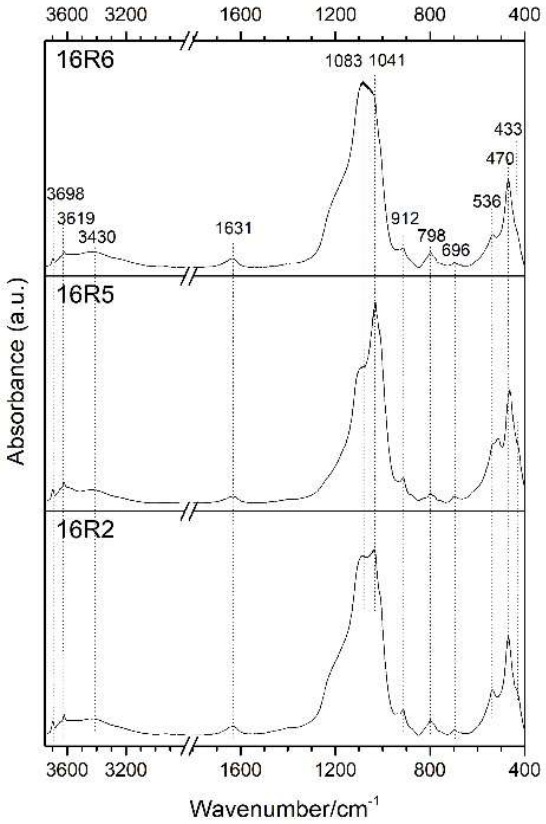


**Fig. 13: FT-IR spectra of the samples 16R_6W_69-70 (at 267.4 mbsf), 16R_5W_16-17 (265,6 mbsf), 16R_2W_16-17 (261,1 mbsf).**

*4.4.7. Raman Spectroscopy*

To characterize the micrometric black and red grains, selected samples were investigated by Raman spectroscopy. Spectra collected on black grains show a strong and wide band at around 635 $cm^{-1}$, and weak bands at 247, 290, 345, and 419 $cm^{-1}$ (fig. 14). Bands at 290, 343 and 635 $cm^{-1}$ represent Mn oxides, and can be assigned either to ranciéite $[(Ca,Mn^{2+},K,Ba)(Mn^{4+},Mn^{3+})_4O_9 \cdot nH_2O]$ (BERNARDINI et al., 2019; FAN et al., 2015), todorokite $[(Ca,Na,K)(Mn^{4+},Mn^{3+})_6O_{12} \cdot nH_2O]$, or cryptomelane $[K(Mn^{4+}{}_7,Mn^{3+})O_{16}]$ (BERNARDINI et. Al. 2019). Since SEM-EDS shows the presence of Ca and K associated with Mn, it is not possible to exclude the presence of any of these phases. Spectra collected on the red grains show the presence of hematite (DE FARIA et al., 2007) (fig. 15), Titanium dioxides are also recognized, especially brookite (ILIEV et al., 2013 ) and anatase (BALACHANDRAN et al., 1982), as well as traces of gypsum [Ca(SO4)•2H2O] (see fig.16).

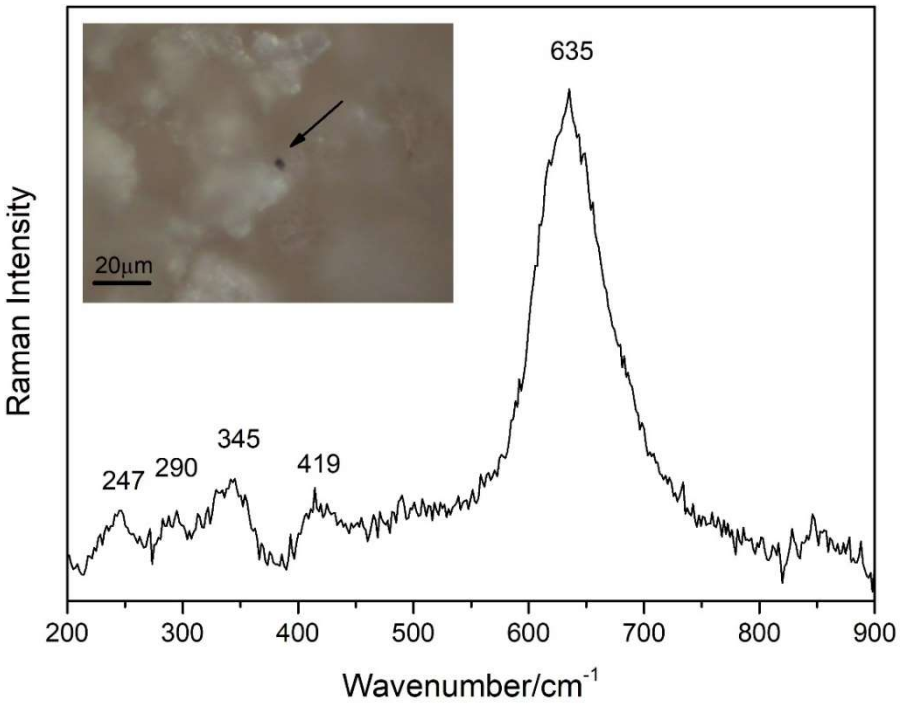


**Figure 14: Raman spectrum of a black Mn-rich grain in sample 16R_5W_16-17 (265,6 mbsf). Spectrum collected at λ = 532 nm.**

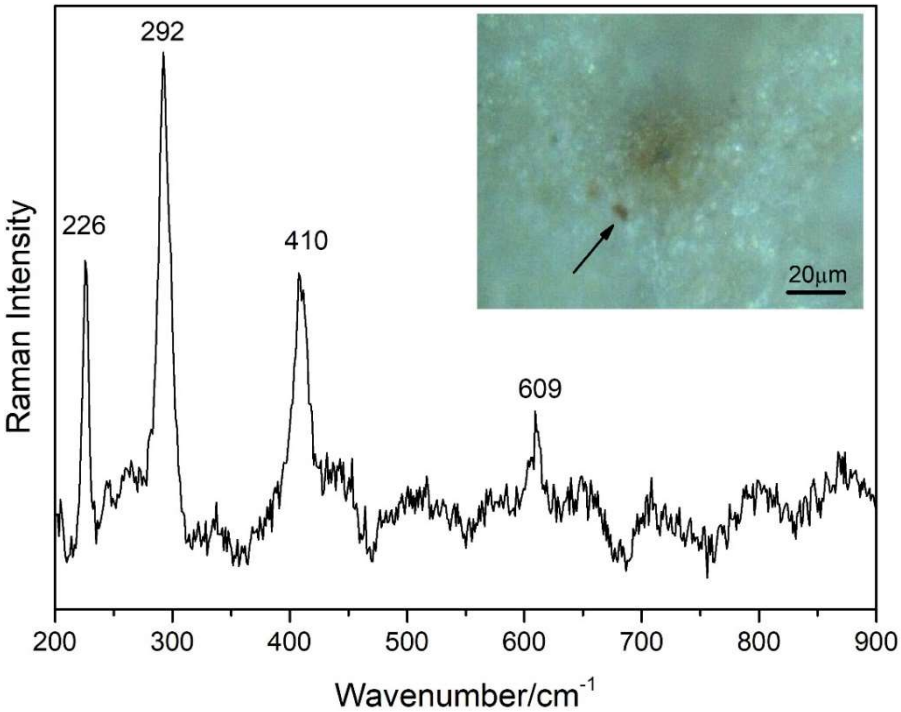


**Figure 15: Raman spectrum of a red Fe-rich grain in sample 16R_4W_41-42 (264.4 mbsf). Spectrum collected at λ = 532 nm**

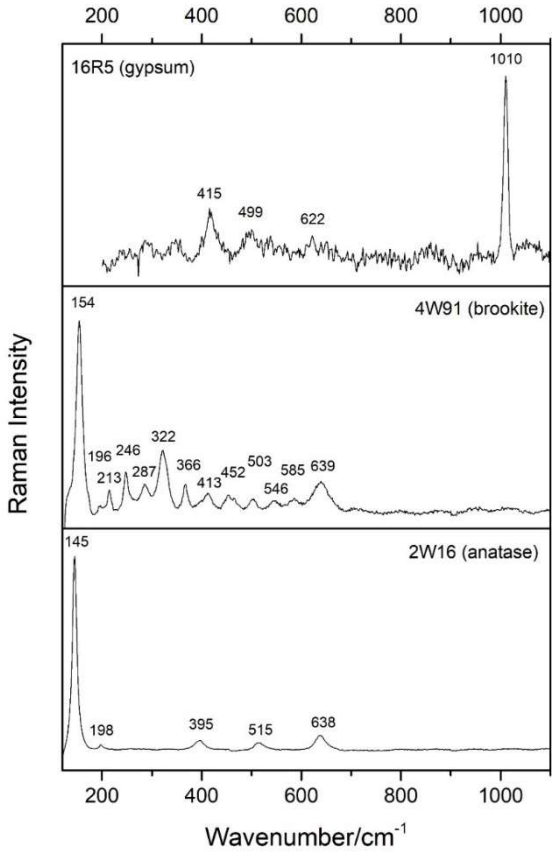


**Figure 16: Raman spectra of gypsum and Ti-oxides. Spectra collected at λ = 532 nm in samples 16R_5W_16-17 (265,6 mbsf), 16R_4W_41-42 (264,4 mbsf), 16R_2W_16-17 (261,1 mbsf)**

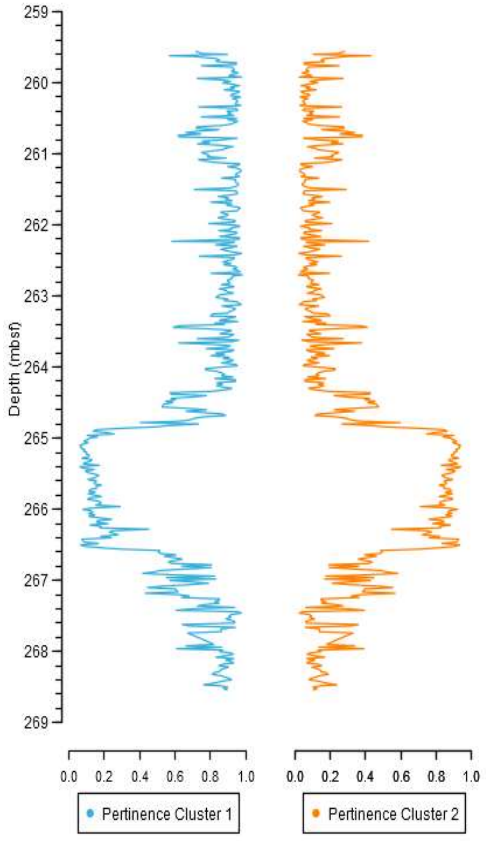


**Figure 17: Cluster pertinence values obtained by the fuzzy c-means algorithm (BEZDEK et al., 1984) for XRF data (Zn, Sr, Al, Si, Cl, K, Ca, Ti, Mn and Fe), Magnetic Susceptibility and reflectance values. Pertinence values show a distinct separate cluster between ~264,8 and 266,6 mbsf.**

*4.4.8. Statistical results*

*Partitioning Cluster Analysis (PCA):* Two major clusters were identified in the dataset, being cluster 1 dominant in the intervals 268.5-266.8 mbsf and 264.8-259.5 mbsf, and cluster 2 limited within the interval between 266.8-264.8 mbsf. Transition intervals occur before and after the cluster 2 interval, (Fig. 17).

*Hierarchical Cluster Analysis (HAC):* Two superclusters subdivided into 6 clusters and two outsiders were identified as follows (fig. 18):

Supercluster A:

- **Cluster 1** (C1) contains all and exclusively the samples from within 264.91-266.41- mbsf, characterized by a relative increase in smectite respect to the other minerals (fig. 12).
- **Cluster 2** (C2) is composed by the first sample above the C1 interval (264.66 mbsf) and a sample at 261.9 mbsf.

**Outsider** at 264.16 mbsf.

Supercluster B:

- **Cluster 3** (C3) is the largest group of values and includes samples from below and above the C1 interval.
- **Cluster 4** (C4) composed only by samples from within 259.66- 260.69 mbsf
- **Cluster 5** (C5) contains the three samples right below the C1 interval (266.65-167.15 mbsf)
- **Cluster 6** (C6) includes the samples at 262.4 and 268.44 mbsf.

**Outsider** at 261.26m.

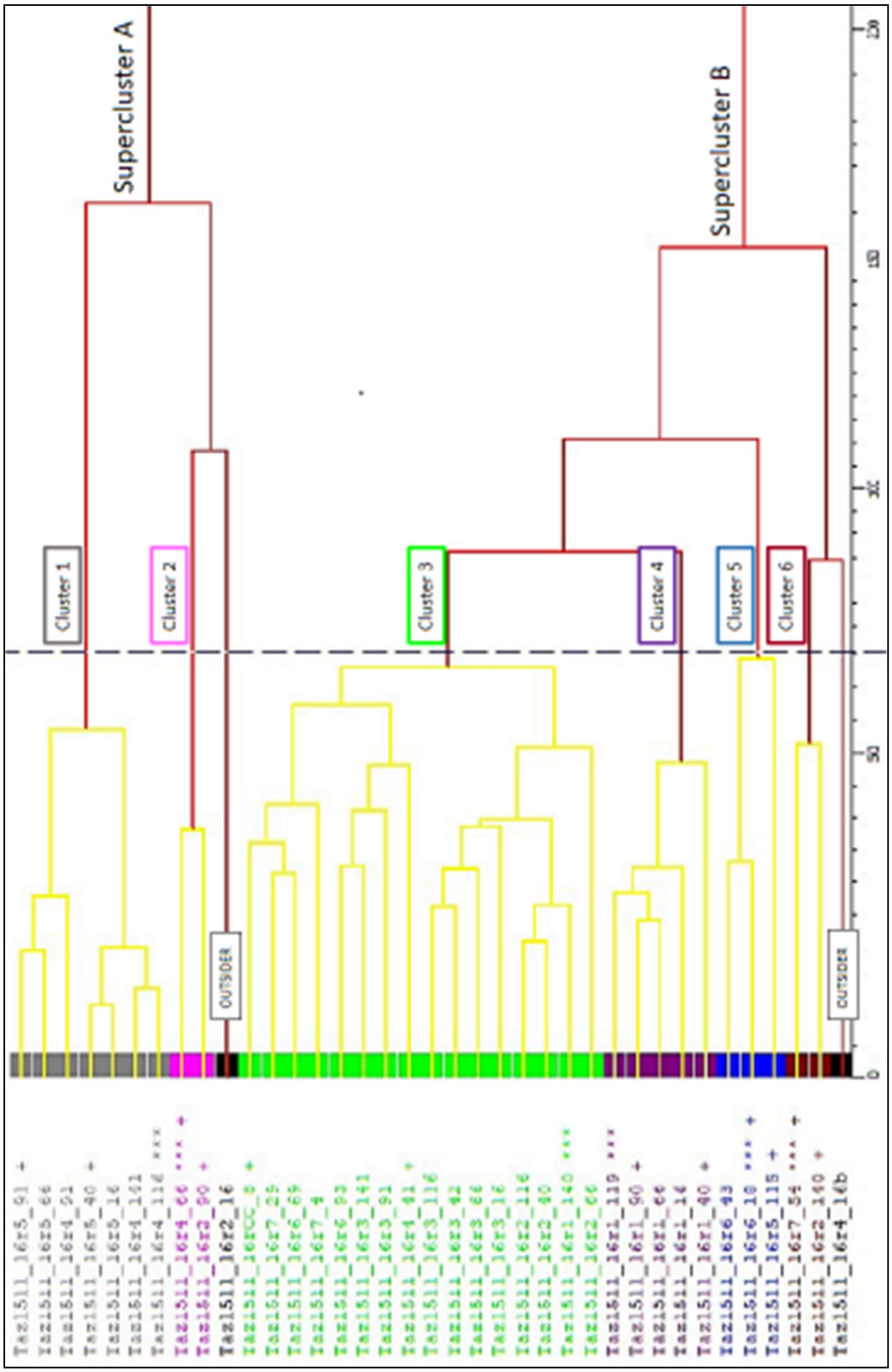


**Fig. 18: Dendrogram for the hierarchical cluster analysis. The samples' names are on the left the six clusters identified by HAC are in the center, and the superclusters A and B are on the right. Three asterisks (***) mark the most representative samples of each cluster.**

*K-mean cluster analysis* was conducted on four clusters, determined by integrating the results of previous cluster analyses. The mean value identified for each cluster is reported in table 1.

| | Sr | Al | Si | Cl | K | Ca | Ti | Mn | Fe | MS |
|---|---|---|---|---|---|---|---|---|---|---|
| **cluster_0** | 94,35 | 155,27 | 132,11 | 78,74 | 118,82 | 62,49 | 125,05 | 319,70 | 125,97 | 19,63 |
| **cluster_1** | 86,84 | 43,18 | 62,06 | 118,89 | 85,65 | 43,18 | 73,79 | 63,81 | 76,18 | 8,77 |
| **cluster_2** | 88,72 | 78,82 | 94,32 | 106,21 | 98,58 | 51,51 | 86,21 | 140,03 | 84,51 | 9,92 |
| **cluster_3** | 56,44 | 47,04 | 62,15 | 113,12 | 82,92 | 42,23 | 66,00 | 1832,19 | 74,24 | 22,37 |

**Table 1: k-means values**

*Pearson correlation:* A strong direct correlation occurs between Al, Si, Fe, K, and Ti, and between Cl and S, whereas Cl is anti-correlated with Si and Al. Mn, Ca, and Sr have no correlation with any element. This method was applied to each of the six stratigraphic intervals identified by the cluster analyses and showed that the correlation coefficients change significantly from within to outside the MECO interval (fig. 19).

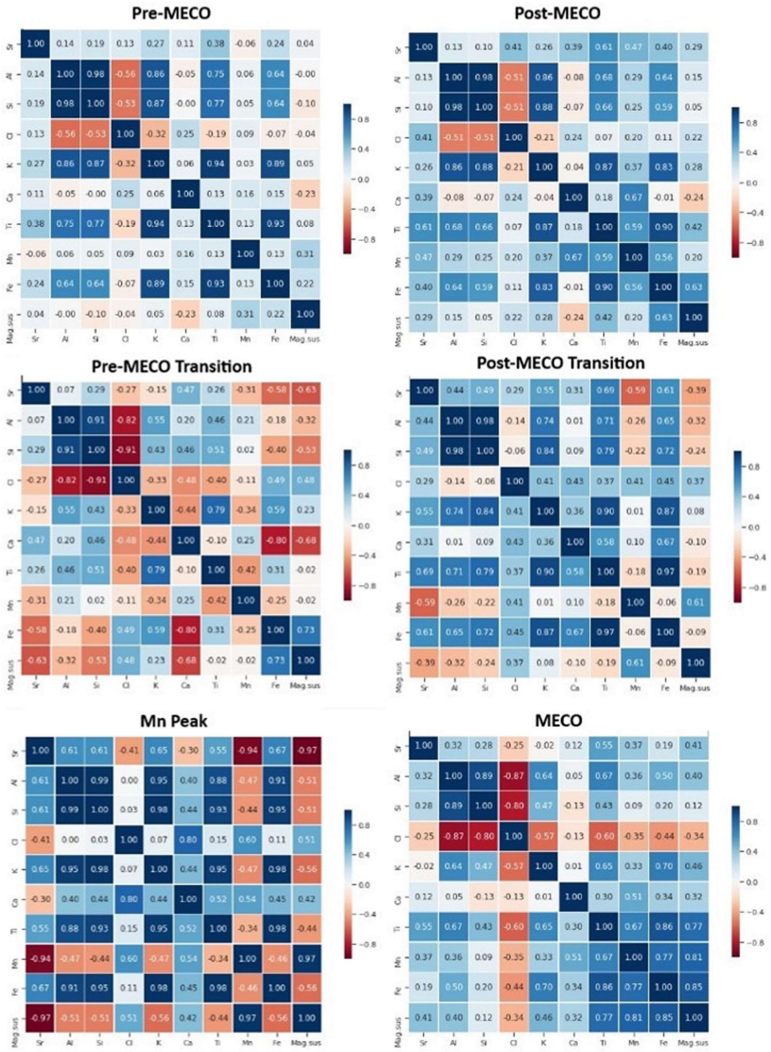


**Fig. 19: Pearson correlation for the main elements (Sr, Al, Si, Cl, K, Ca, Ti, Mn, Fe) and MS in the six identified stratigraphic intervals.**

## *4.5. Discussion*

### *4.5.1. Middle Eocene paleoceanographic changes over the TAP*

The MECO event is defined according to the negative oxygen isotope anomaly at the base of the paleomagnetic Chron C18n (BOHATY et al., 2009). Therefore it has been characterized mainly in pelagic carbonate successions deposited at bathyal depths, yielding well-preserved carbonate for stable isotopes measurements. Recognizing this event in successions devoid of carbonate, such as those below the CCD, is challenging. In the IODP Core U1511B the MECO is clearly recognizable thanks to the magneto-bio stratigraphy and the MS anomaly, and this represents a unique opportunity to study this event in an abyssal setting. The combination of the results of the different cluster analyses allows us to identify six stratigraphic intervals that show how the paleoceanographic conditions changed over the TAP in response to the MECO event (Fig. 19):

1. PRE-MECO (268.54-267.21 mbsf): Consists mainly of radiolarian and diatoms, with smectite (30-40%), illite (20-30%), quartz (15-20%), and kaolinite (10-15%). All the terrigenous elements (Al, Ti, Fe and K) are directly correlated, whereas Cl is anti-correlated with Si and Al. Mn correlates moderately with Fe and poorly with MS. K-means show generally low MS and low counts for all the elements but Cl. This interval represents conditions with a stable circulation and a well-mixed water column, supplying oxygen at the bottom and nutrients at the surface, stimulating the productivity of bio-siliceous organisms.
2. PRE-MECO TRANSITION (267.21-266.57 mbsf): This is a 0.66 m thick interval, corresponding to ~66 kyr, considering the sedimentation rate of SUTHERLAND et Al. (2019). Smectite, which represents 40-50% of the non-biogenic fraction, starts increasing, whereas all the other minerals decrease. Trends of chemical elements change significantly, as Sr decreases whereas MS and all detrital elements start increasing. This expresses a lowering biogenic silica input and consequent increase in clay fraction that gets less diluted, representing the beginning of a change in the paleoceanographic conditions over the TAP towards the MECO scenario.
3. MECO (266.57-264.85 mbsf): Consists of 1.72 m of clay with biosilica, which is significantly less abundant than in the former intervals, and consists of sponge spicules and few radiolarians (SUTHERLAND et Al. 2019). This indicates a decrease in the planktonic biosiliceous productivity at the surface (diatoms and radiolarians), leaving only the contribution of the sponge spicules, delivered from shallower benthic environments. This change in sediment composition is confirmed by the increasing

trend of all detrital elements and MS, indicating less dilution of the terrigenous fraction. Moreover, physical properties show higher sediment density, reflecting the drop of the porous biosiliceous fragments and the consequent increase of clays, which are more compactable (SUTHERLAND et Al 2019). This change induces also a decrease in sedimentation rate, explaining why, by applying the value of 10 m/Myr estimated by SUTHERLAND et al. (2019);, the duration of the MECO at this site results 172 kyr, instead of ~500 kyr observed in most of the records (e.g. BOHATY et al., 2009; GIORGIONI et al., 2019). An important change occurs also in the clays composition, with smectite increasing up to 70% and illite decreasing down to 20% (fig.12) as is clearly shown by the diffractograms (see fig. 20). The major increase in smectite within the MECO interval and the significant lowering in the biogenic input expresses a change in sediment source due to bottom currents modifications. This evidence indicates a strong change in the paleoceanographic conditions over the TAP during the MECO event, with a more stratified water column and consequent decrease in biosiliceous productivity at the surface.

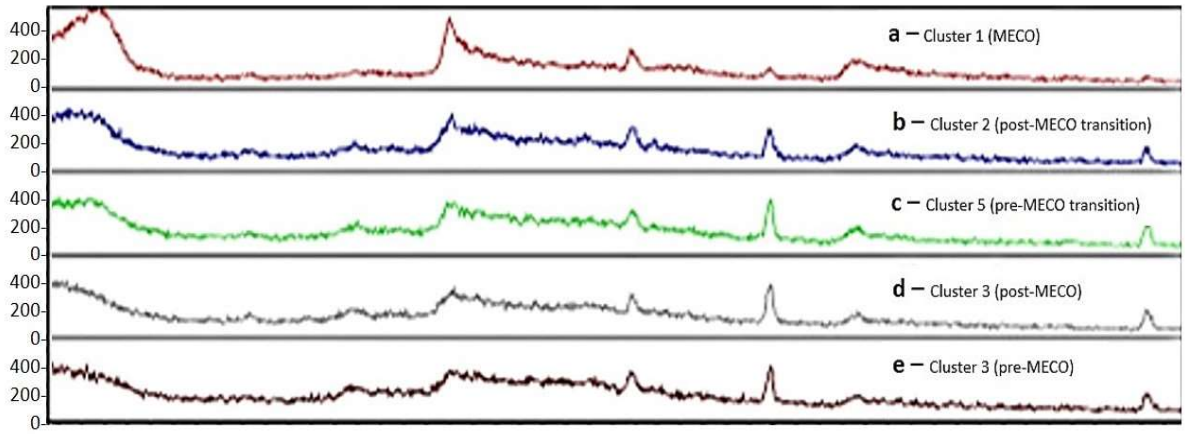


**Fig. 20: comparison of diffractograms for the most representative sample for different clusters of the HAC. (a) sample at 265,26 mbsf within the MECO interval classified in C1 with the characteristic peak of the expansive clays at low theta degrees; (b) sample from the post-MECO transition at 264,68 mbsf classified as C2; (c) sample from the pre-MECO transition at 266,66 mbsf classified in C5; (d) sample from the post-MECO interval at 262,64 mbsf classified in C3; (e) a sample from the pre-MECO interval at 267,62 mbsf classified in C3.**

4. POST-MECO TRANSITION (264.85-264.57 mbsf): After the MECO there is a brief transition of ~28 kyr, with decreasing smectite respect to illite and other minerals. In this interval all the elements shift back to Pre-MECO values, except for Mn, which presents a highly fluctuating trend. K-means and Pearson correlation results also agree with this evidence. These conditions are limited to a particularly thin interval above the MECO, indicating that the end of the typical MECO conditions on the TAP was rather

abrupt. By comparing it with the pre-MECO transition, it took twice longer to force the system into the MECO scenario than to switch it back.

5. MANGANESE PEAK (264.57-264.33 mbsf): A prominent Mn peak occurs in a 24 kyr long interval, 28 kyr after the end of the MECO. K-means Mn values here are six times higher than in the MECO and 29 times higher than in the Pre-MECO intervals. Alongside Mn, only Sr changes and shows a negative peak (Fig. 10). It is worth noting the lack of correlation between Mn and Fe, which, instead, are tightly correlated in the other intervals, being both linked to oxide phases (fig. 14-16). Therefore, the Mn peak is not due to an increase in hydrothermal activity, because, in this case, a concomitant increase in Fe and Sr would be expected. MS also increases and is strictly correlated with Mn (fig. 10 and 19). As the MS signal is mainly biogenic in this record, as confirmed by the FORCs measurements, such correlation may reflect a Mn rich environment that forces this element into the biogenic magnetic crystals. Recent studies demonstrate that magnetotactic bacteria can incorporate small but significant amounts of Mn, if they grow in an environment where this element is abundant (KEIM et al., 2009, TANAKA et al., 2012; PROZOROV et al., 2014).
6. POST-MECO (164.33-262.90): This interval is represented by the same cluster assemblage as the Pre-MECO, and all Pearson values are also very similar. This indicates the complete restoration of Pre-MECO environmental conditions after the MECO perturbation.

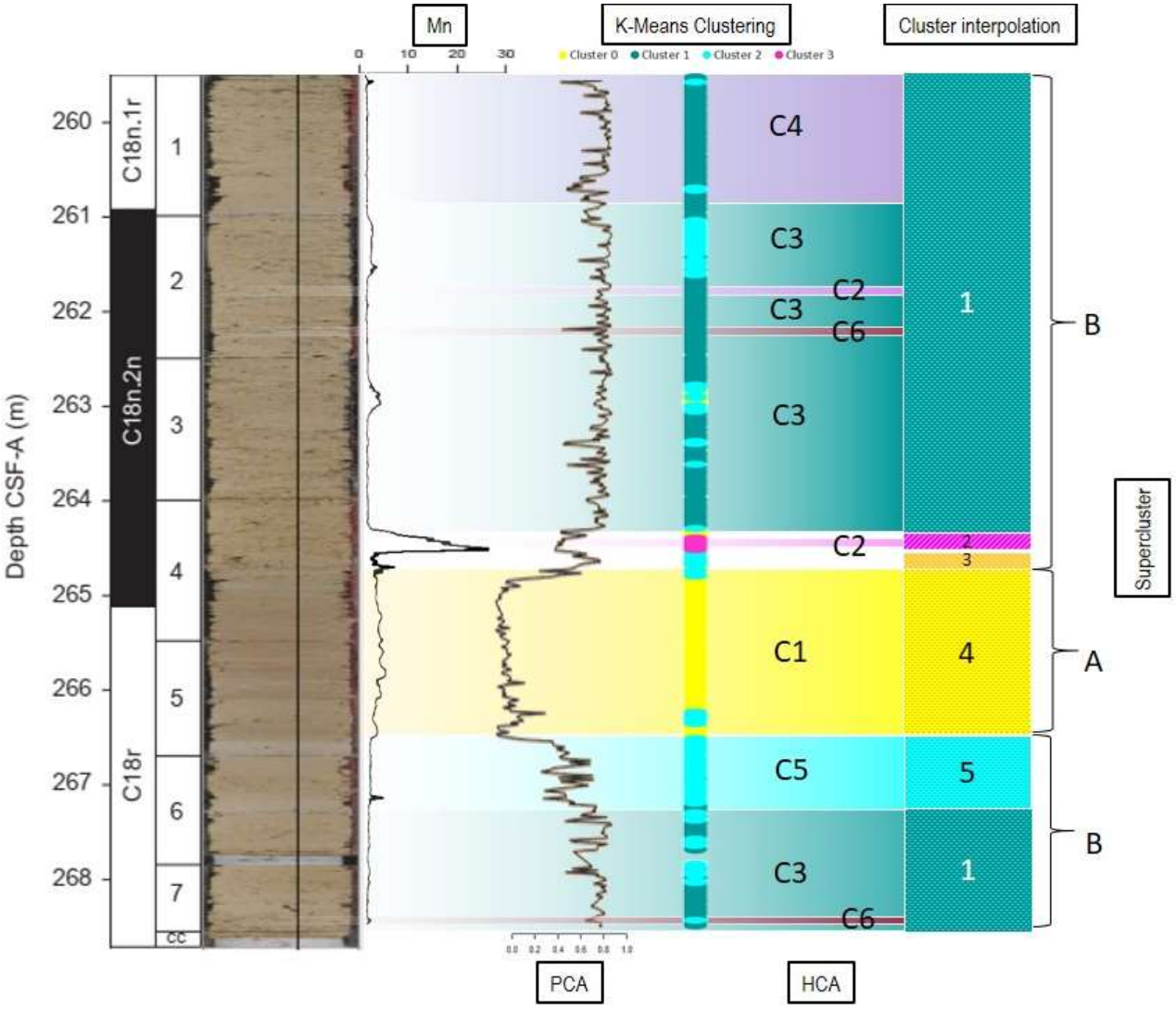


**Fig. 21: Summary figure for statistical analyses and interpolated cluster subdivision**

*4.5.2. MECO abyssal oceanographic response*

The variations described allow us to create a model of the changing conditions at the bottom of the TAP during the middle Eocene (fig. 22). SUTHERLAND et al. (2019) observed that Mn is abundant throughout the entire IODP Core U1511B, as testified by several rhodochrosite nodules and high Mn content in pore waters. Mn can be delivered to this site by hydrothermal fluids, which reach the TAP since its formation, in the Late Cretaceous (GAINA et al., 1998; SUTHERLAND, 1999). However, no nodule or any other macroscopic Mn-bearing diagenetic feature occurs throughout the core U1511B-16R, therefore, the Mn peak is related to an increase in the micrometric Mn oxides, recognized with Raman spectroscopy. Ranciéite was detected, although todorokite and cryptomelane cannot be excluded. The average valence of Mn is close to 4 in ranciéite, 3.7 in cryptomelane, and 3.9 in todorokite (CHALMIN et al., 2009). We also detected hematite, in which Fe occurs as $Fe^{3+}$. Such high Mn and Fe oxidation states suggest

relatively well oxygenate bottom waters at the time of the minerals' formation. Besides, todorokite could be related to biological processes (MANDERNACK et al., 1995).

Mn solubility in seawater is controlled by redox potential and pH, being more soluble in reducing or acidic waters (CALVERT & PEDERSEN, 1993 and 1996). Since minerals with highly oxidized Mn occur within the MECO interval, a shift to reducing conditions during this event can be excluded. Therefore, the Mn record can be explained with relatively well-oxygenated bottom water that during the MECO became acidic, and thus got enriched in dissolved Mn. When the pH increased again, after the end of the MECO, induced the sudden precipitation of the dissolved Mn, testified by the Mn anomaly. The lack of a correlation between Fe and Mn in the post-MECO transition and Mn peak intervals confirms this interpretation, since they are both sensitive to redox changes, but Fe is less influenced by pH (LANGMUIR, 1997; ROY, 1997). Therefore, Fe oxides precipitation persisted during the MECO, whereas most of the Mn remained dissolved. The slight increase in Mn content within the MECO interval can be attributed to the lower sedimentation rate, which concentrated the authigenic minerals. The tight correlation between Mn and MS within the MECO and Mn peak intervals suggests that Mn oxides precipitation could have also been catalysed by microbial activity, which increased during the MECO. Moreover, a larger amount of smectite respect to illite deposited onto the TAP during the MECO, this suggests a major re-arrangement in bottom water circulation, which created a more stratified water column and brought a new, more acid, water mass, which also delivered smectite to this region. This may also have intensified the bottom water flux and sediment winnowing, which decreased the sedimentation rate. Such major deep circulation changes represent the response of the complex oceanographic circulation of the SO to the MECO climatic warming (NELSON and COOKE, 2001; CRAMWICKEL et al., 2019).

Major circulation changes have been described in previous studies associated with the MECO climatic warming, at surface to bathyal depths (e.g. BOHATY et al., 2009; WARNAAR et al. 2009; BIJL et al., 2010; MOEBIUS et al., 2014; CRAMWICKEL et al 2019; GIORGIONI et al., 2019). Here we show that deep modifications occurred also in the abyssal circulation in the SO and show not only the link of the MECO with ocean acidification, identified by BOHATY et Al. (2009), but also that acidified waters reached abyssal depths. In order to acidify the ocean water it is necessary to add $CO_2$ into the system. However, a stratified water column and an efficient biologic pump are also required to acidify the deepest environments (MARINOV et Al., 2008). Such configuration in circulation could have maintained low pH and warming conditions for hundreds of thousand years, so explaining in part the conundrum related to this

event (SLUIJS et al., 2013). On the other hand, the source of carbon that triggered the acidification still remains uncertain and perhaps it is related to C-cycle instability induced by orbital forcing (GIORGIONI et Al., 2019). Even though the main trigger of the MECO is still unclear, we showed that oceanic circulation played a key role during this event.

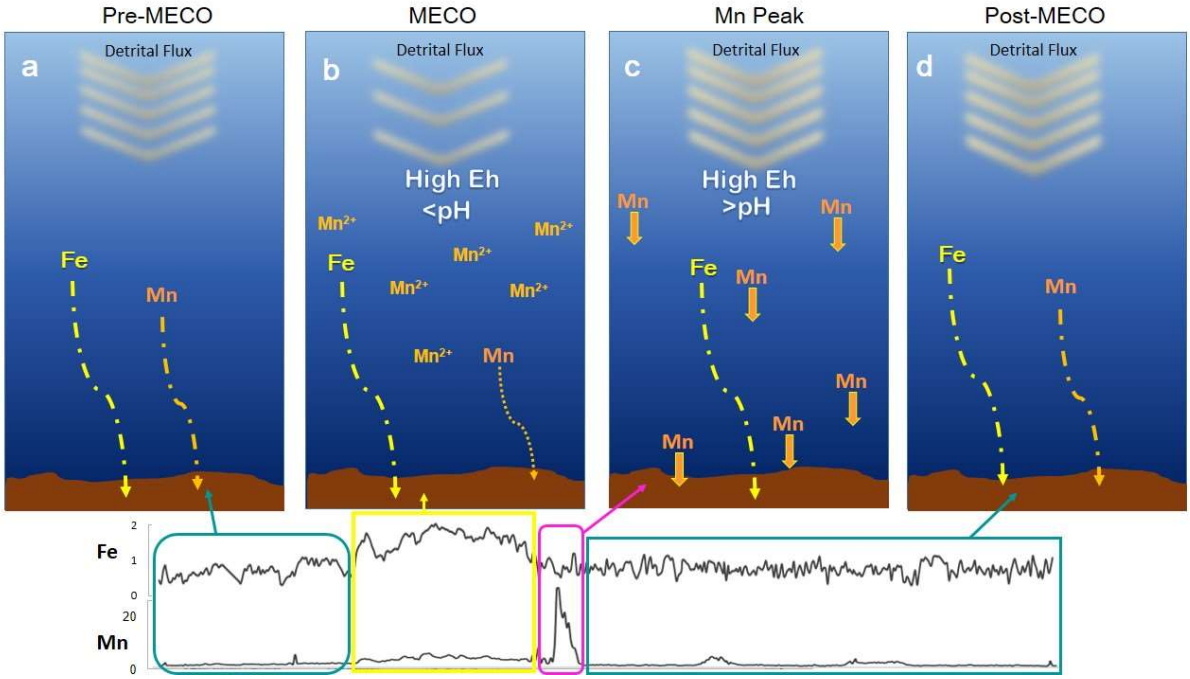


**Fig 22: Environmental Model showing the oceanic bottom conditions at the Tasman Plain during the middle Eocene, respect to the variation in Mn and Fe content between the water and the sediment.**

*4.5.3. MTB and their occurrence in the TAP*

The presence of MTB magnetofossils in core U1511B16R was identified and correlated with the MS variations along the core by Liao Chang (personal communication) and confirmed by FORCs measurements. During the MECO interval the signal of the MTB is higher than in the other intervals (see fig. 6) indicating that they were highly producing in this interval. This is in line with the studies that correlated the presence of MTB with warmer climates.

It is interesting to notice how in this core the signal of MTB and of MS are correlated and that the signal of Mn is correlated with MS. This could imply that the Mn is bound to the magnetic crystals produced by MTB and it might be first record of Mn-doped magnetosomes in the wild. Until some years ago, biogenic magnetite was considered to be always chemically pure, but recent studies demonstrate that MTB magnetosomes can incorporate a small, but significant quantity of other elements, especially Mn. MTB grown in environments with high concentration of Mn produce Mn-doped magnetosomes that have only slight (if any) macroscopic differences with the pure magnetite of the non-doped magnetosomes. Moreover MTB can live normally in

environments rich in Mn and poor in Fe without losing their ability of biosynthesize magnetite (KEIM et al. 2009, TANAKA et al., 2012; PROZOROV et al. 2014). In all these cited studies MTB cell growth seem to be unaffected by the presence of a high concentration of Mn and had a negligible effect on the number and size of magnetosomes.

Mn is bioavailable only in its dissolved form, therefore MTB living at the bottom during the MECO, as stated, were in an environment rich in dissolved Mn and could have absorbed Mn and biomineralized it in their crystals. At the end of the MECO, when the conditions at the bottom changed and were not that favourable anymore, the MTB community begun to suffer and die. This would explain why the Mn peak after the MECO is correlated to the MS peak: the magnetic signal in this interval is, at least partially, represented by a massive death of MTB that were highly producing during the MECO and that are dying in this interval causing a high sedimentation rate of the magnetofossils. The impossibility to identify Mn minerals with XRD implies that the Mn minerals crystals found in this interval are too small. We know that magnetosomes contain nanometric crystals not detectable by XRD, and it has been proved that MTB are able, in case of Mn-rich water, to produce in laboratory experiments Mn-doped magnetosomes (KEIM et al. 2009, TANAKA et al., 2012; PROZOROV et al. 2014). This could be the first record of naturally occurring Mn-doped magnetosomes, to test this hypothesis more studies should be conducted to characterize in detail the magnetofossils and their chemical composition.

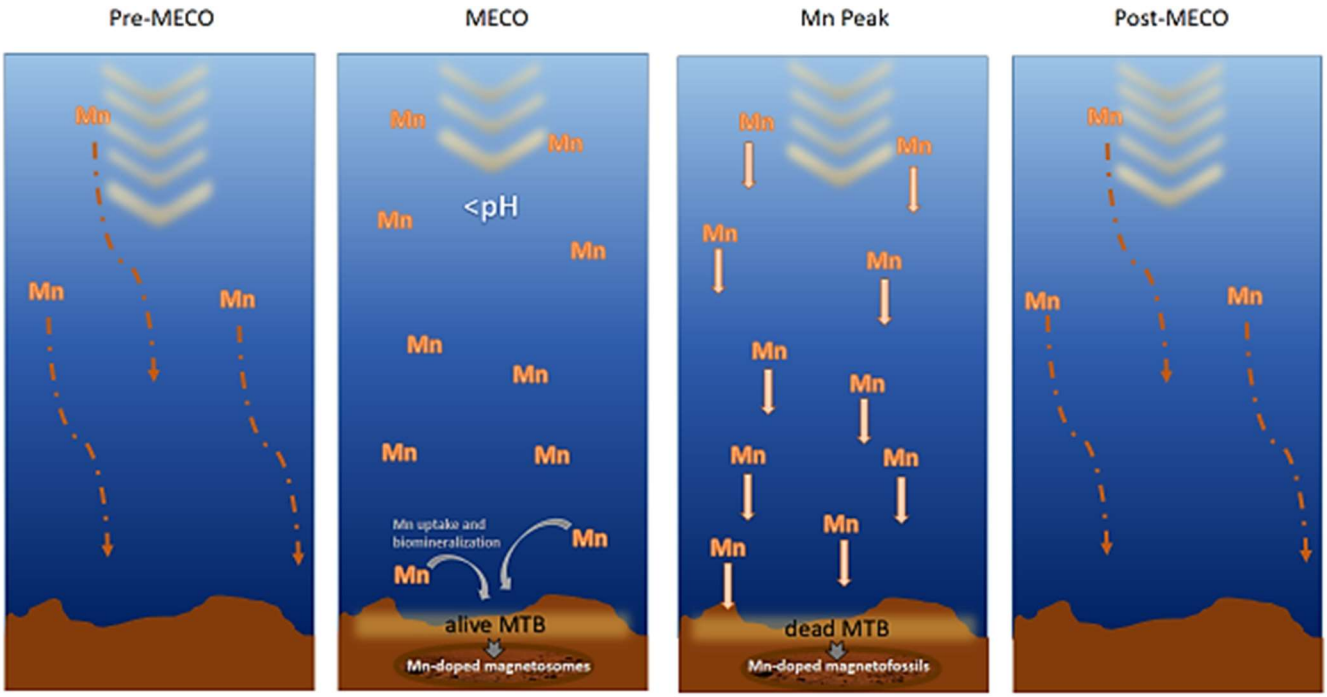


**Fig. 23: Environmental Model of the oceanic bottom conditions at the Tasman Plain during the middle Eocene, showing the possible interference of the MTB**

# 5 – CANANEIA: DIVERSIONS OF THE RIBEIRA RIVER FLOW AND THEIR INFLUENCE ON SEDIMENT SUPPLY

**This work produced an article published in Frontiers in Earth Sciences with the title: 'Diversions of the Ribeira River Flow and Their Influence on Sediment Supply in the Cananeia-Iguapé Estuarine-Lagoonal System (SE Brazil)' by Flaminia Cornaggia, Luigi Jovane, Luciano Alessandretti, Paulo Alves de Lima Ferreira, Rubens C. Lopes Figueira, Daniel Rodelli, Gláucia Bueno Benedetti Berbel and Elisabete S. Braga**
https://doi.org/10.3389/feart.2018.00025

***Abstract***

The Cananéia-Iguapé system is a combined estuarine-lagoonal sedimentary system, located along the SE coast of Brazil. It consists of a network of channels and islands oriented mainly parallel to the coast. About 165 years ago, an artificial channel, the Valo Grande, was opened in the northern part of this system to connect a major river of the region, the Ribeira River, to the estuarine-lagoon complex. The Valo Grande was closed with a dam and re-opened twice between 1978 and 1995, when it was finally left open. These openings and closures of the Valo Grande had a significant influence on the Cananéia-Iguapé system. In this study, we present mineralogical, chemical, paleomagnetic, and geochronological data from a sediment core collected at the southern end of the 50 km long lagoonal system showing how the phases of the opening and closure of the channel through time are expressed in the sedimentary record. Despite the homogeneity of the grain size and magnetic properties throughout the core, significant variations in the mineralogical composition showed the influence of the opening of the channel on the sediment supply. Less mature sediment, with lower quartz and halite and higher kaolinite, brucite, and franklinite, corresponded to periods when the Valo Grande was open. On the other hand, higher abundance of quartz and halite, as well as the disappearance of other detrital minerals, corresponded with periods of absence or closure of the channel, indicating a more sea-influenced depositional setting. This work represented an example of anthropogenic influence in a lagoonal-estuarine sedimentary system, which is a common context along the coast of Brazil. Here the signal of MTB was produced by living bacteria in the first few cm of the core, the low MTB production imply a non-optimal environment for MTB. It is not clear if the clay composition is the limiting factor.

### *5.1. Introduction*

The Cananéia–Iguapé estuarine-lagoonal system (Figure 24) is located in a large portion along the southern coast of the São Paulo State (Brazil), at latitude between 24°50′ and 25°40′ South and longitude between 47°20′ and 48°20′ West. This region is characterized by a group of four islands, separated by tide channels, coastal lagoons, little estuaries, and the Ribeira de Iguapé River that reaches the northern part of the hydrological system by the Valo Grande channel (SCHAEFFER-NOVELLI et al., 1990).

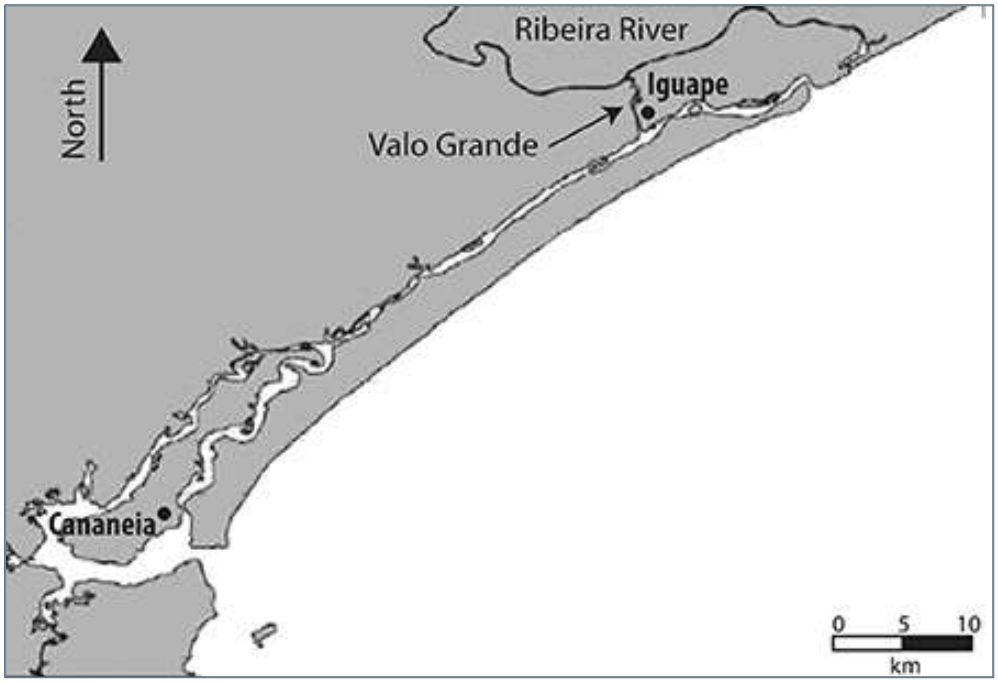


**Fig. 24: Map of the Cananeia-Iguapé System.**

The Ribeira River has the largest drainage basin of the S-SE Brazilian coast (from 22°S to 30°S), with an area of about 25,000 km$^2$ (BONETTI FILHO and de MIRANDA, 1997), with an annual average discharge of 773.56 m$^3$/s (BÉRGAMO, 2000). The outflow of the Ribeira River is strongly influenced by the subtropical climate and in its lower course varies from about 300 to more than 1,200 m$^3$/s (MAHIQUES et al., 2009; 2013).

The bedrock of the Cananéia-Iguapé Coastal Plain consists of a metamorphic basement of pre-Cambrian age. Different types of rock outcrop along the Ribeira River, such as quartzites, amphibolites, and green schists; intruded by granites, adamelites and granodiorites. Mesozoic intrusive alkaline rocks crosscut this basement complex and outcrop in various locations (RICCOMINI, 2017; de SOUZA et al., 1996). One of these outcrops forms the hill of São João (also called the Cananéia Alkaline Massif), in the municipality of Cananéia, which is the part of land closest to our core location. This hill is 137 m height and is surrounded by a coastal plain, filled with Pleistocene marine deposits (Cananéia Formation) and Holocene sediments of

beach and mangrove swamp environments (see Figure 25) (RICCOMINI, 1995; SUGUIO et al., 2003).

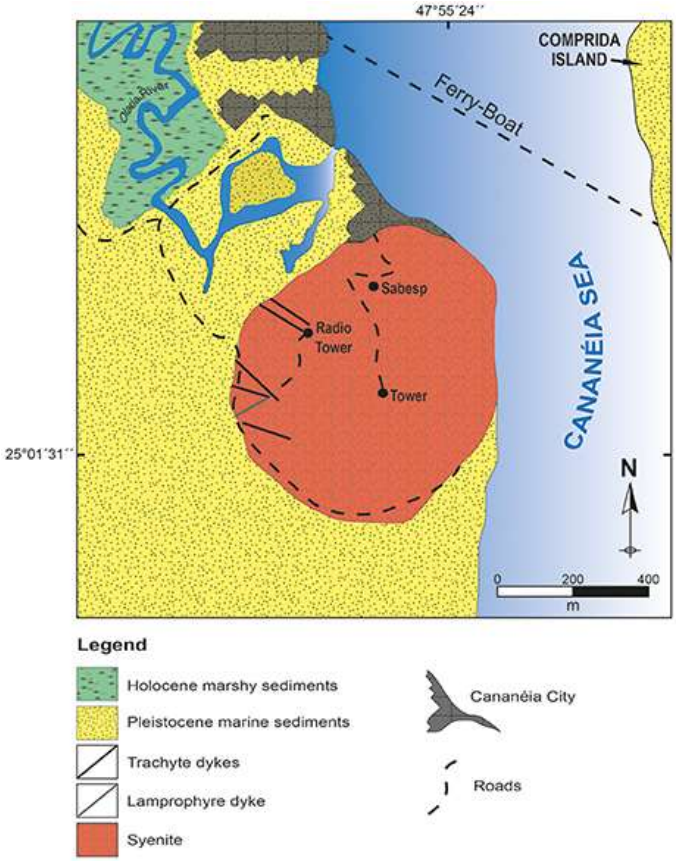


**Fig. 25: Geologic map of the Cananéia Alkaline Massif area (adapted from Riccomini, 1995 with permission).**

The Valo Grande is a 4 km long artificial channel connecting the Ribeira River to the Cananéia-Iguapé lagoon. It was excavated to facilitate the transportation of agricultural goods from the country lands to the harbor of Iguapé city, between 1827 and 1852 (GEOBRÁS FUNDACÕES, 1966; MAHIQUES et al., 2013). However, it began to be open to navigation in 1832 (Suguio and Petri, 1973). The channel was initially about 4.4 m wide and 2 m deep, but it quickly widened due to the high erosion produced by the strong stream. At the end of the XIX century, it was already wider than 100 m and deeper than 10 m (GEOBRÁS FUNDACÕES, 1966).

According to da Silva Teles (1998), prior to the opening of the Valo Grande channel the river discharge was minimal in the lagoon, which was controlled mainly by tidal fluctuations and coastal currents. Since the opening of the Valo Grande, the coastal plain suffered drastic erosion, leading to a reduction of cultivable and inhabitable areas (BÉRGAMO, 2000; MAHIQUES et al., 2009). Consequently, a dramatic increase in sediment deposition occurred into the adjacent lagoonal setting, forming several new sediment bars, including the island of Iguapé, and filled the port completely, making it inoperative by the late twentieth century

(TELEGINSKI, 1993). Moreover, changes in the fluvio-marine dynamics of the region introduced radical variations in temperature, salinity, currents, and water turbidity (ITALIANI and MAHIQUES, 2014).

In 1978, in response to the local people's request, the state government provided the construction of a dam to close the Valo Grande. This closure increased the salinity of the lagoon and caused a return of the seasonal flooding in the areas downstream the Valo Grande, which were occupied with crops at that time. Since then, major floods jeopardized the agricultural activities and the urban settlements of the region, until 1983, when the dam, already damaged by the floodings, was completely demolished by the local inhabitants. Subsequently, the dam was partially rebuilt but was unable to resist the continuous floodings and the sediment deposition. Therefore in 1995 it was completely demolished and, since then, the flux coming from the Ribeira river through the Valo Grande controls the geomorphological and ecological characteristics of the region (ITALIANI and MAHIQUES, 2014).

The various phases of opening and closure of the Valo Grande produced significant alteration of the sediment supply in the area of Cananéia-Iguapé. In this work we analyze bulk sedimentary mineral assemblages, sediment grain size, sediment magnetic properties, and pore water chemistry from a sediment core, which was collected in the lagoon near the southern connection to the sea, and from samples of the bedrock of the São Jõao Hill (also known as Cananéia Alkaline Massif), which represents the bedrock nearby the core site (RICCOMINI, 1995). The core was collected on the southern end of the lagoon, downstream to the main flow. This location receives sediment from all the different inputs into the sedimentary system and thus is ideal to assess the extension and the intensity of the disturbances created by the opening of the channel.

### *5.2. Materials and Methods*

The core CAN-N01 was collected using a gravity corer at −25.023831, −47.921750 in the Lagoon, south of the city of Cananéia. The core is 137 cm long with a 7.5 cm of diameter and was sampled each 2.5 cm.

Samples of the local bedrock, the Cananéia Alkaline Massif, forming the São João hill, were collected from an outcrop at −25.026223, −47.923203. The collection sites are shown in Figure 26.

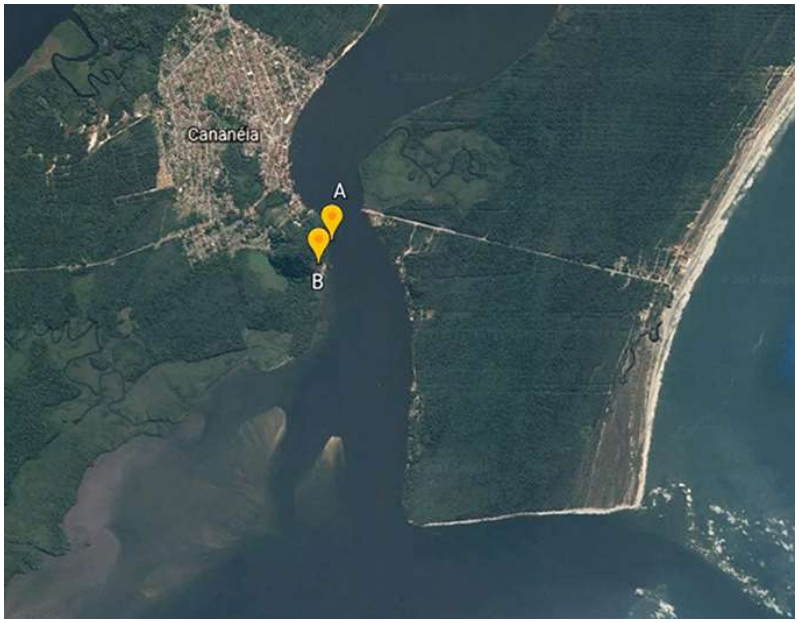


**Fig. 26: Location of sampled points. (A) CAN-N-01, (B) outcrop of São Jõao hill, Cananeia region. São Paulo, Brazil.**

All the measurements for this study were performed in the laboratories at the Institute of Oceanography of the University of São Paulo. The samples and parameters analysed are listed below.

*5.2.1. Grain Size*

The samples were collected continuously along the core with 5 cm spacing. Carbonate constituents were removed with a 10% HCl solution in a beaker over a hot plate at 80°C, put inside an extraction hood while stirring hourly and adding more solution as it saturated. Afterwards, the samples were the washed at least twice, drained, and dried in an oven at a temperature of above 60°C for approximately 24 h.

Organic matter was removed with a 10% H-peroxide solution in a beaker over a hot plate, kept inside an extraction hood, at approximately 80°C, until the solution became colorless and changing the solution every 2 days. At the end, the samples were washed at least twice with distilled water. Grain sizes of 27 samples were determined using a Malvern Mastersizer-2000 Laser analyzer®.

*5.2.2. Pore Waters*

Pore water was extracted soon after core collection using Rizosphere® needles with diameter of 2.5 and a mean pore size of 0.15 μm to avoid fine sediment particles in pore waters. The extraction was performed in a regular interval distance of 10 cm. The water samples obtained (±10 mL) was fractionated and refrigerate to 4°C for dissolved nutrients ($NH^{+}_{4}$, $PO^{3-}_{4}$ and

$Si(OH)^{-}_{4}$) using colorimetric methods with a Biospectro®SP22 spectrophotometer. The analyses of nutrients were performed at the Laboratory of Biogeochemistry of Nutrients, Micronutrients and Traces in oceans (LABNUT-IOUSP). N-ammonium concentration was determined using Tréguer and Le Corre (1975) method with a detection limit of 0.02 μmol $L^{-1}$ and a precision of ±0.01 μmol $L^{-1}$. Dissolved phosphate and silicate concentrations were determined using the recommendation of Grasshoff (1983) based on the molybdenum blue complex with a detection limit of 0.01 for phosphate and 0.1 μmol $L^{-1}$ for silicate and a precision of ±0.01 and ±0.1 μmol $L^{-1}$ respectively.

*5.2.3. Paleomagnetism*

In order to study in detail the magnetic properties of the core, a U-channel sample spanning the entire length of core (137 cm) was collected. Discrete oriented samples in cylindrical plastic boxes were also collected every 2.5 cm. The U-channel was firstly used to study the natural remanent magnetization (NRM). To study the presence of primary and secondary magnetic components we applied an alternating field (AF) stepwise demagnetization, with steps of 0, 25, 50, 750, 100, 150, 20, 250, 300, 400, 500, 600, 700, 800, 900, and 1,000 mT. After each step, the u-channel was measured with a resolution of 1 cm using a 2G- Long Core Squid cryogenic magnetometer, located in a magnetically shielded room. The resultant curves were deconvoluted and analyzed using the software developed by Xuan and Channell (2009) and the principal component analysis of Kirschvink (1980), in order to isolate the characteristic remanent magnetization (ChRM).

*5.2.4. Environmental Magnetism*

Different rock magnetic measurements were performed to characterize the magnetic mineralogy of the core. Mass-dependent magnetic susceptibility was determined on discrete samples using an Agico KF1 Kappabridge. Artificial magnetic fields of known characteristics were used in order to study the response of the samples in different conditions and the following parameters were determined: (a) anhysteretic remanent magnetization (ARM), which was measured first by imposing a 0.1 mT DC bias field while applying a 0.1 T demagnetizing alternating field, and then by progressively demagnetizing via AF with fields of 50, 100, 150, 200, 250, 300, 400, 500, 600, 700, 800, 900, 1,000 mT; (b) Isothermal remanent magnetization was imparted by applying a 1.0 T direct field (IRM@1.0), after measuring the magnetization Backfield IRM was imparted by applying a direct field of 0.1 (IRM@-0.1) and 0.3 mT (IRM@-0.3) in the opposite direction (e.g., KING and CHANNELL, 1991; VEROSUB and ROBERTS,

1995; JOVANE et al., 2013). From these parameters the S-ratios were calculated (S-Ratio300 as IRM@0.3/IRM@1.0; and S-Ratio100 as IRM@0.1/IRM@1.0), which measure the relative abundance of high coercivity (e.g., hematite, goethite) and low coercivity (e.g., magnetite) minerals. The hard isothermal remanent magnetization (HIRMs), which reflects the concentrations of high coercivity minerals, was calculated as (HIRM300 = (IRM@0.3+IRM@1.0)/2 and HIRM100 = (IRM@0.1+IRM@1.0)/2); the relative magnetic grain size variations were estimated as ARM/IRM@1.0 (Evans and Heller, 2003). In order to perform the measurements with the 2G Cryogenic Magnetometer we used the Laboratory of Paleomagnetism of the Institute of Astronomy, Geophysics and Atmospheric Sciences of the University of São Paulo, Brazil.

*5.2.5. First-order reversal curve (FORC)*

FORCs were analysed at the Centro Oceanográfico de Registros Estratigráficos (CORE) Laboratory, Instituto Oceanográfico, Universidade de São Paulo, Brazil using a Lake Shore Cryotronics Inc. vibrating sample magnetometer, and FORC diagrams were elaborated using the FORCINEL 3.0 software (HARRISON and FEINBERG, 2008).

*5.2.6. Geochronology*

A set of 11 samples for gamma spectrometry analysis were taken every 4 cm within the first 40 cm of the core, and then the material was prepared and analyzed following Figueira (2000) and Neves et al. (2014) recommendations. At first, the samples were lyophilized and homogenized, and 10 g were weighted and sealed in a container specific for gamma counting. After 21 days, the samples were counted in an EG&G ORTEC low-background gamma spectrometer (model GMX25190P, 1,79 keV FWHM for the $^{60}$Co 1,33 MeV peak). An identical empty container was used to determine the background radiation of the detector and a source of $^{241}$Am was used to determine the self-absorption factor of the samples. The samples were counted for 70,000 s and the photopeaks used in this analysis were 46.52 keV for $^{210}$Pb, 609.31 keV for $^{226}$Ra and 661.67 keV for $^{137}$Cs. The quality control of this technique was assessed by measuring the same nuclides in certified reference materials (IAEA300, IAEA315, and IAEA326), and met all quality requirements, with statistical deviations and errors below 10%. Model CIC (Constant Initial Concentration) with unsupported $^{210}$Pb (ROBBINS and EDGINGTON, 1975) was used to measure the sedimentation and rates and to create an age model for the core.

*5.2.7. Mineralogy*

Approximately 1 $cm^3$ of sediment per sample was hand grinded in a jade mortar and then sieved through a 63 μm sieve. X-ray diffraction measurements were performed with an Olympus BTX II Benchtop X-ray Diffraction/X-ray Fluorescence device. The resulting X-ray diffraction data were processed using the Panalytical High Score Plus software, which includes the American Mineralogist Crystal Structure Database (AMSCD) and the Crystallography Open Database (COD). To determine the optimal number of expositions, diffractograms were obtained with different exposure times, and the best time/resolution was found at 100 exposures. Runs with more than 100 exposures did not yield significant improvement in mineral quantification, in agreement with Davis et al. (2015).

*5.2.8. Hierarchical cluster analysis (HAC):*

XRPD data collected with the Olympus BTX II Bench-top XRD were analysed with the PANalytical High Score Plus software for cluster analysis. The software analyses the diffractograms profiles and peaks and groups the samples on the base of their similarity. For each cluster the software identify the most representative sample.

### *5.3. Results*

*5.3.1. Grain Size*

The results, presented using the Particle Size Distribution (PSZ) (Figure 27), showed high concentrations of fine and very fine sand (respectively on average 45.2 and 32.7%), with minor coarse sand, silt, and clay. No significant variations in grain size are observable throughout the core.

*5.3.2. Pore Waters*

The nutrients concentrations in pore waters are shown in Figure 28.

Concentration of N- ammonium ranged from 685 to 3,282 μmol $L^{-1}$. The values showed an increasing trend downcore, except from a value at 90 cm that decreased to 757 μmol $L^{-1}$. Phosphate concentration ranged from 104,6 to 291,7 μmol $L^{-1}$. The values showed an increasing trend downcore except at 20 cm that dropped from 170,3 to 104,6 μmol $L^{-1}$, and at 120 cm that dropped to 177,3. Silicate values ranged from 640.2 to 836.2 μmol $L^{-1}$, with irregular distribution.

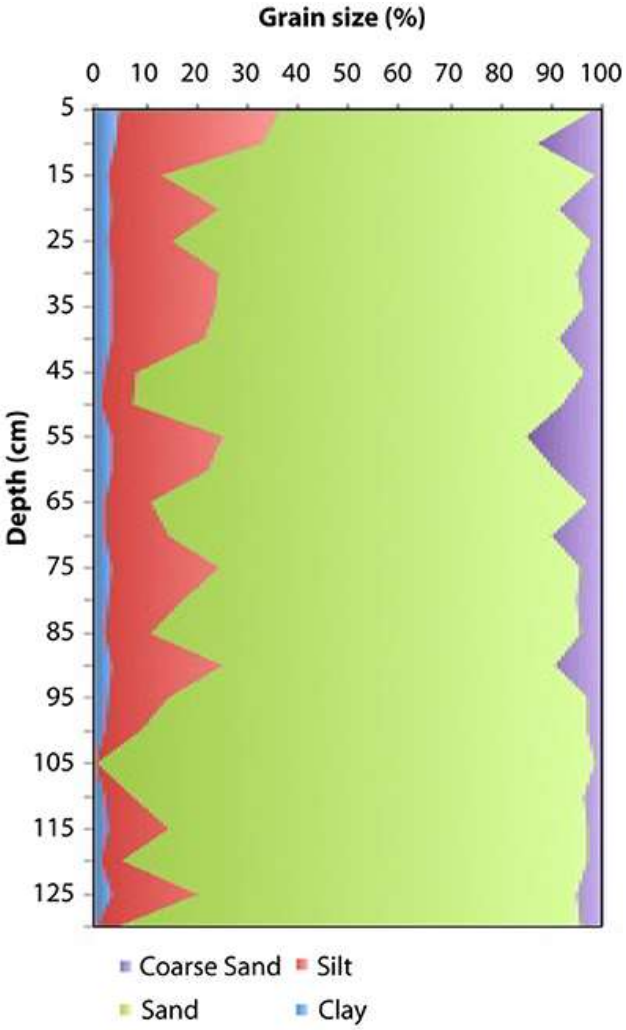


**Figure 27: Distribution of grain size in core CAN-N-01 profile.**

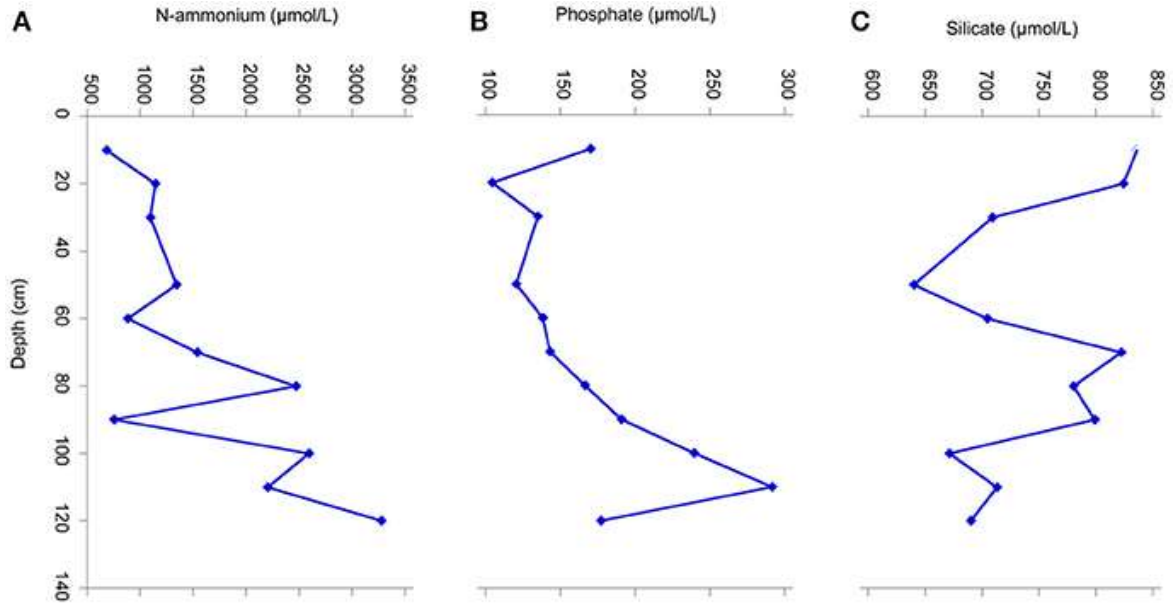


**Figure 28. Distribution profiles of dissolved nutrient concentrations in pore-waters: (A) N-Ammonium, (B) Phosphate, (C) Silicate for core CAN-N-01.**

*5.3.3. Magnetic properties*

Following the AF demagnetization process, the vast majority of the samples showed a particular pattern in the variation of intensity of the NRM, which decreased until 400 mT of AF, and then rose again, suggesting that the sample had acquired gyroremanence (GRM). The presence of an early gyroremanence precluded the study of the behavior of the sample at higher alternating fields.

The PCA analysis showed that the ChRM always had negative inclinations, as expected, with mean inclination of −37.2° ($\alpha_{95}$ of 1.6°), (Figure 29) that is perfectly in agreement with the expected value of −37.9° for the locality (as calculated with the Model WMM integrated between the years 2012 and 2014).

A secondary component was recognizable at low demagnetization fields, usually up to 100 mT, with lower inclinations, and was interpreted as a viscous remanent magnetization (VRM) carried by a very low-coercivity mineral.

The results of the environmental magnetic studies are summarized in Figure 29. The various parameters show little to no features, with almost constant values along the core. Relative concentration parameters, such as susceptibility, ARM are the most variable. A few positive peaks in NRM and ARM can be interpreted as an increase in the relative abundance of magnetic minerals, while negative peaks can be interpreted as a decrease. The peak at 5 cm found in the IRM and ARM curves could represent an increase of the fine grained magnetite crystals in the sediment, comparable with the features found in sediments from Mamangua (RJ, Brazil), that are interpreted as the presence of living magnetotactic bacteria producing biogenic magnetite (RODELLI et al., 2019).

S-Ratios give information about the relative concentration of high and low (for S-Ratio300), and middle and low (S-Ratio100) coercivity minerals. The two curves have a similar behaviour, with almost constant values close to 1 for the S-Ratio300 and 0.4 for the S-Ratio100 throughout the core. The variation along the core is minimal, with only a slight increase in the interval between 80 and 90 cm. The HIRMs curves also show almost no variation, with only some minor variations at 40 and 75 cm that should represent small fluctuations in the abundance of high coercivity minerals.

*FORCs* have been measured in the first three samples at the top of the core, where ARM and IRM values are higher and the grain size values are low, suggesting the possibility of the presence of biogenic magnetite (results in figure 30). The first sample (0-2,5 cm) shows a signal of detrital magnetite only, the second sample (2,5-5cm) shows a weak but distinct signal of MTB as the magnetosomes are behaving as a single crystal. The third sample (5-7,5 cm) shows

a substantially empty field, meaning that there are no relevant interactions at the given parameters, therefore a lack (or very low concentration) of magnetic minerals in the coercivity range 0-100 mT.

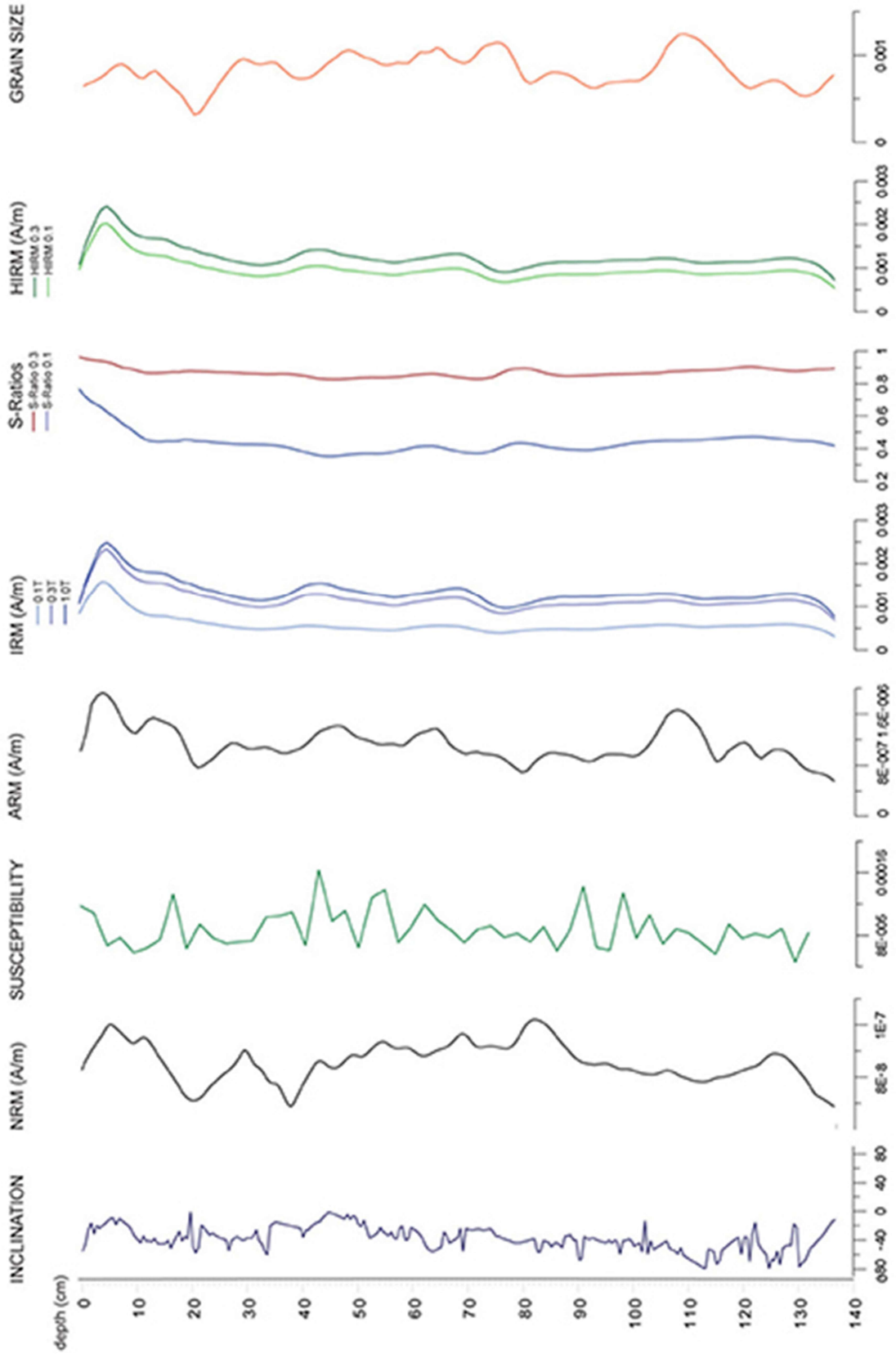


**Figure 29. Distribution of paleomagnetism data for core CAN-N-01.**

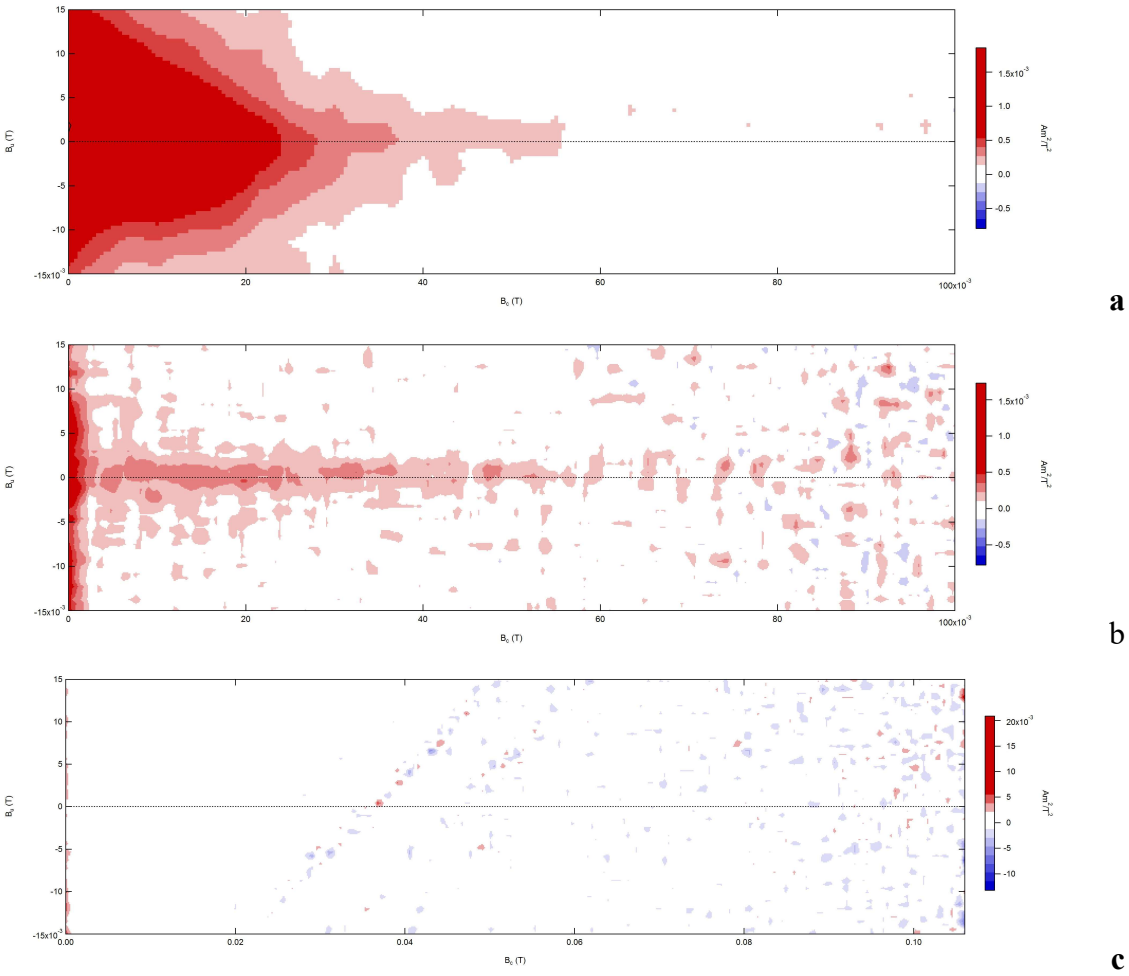


**Fig. 30:FORCs results for samples at 2.5, 5 and 7,5 cm depth of core CAN-N01 showing: a)non-biogenic magnetite; b) the typical ridge of magnetosomes; c)lack (or very low concentration) of magnetic minerals in the coercivity range 0-100 mT**

### *5.3.4. Geochronology*

Model CIC was applied to the vertical profile of $^{210}$Pb (Fig. 31) and the calculated sedimentation rate was 0.43 ± 0.02 cm yr$^{-1}$. The exponential decay of $^{210}$Pb ($r$= 0.87, $p$< 0.05; $\chi^2$ = 0.44, $p$ < 0.05) shows that the sedimentation rate underwent little variations within the core. If any variation occurred, it was limited to the 8–12 cm of the core, and it is not statistically significant to the overall calculation, given the fit quality obtained from the statistical parameters presented above. Moreover, this result is supported by the vertical distribution of $^{137}$Cs, which estimates a mean sedimentation rate of 0.39 ± 0.02 cm yr$^{-1}$ for the first 40 cm of the core based on its horizon of maximum activity (corresponding to the nuclear fallout maximum of 1963 from past atomic tests).

The age model of the core was created, estimating a deposition year of 1920 for the 40-cm-deep layer of the core. Given that it was not observed evident changes in the sedimentation rate

within the core, the age model created with the CIC model was extrapolated throughout the entire core.

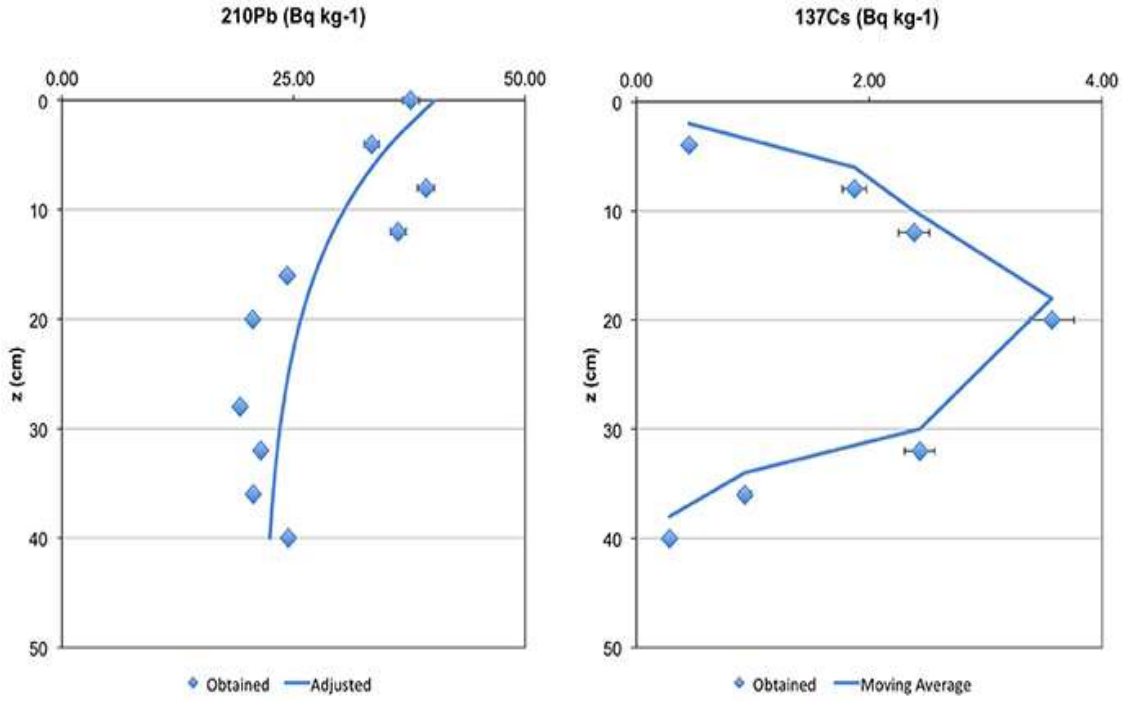


**Figure 31: Vertical distribution of 210xsPb and 137Cs for core CAN-N-01.**

### *5.3.5. X-Ray Diffraction*

XRD analysis of the sediment core revealed three main mineralogical assemblages: (i) quartz around 99% and halite; (ii) quartz around 80%, and a minor fraction dominated by brucite; (iii) quartz between 60 and 80%, and a minor fraction dominated by kaolinite (Figure 32).

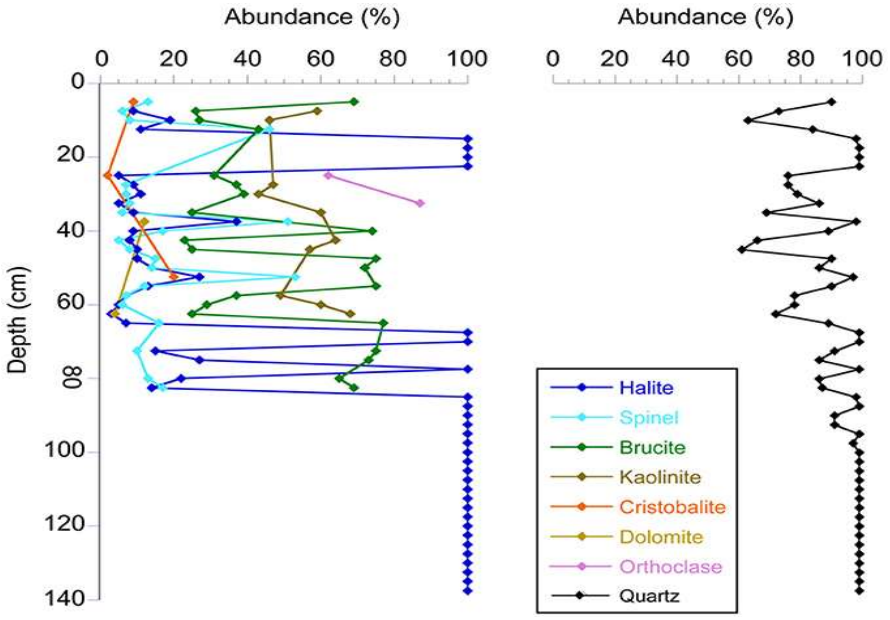


**Figure 32: Mineralogical distribution for core CAN-N-01: concentration of quartz on the right side and minor mineral fraction on the left side. Minor mineral abundances are expressed as normalized respect to quartz.**

The interval from the top of the core to 65 cm depth is dominated by the mineralogical assemblages (ii) and (iii), with lower quartz content. Only a brief interval, between 15 and 22.5 cm, is dominated by the assemblage (i). Down-core, quartz content increases and below 95 cm it reaches the abundance of 97% or higher, with only halite as a minor mineral fraction. Halite is precipitated from pore water once the sample is colected and dried, thus it is not originally part of the mineralogical assembly.

| Sample | Albite (%) | Orthoclase (%) | Quartz (%) | Scapolite (%) |
|---|---|---|---|---|
| BR1 | 57 | 17 | 25 | 1 |
| BR2 | 65 | 19 | 15 | 1 |
| BR3 | 62 | 21 | 16 | 1 |
| BR4 | 60 | 21 | 18 | 1 |
| MEAN CONTENT | 61 | 19,5 | 18,5 | 1 |

**Table 2: Mineralogical composition of the bedrock samples.**

The XRD analysis of the bedrock samples yielded the results shown in Table 2. Our results are in agreement with previous studies on the bedrock in this area, which found intrusive rocks, saturated or oversaturated in silica, with Na-feldspar more abundant than K-feldspar (SPINELLI and GOMES, 2009).

*5.3.6. HAC*

The software divided the diffractograms in 5 cluster (fig. 33). We have considered the main three according to the hierarchy of the analysis, namely cluster 1, cluster 2 and cluster 3. Cluster 1 is dominant at the bottom of the core (below 90 cm depth) and between 15 and 22,5 cm depth, cluster 2 and 3 are intercalated throughout the rest of the core. This confirms the mineralogical analysis observations.

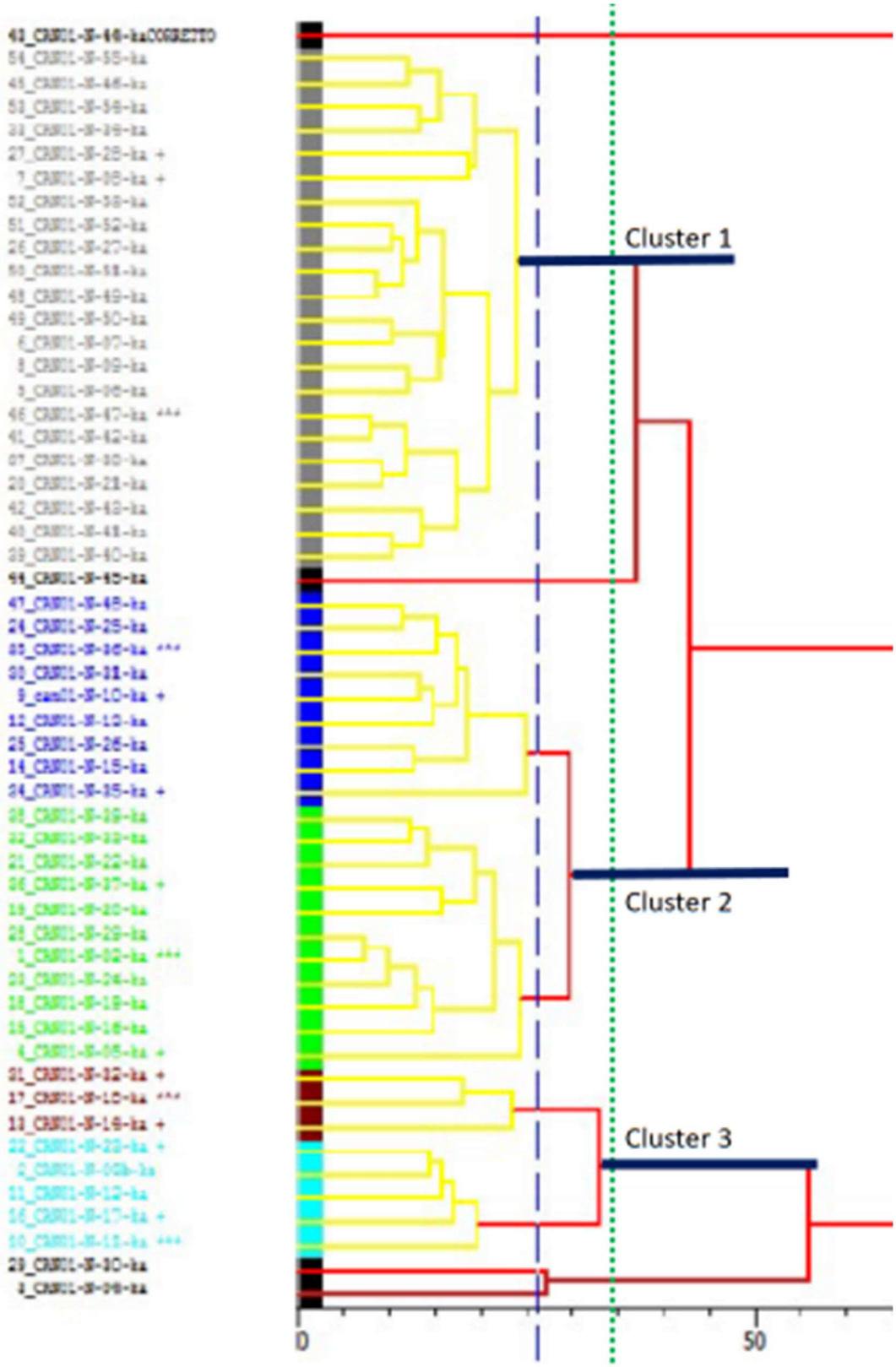


**Fig.33: dendrogram for HAC for Cananeia N01. With the dotted blue line in indicated the cut off generated by the software which recognized 5 clusters. With the dotted green line is indicated the cut off considerated significant for this study. Three major clusters were identified as cluster 1, cluster 2 and cluster 3 and underlined in green. We can observe that cluster one remained the same after the moving of the cut off line, cluster 2 and 3 where created by merging of two clusters each, always following the similarity hierarchy created by the HAC analysis.**

### *5.4. Discussion*

The core was collected close to where the water flows out of the lagoon to the sea, in a moderate energy environment, mainly controlled by the currents flowing parallel to the coast. In this context the lack of significant grain size variations along the core, indicates that the energy of the system remained constant during the deposition of the entire interval and therefore, the changes observed in the mineralogical assemblages must be related to the sediment supply, rather than to the depositional processes.

According to the age model of the core, the opening of the Valo Grande channel in 1852 should occur at 70 cm depth, whereas its closure with the construction of the dam in 1978 at 16 cm, and the re-opening of the channel in 1983 at 13 cm. The results of the environmental magnetic studies show almost constant values along the core. The positive correlation between ARM and IRM peaks and the magnetic grain size suggest that the variation in concentration of magnetic minerals is accompanied by variations in the relative magnetic grain size, with a general trend of bigger grain size during periods of low concentration and vice-versa. S-Ratio curves showed that the most predominant magnetic minerals are of low to middle coercivity, probably low-Ti magnetite (OZIMA and LARSON, 1970). The peak in the IRM, S-Ratios, and HIRMs curves occurring at 5 cm represent an increase of fine grained magnetite crystals in the sediment, comparable with those found in Mamangua (RJ, Brazil), that were interpreted as indication of living magnetotactic bacteria producing biogenic magnetite (RODELLI et al., 2019). This interpretation is also supported by FORCs measurements. In figure 33 is shown in detail the mineralogical composition of the Cananeia core where the FORCs were measured. It can be observed that around 5 cm depth, where MTB were detected, quartz drops from nearly 90% to nearly 60%, whereas clay minerals, represented by kaolinite,increase up to 60% of the minor mineral fraction (and about 25% of the bulk mineralogical composition).

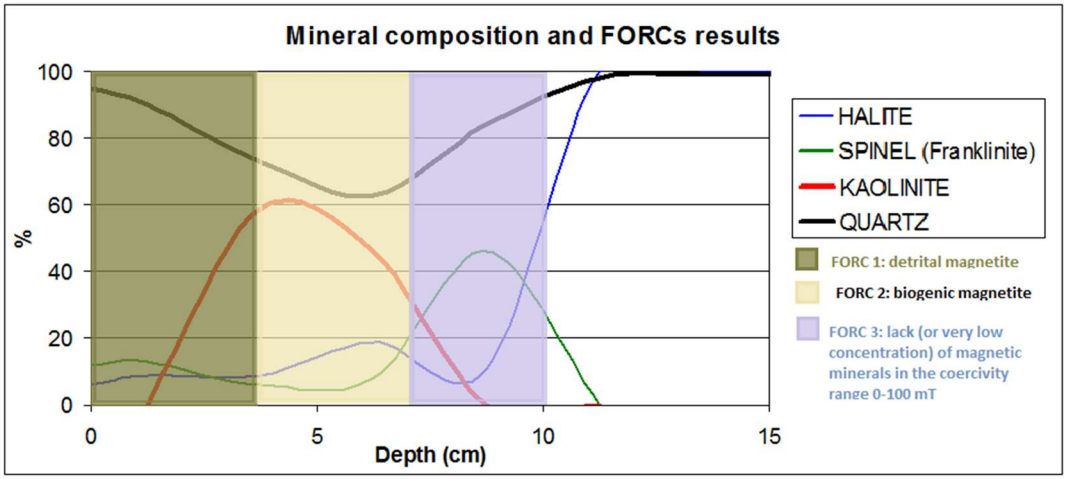


**Fig. 33: XRPD and FORCs results for the first 15 cm of the core CAN-N-01 in Cananeia. Quartz and minor mineral are represented here in the same graphic, but were analyzed separately.**

Pore water oxygen concentration data are not available for this core, however, considering that the core was collected in a shallow setting with relatively high energy, it is reasonable to exclude an abrupt modification of the oxygen content immediately below 5 cm depth. Nutrients concentrations varied throughout the core despite the homogeneity of the grain size (Fig. 27 and 28). This indicates fluctuations in redox conditions and in the amount of organic matter. The N-ammonium showed a minimum after the first opening the Valo Grande, and another one in the recent horizon, after the last opening. As N-ammonium is a product of anaerobic destruction of organic matter, its decrease could be associated with organic matter decomposition in the presence of enough dissolved oxygen to allow the formation of nitrite and nitrate, which is corroborated by the increase of phosphate and silicate at this level. Phosphate also decreased from the opening of the Valo in 1852, contrary to N-ammonium, which increased toward the surface of the sediment. This could be the effect of the recent exploitation of phosphogypsum in the upland (BERBEL et al., 2015). Silicate concentrations increased soon after the opening of the Valo Grande, signalizing an increase of silicate input. The increase of silicate is an excellent indicator of terrestrial and mineral inputs. In the recent horizon, the increase in silicate and phosphate can indicate higher terrestrial input, showing a return of the effective anthropogenic interference. For Braga et al. (2000), environments that suffered from anthropogenic nutrients enrichment may present high levels of eutrophication. This can produce frequent and periodic episodes of low oxygenation in the water column, due to high nutrient supply and high primary production rate that consumes the oxygen (GRAY et al., 2002; SMITH and DEMOPOULOS, 2003).

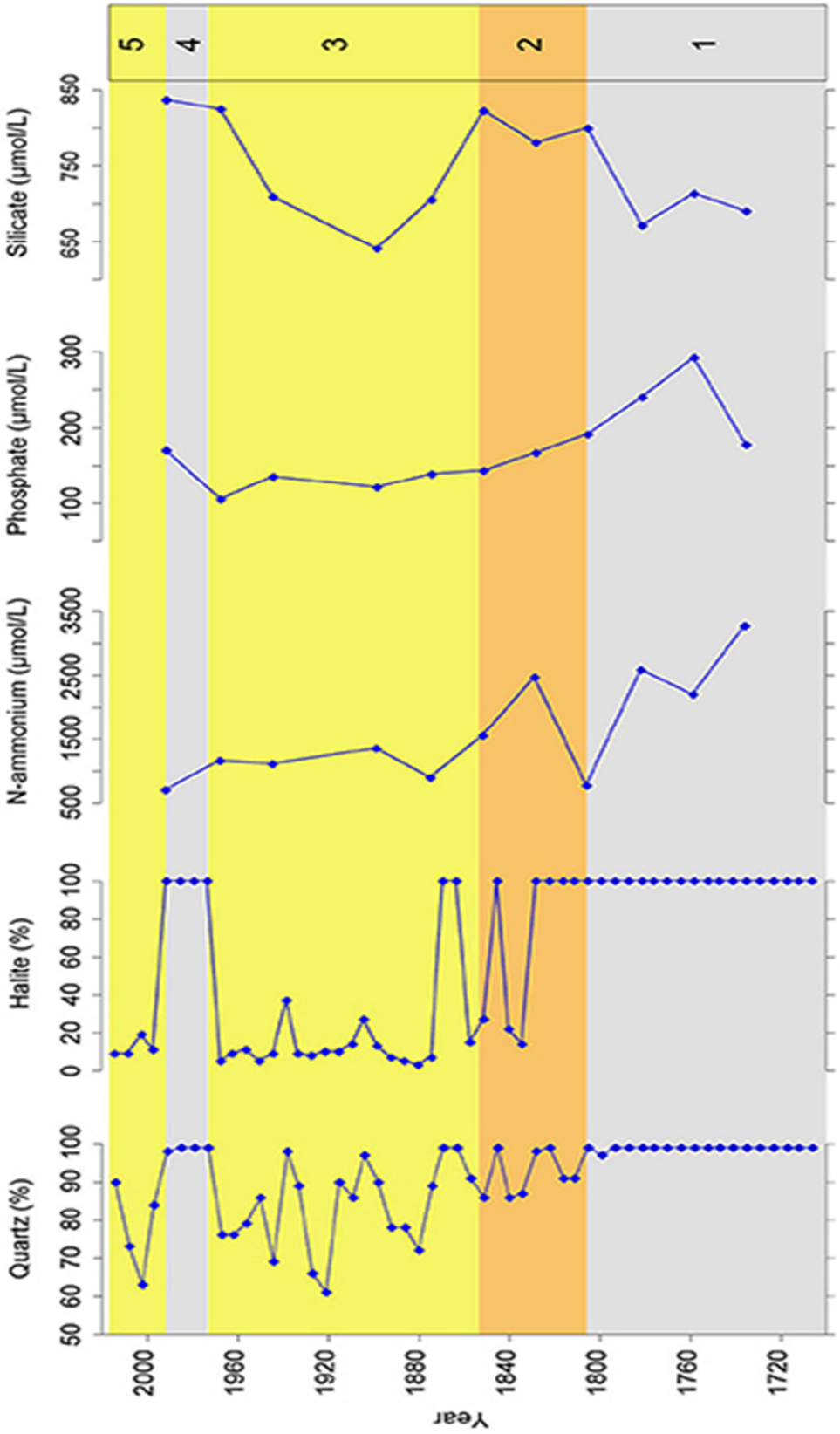


**Fig. 34: Major mineral concentrations and pore water results over time for core CAN-N-01. Dating before 1850 has been extrapolated from the sedimentation rate. (1) Period before the construction of the Valo Grande channel; (2) Period during the construction of the Valo Grande channel; (3) Period during which the Valo Grande channel was completely open; (4) Period of the closure of the Valo Grande channel with a dam; (5) Period after the destruction of the dam and complete re-opening of the Valo Grande channel.**

Mineralogical analyses show that halite and quartz have similar trends throughout the core, with maximum values corresponding to the periods when the Valo Grande channel was closed and decreasing when it was open (Figure 34). They have a marked increase between 15 and 22.5 cm, where the mineralogical assemblage (i) replaces the others. Besides, an alternation between the mineralogical assemblages (ii) and (iii) dominates from the top to the depth of 67.5 cm, where quartz content begins to increase and the mineralogical assemblage (i) becomes more frequent. Mineralogical assemblage (i) predominates 90 cm depth down-core.

Halite precipitates from pore water trapped in the sediments at the time of deposition,therefore its presence indicates the absence of riverine input that freshens the water. Our data suggest that, during the periods of absence or closure of the Valo Grande (between 1978 and 1983 and before 1827), the Ribeira River entered in the sea more northwards and did not supply significant amount of sediment and fresh water to the Cananeia–Iguapé aquatic environment.

The mineralogical composition of the sediment core indicates that during the time when the Valo Grande was opened, the sediments were characterized by lower quartz content and significant amounts of kaolinite, brucite, and franklinite, which corresponds also to a slight increase in detrital magnetite, estimated from environmental magnetic analyses. These minerals may have come from the alteration and erosion of the metamorphic basement forming most of the bedrock of the region and transported there by the opening of the Valo Grande. On the other hand, before the construction of the Valo Grande and during its closure, the sedimentary supply into the lagoon was controlled by sea currents, parallel to the coast, which delivered more mature sediments composed mainly by quartz. Our data show that the sedimentary input into the lagoon changed during the last 165 years in response to the openings and closures of the Valo Grande channel. These variations are well displayed by the mineralogical assemblages, despite the homogenous grain size and environmental magnetic parameters.

### *5.5. Conclusions*

Here, we presented detailed mineralogical, grain size, environmental magnetic, geochronological, and pore waters profiles of a sedimentary core from the southern portion of the estuarine-lagoonal system, near the Cananeia city. Despite the homogeneity of the grain size throughout the approximately 300 years long interval, significant variations in the mineralogical composition of the non-quartz material revealed the influence of the opening of the channel on the sediment supply in the downstream part of the lagoon. Sediments with lower quartz and halite, and higher kaolinite, brucite, and franklinite contents corresponded to periods of freshwater input into the lagoon, due to the opening of the Valo Grande channel. Higher

abundance of quartz and halite and the disappearance of the other detrital minerals corresponded with periods of closure or absence of the channel, during which the setting was more sea-influenced. These results are corroborated by pore water dissolved nutrients. As estuarine-lagoonal sedimentary systems are rather common along the coast of Brazil, the case presented in this study could have several analogues in still less studied settings.

The presence of living and producing MTB at this site is very low and limited to a very small interval, at around 5 cm depth. This implies that their living conditions at this site are not favourable. The clay content throughout the core is quite low (between 16 and 25% of the total mineral assemblage), with the highest value in the interval in which the MTB were found. Although this simple correlation is not sufficient to claim that the clay content is the main controlling factor on the productivity of MTB, it is also evident that other important ecological parameters, such as nutrients and dissolved oxygen, do not seem to display the same abrupt variations with depth. More specific analyses, such as a characterization of the mode of life of the MTB in this specific setting and of the magnetosomes can contribute to enlighten this relationship.

# 6 - THE MAMANGUÁ RÍA: BIOGENIC MAGNETITE IN A CHEMICALLY STRATIFIED SEDIMENTARY ENVIRONMENT.

**This work is part of an article published as Rodelli et al. 2019 in the Journal of Geophysical Research: Solid Earth, with the title "Diagenetic Fate of Biogenic Soft and Hard Magnetite in Chemically Stratified Sedimentary Environments of Mamanguá Ría, Brazil'.**


## *Abstract*

MTB synthesize magnetite and greigite crystals in the water column or uppermost sediment. Dissolved iron and oxygen contents are known limiting factors for MTB production and preservation of biogenic magnetite. Understanding the processes that link MTB to their living environments is fundamental to reconstructing past chemical variations in the water column and sediment, and for using the magnetic properties of biogenic magnetite as environmental proxy indicators. In this case study the environments appears very favourable for MTB that are highly abundant within the uppermost 30 cm of the core. Sediment supply did not change significantly throughout the studied core, so that sediment composition and relative nutrient abundances are likely to have been almost constant. Sedimentary oxygen content and redox potential measured in pore waters within the studied sediments are the main factors controlling the presence or absence of living magnetotactic bacteria. Biogenic magnetite is present only where redox potential and dissolved oxygen concentrations are high enough to allow magnetite producing MTB to live or biogenic magnetite to be preserved. The abrupt transition between relatively well oxygenated and oxygen depleted sediment is marked by the death of magnetite producing MTB and by the rapid dissolution of the magnetosomes. Therefore, MTB production in this context is not limited by the mineralogical composition and the presence of clay in the sediment, rather by others factors, such as pore water oxygen content.

## *6.1.Introduction*

Studying the natural distribution of MTB can be useful for understanding water column and sedimentary environments. Recent studies have suggested that the abundance of different morphologies of magnetosomes crystals varies in accordance with sedimentary oxygen content. MTB that produce equant octahedral biogenic soft (BS) magnetite crystals live in more oxygenated environments, while the MTB producing the more elongate biogenic hard (BH) magnetite crystals in less oxygenated ones (e.g. CHANG et al., 2013, 2018; EGLI, 2004; YAMAZAKI, 2012; YAMAZAKI & SHIMONO, 2013, RODELLI et al., 2019). BS and BH magnetite react differently to the environmental oxygen depletion, as BS is more prone to dissolution in anoxic environments than BH magnetite.

We present an integrated study of magnetic properties, pore water chemistry, and lithology of surface sediments from a coastal ría environment in the Saco do Mamanguá (Rio de Janeiro, Brazil) (BENITES et al., 2015; RODELLI et al., 2019) as it represents a favourable environment for MTB, as demonstrated by the high presence of MTB in the surface sediments.

### *6.1.1. Geological Setting*

The Mamanguá ría is located in the Ilha Grande Bay, along the SE coast of Brazil, and it is part of the Municipality of Paraty (RJ, Brazil). It has an elongated shape, roughly 11 km long and 2 km wide (Fig. 35). The Mamanguá ría has a restricted circulation and a weak tidal action, which ranges between 64 and 125 cm (BERNARDES, 1996). The inner part receives organic matter from the continent, like in an estuary, whereas the outer part is influenced by marine production (SPERA, 2012). Surface sediments are predominantly composed of clay and silt with high organic phosphorus content indicating a significant contribution of nutrients coming from land (TEIXEIRA, 2009). Gas seepages have been reported from shallow depths below the seafloor (BENITES et al., 2015). The ría margins are composed of granites linked to the Araçuaí orogen (ALMEIDA, 1977) and covered by Atlantic forest, which contributes to the formation of extensive lateritic soils (RODELLI et al., 2019).


**Fig. 35: Map and position of the Mamangua ria and core 9. (RODELLI et Al.2019)**

This study focuses on Core 9M (411cm long), which was collected with a vibracore at 23° 16' 33" latitude South and 44° 38' 6" longitude West, at a water depth of 7.2 m, within the inner part of the riá (figure 35). The core was analysed by collaborators for magnetic properties, pore water chemistry, grain size, and petrographic properties, which were used to integrate the XRPD results generated in the development of this work. This core was chosen for this PhD work as representative of a favourable and stable environment for MTB.

## *6.2. Methods*

### *6.2.1. Pore Water Chemistry*

Pore water analyses on sediments were carried out on a shorter (170cm) core collected at the same site via gravity corer, as the vibracore potentially mixes the water within the sediment. Pore water samples were extracted every 10 cm as soon as the core was collected, using rizosphere ® needles to filter out any sediment particle. Collected water was used to measure Dissolved Oxygen (DO) and Eh. All measurements were performed in a controlled, nitrogen atmosphere. DO was measured with a DO probe connected to a VWR sympHony bench-top meter, while Eh was measured with a HACH SensION portable meter.

### *6.2.2. Mineralogy*

Samples for X−ray Powder diffraction (XRPD) analyses were collected at 10 cm stratigraphic intervals and prepared by hand pulverizing ~0.2 g of bulk sediment in a mortar. Samples were analysed with an Olympus® BTX Benchtop XRD/XRF diffractometer using Co−K radiation,

operated at 30 kV and 0.326 mA, over the 2θ range of 5°–60°, with a step size of 0.05° (results are a stack of 60 exposures to X−rays, each of 15 s duration). Mineral identification and analysis was carried out using the XPowder software (Version 2010.01.15 PRO), which uses the PDF2 International Centre for Diffraction Data database.

### *6.2.3. Grain Size*

About 5 g of sample from 10 cm stratigraphic intervals were treated with 10% hydrogen peroxide to remove organic matter, and with 0.05 g of pyrophosphate added to each sample to avoid clay mineral flocculation. The measurements were performed with a Bluewave Microtrac system.

### *6.2.4. Petrophysical Properties*

Petrophysical properties were measured using a GEOTEK multisensor core logger, with piezoelectric ceramic transducer for P wave velocity measurements, a Bartington Instruments loop sensor for magnetic susceptibility measurements, and natural gamma−ray counters for natural gamma−ray spectroscopy, density, and porosity measurements.

### *6.2.5. Radiocarbon Dating*

Six bivalve shell specimens were chosen from Core 9M at depths of 54, 162, 220, 314, 320, and 409 cm for $^{14}C$ dating. All bivalves were closed, articulated, and in life position, with no evidence of transport and sediment reworking. The shells were sent to two external laboratories (ICA, Inc. and the Physics Department, University of Arizona) for radiocarbon dating using accelerator mass spectrometry.

### *6.2.6. Magnetic Properties*

Detailed magnetic measurements were made continuously throughout the core on U-channel samples with 2 × 2 cm cross section and length <1.5 m (WEEKS et al., 1993). Discrete oriented samples were collected at 5-cm intervals in plastic cylinders.

The *Natural Remanent Magnetization* (NRM) was analyzed with a 2-G Enterprises superconducting rock magnetometer located in a magnetically shielded room at the Paleomagnetism Laboratory, Instituto de Astronomia, Geofísica e Ciências Atmosféricas, Universidade de São Paulo, Brazil. Samples were measured at 1 cm intervals, where consecutive measurements are not independent due to the 4.5 cm half-width of the response

function of the magnetometer (e.g., WEEKS et al., 1993). To identify primary and secondary magnetic components, stepwise Alternating Field (AF) demagnetization was used, with steps of 0, 2.5, 5, 7.5, 10, 15, 20, 25, 30, 40, 50, 60, 70, 80, 90, and 100 mT. Data were analysed with the software of Xuan and Channell (2009) to isolate the characteristic remanent magnetization, using principal component analysis (Kirschvink, 1980), and deconvolution was applied. The magnetometer response functions were measured using an internal standard. Edge effects due to the half-width of the magnetometer response function require data removal from the first and last 5 cm of each U-channel to avoid artefacts during deconvolution.

*Anhysteretic Remanent Magnetization* (ARM) was imparted by imposing a 0.1-mT direct current (DC) bias field while demagnetizing the sample in a 0.1 T AF. The ARM was then measured and progressively AF demagnetized with fields of 5, 10, 15, 20, 25, 30, 40, 50, 60, 70, 80, 90, and 100 mT.

*Isothermal Remanent Magnetization* (IRM) was imparted by applying a 1.0 T direct field (IRM@1.0) and a backfield IRM was then imparted by subsequently applying DC fields of 0.1 T (IRM@-0.1) and 0.3 T (IRM@-0.3) in the opposite direction. U-channel ARM and IRM data were processed and deconvolved with the software of Xuan and Channell (2009). Parameters were calculated as follows: (i) S ratio (as IRM@-0.3/IRM@1) and (ii) Hard IRM (HIRM) (as [IRM@-0.3+IRM@1]/2) (JOVANE et al., 2013; VEROSUB and ROBERTS, 1995).

### *6.2.7. First-order reversal curve (FORC)*

FORCs were analysed using a Lake Shore Cryotronics Inc. vibrating sample magnetometer at the Centro Oceanográfico de Registros Estratigráficos (CORE) Laboratory, Instituto Oceanográfico, Universidade de São Paulo, Brazil. FORC diagrams were produced using the FORCINEL 3.0 software (HARRISON and FEINBERG, 2008).

### *6.3.Results*

#### *6.3.1. Sedimentation Rate*

Although it was not possible to calibrate the radiocarbon results due to uncertain marine reservoir corrections in this environment, the obtained ages can be used to estimate the mean sedimentation rate for Core 9M. Results, as shown in Fig. 36 are consistent, regardless of the laboratory in which they were analysed. The sedimentation rate was stable throughout Core 9M with a mean value of 1.15 m/kyr.

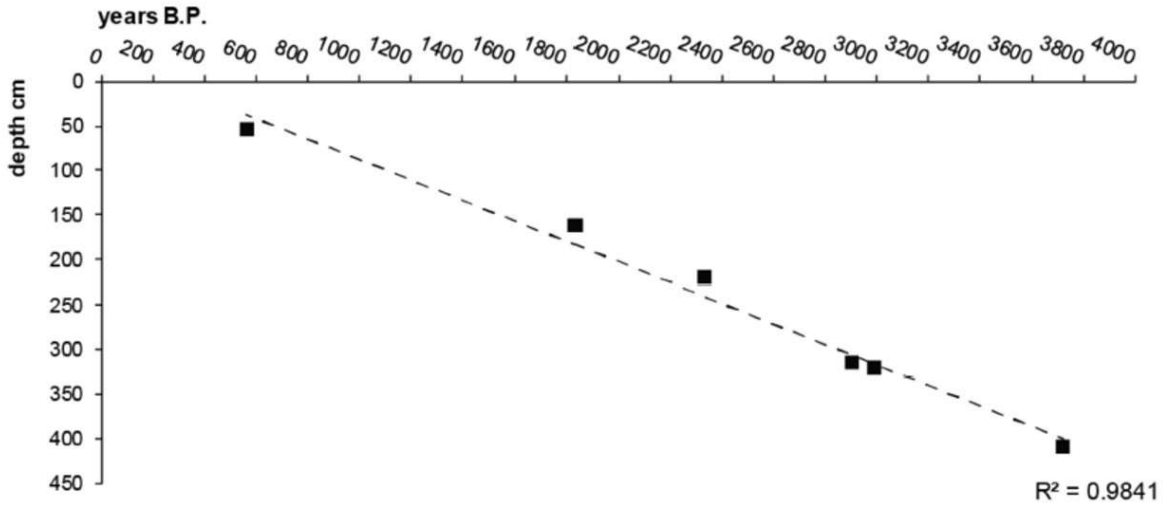


**Fig. 36: age-depth plot (Rodelli et al. 2019)**

#### *6.3.2. Pore Water Chemistry*

DO and Eh ( fig. 37) have higher values in the uppermost 35 to 45 cm and drop sharply below 50 cm. Mean values for the uppermost 40 cm of Core 9 are 3.37 mg/L for DO and 146 mV for Eh, while from 40 cm to the bottom they are 0.72 mg/L and −272 mV, respectively. The results present the already established pattern, with high values in the topmost part and lower values below (BALZER, 1982).

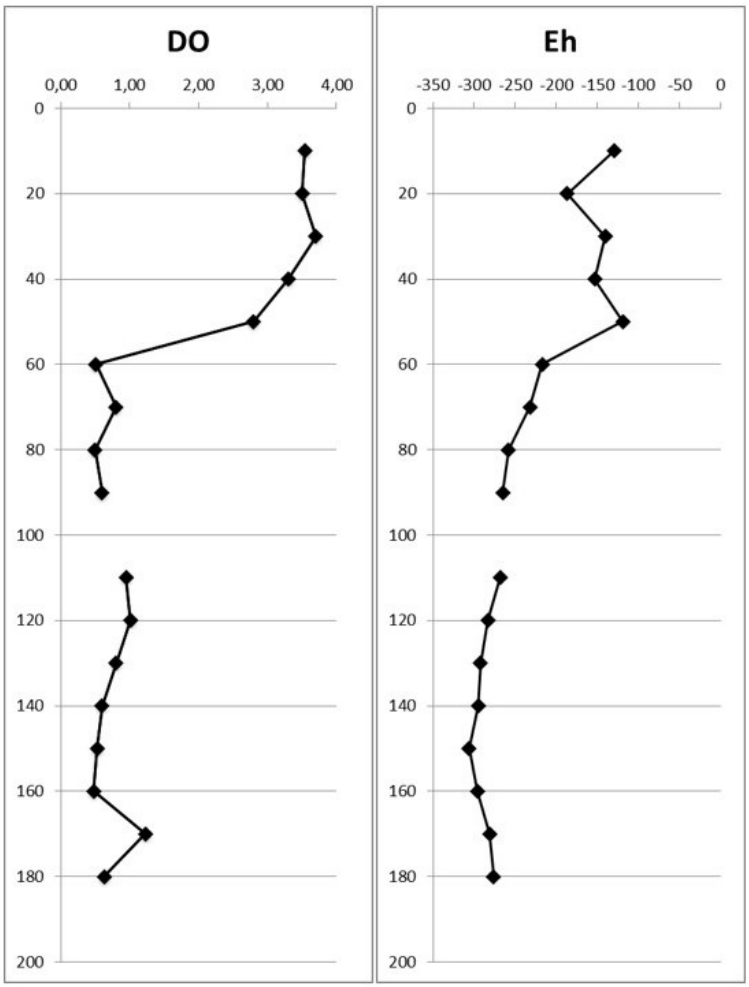


**Fig. 37: pore waters DO results**

### *6.3.3. Mineralogy*

XRD patterns indicate the presence of four principal mineral phases: quartz, Na-feldspar, kaolinite, and illite (Figure 38). The proportion of these phases does not vary significantly downcore, with mean concentrations of 45%, 23%, 12%, and 20%, respectively. This constant mineralogical composition suggests that sediment provenance did not change throughout the studied time interval.

### *6.3.4. Petrophysical Properties*

All petrophysical results are shown in fig. 38. The mean p wave velocity is 1437 m/s for most of the core, although it is slightly lower in the upper 25 cm of sediment where water content is higher. Density follows the same pattern and increases from about 1.4 g/cm$^3$ to a steady value of 1.99 g/cm$^3$. Downcore volume normalized susceptibility values of the whole core are relatively stable at about 3.4 (microSI). Natural gamma rays have low counts per second, with

a mean value of 64.8 cps, and slightly higher counts in the uppermost 5 cm of the core, and a maximum of 71 cps at 2.3 mbsf.

### *6.3.5. Grain Size*

The results (fig. 38) show a quite steady composition throughout the core, with prevalence of clay (around 40%) and silt (around 50%). there are two exceptions in the top meter where two sections, around 30 and around 90 cm depth, show an increase in sand composition reaching about 15%.

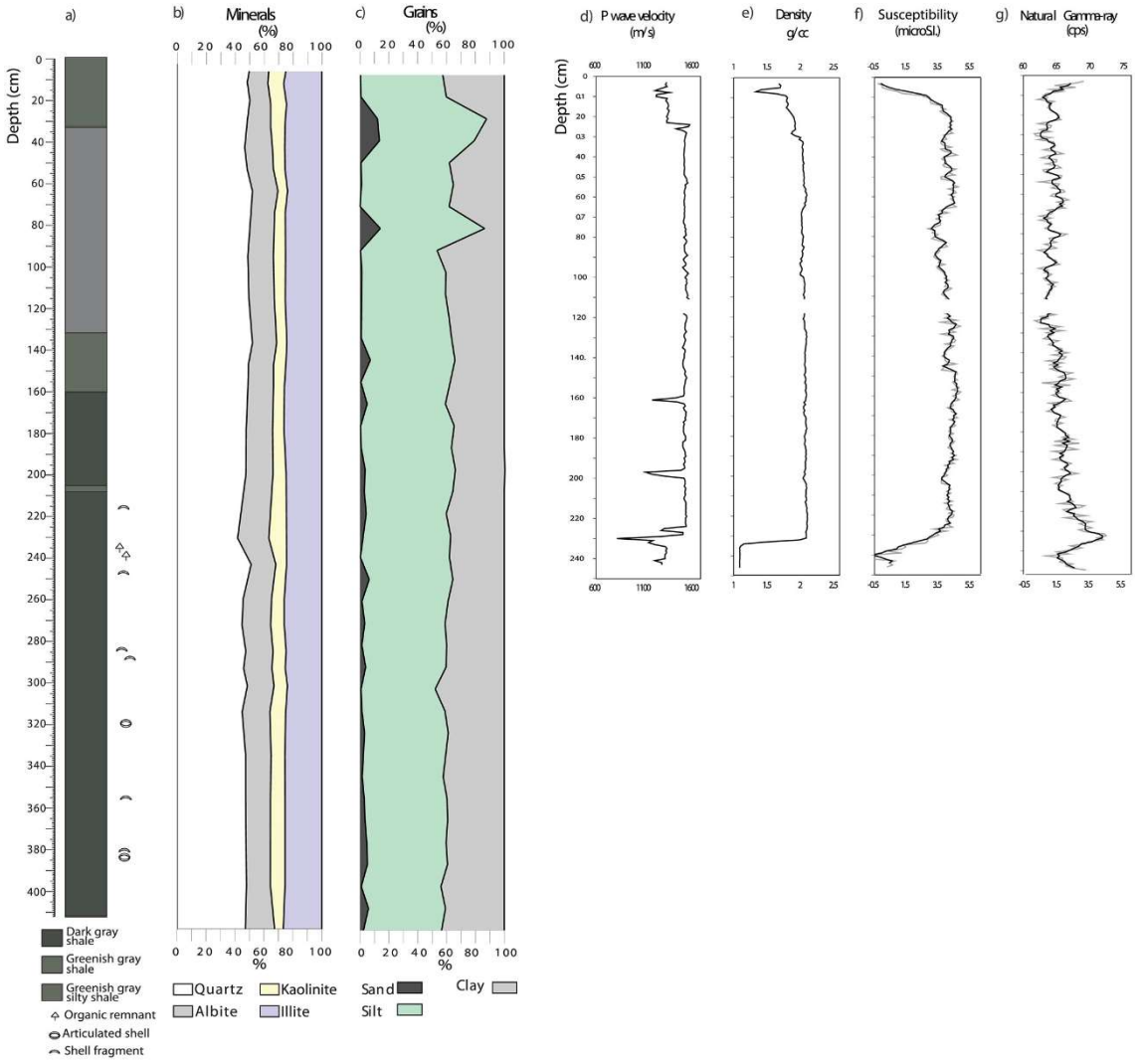


**Fig. 38:Bulk mineralogical and petrophysical property variations. (a) Lithological log, (b) relative abundance of the four main mineral constituents (quartz, albite, kaolinite, and illite), (c) downcore grain size distribution variations expressed as a percentage of the total sediment of the core collected with a vibracorer (Core 9M), and (d–g) multisensor core logger downcore parameter variations for the core collected with a gravity corer (Core 9). Raw susceptibility and natural gamma ray data are shown in light gray, with a running 3-point average in black. (RODELLI et al. 2019)**

### *6.3.6. Magnetic Properties*

The environmental magnetic curves show a distinct pattern, with the uppermost 35 cm having high values for all parameters, especially, ARM, and IRM intensities (fig. 39). Below this depth, the values for the curves drop abruptly and maintain almost constant very low values. Consistently high values of NRM, ARM, and IRM indicate high magnetic mineral concentrations.

- ARM/IRM, also called the magnetic grain size curve, is sensitive to magnetic grain size and high values indicate a high fraction of fine-grained and Single Domain (SD) magnetic crystals (EVANS and HELLER, 2003), which is typical of biogenic magnetite, in the uppermost 30-35 cm of the core. The shift that occurs at 40 cm is consistent with the rapid decrease of concentration of magnetic minerals and an increase in magnetic particle size.
- The S-ratio gives information about the relative concentration of high and low coercivity minerals. S ratio values are consistent with the dominance of magnetite, except at 40 cm, which is consistent with a dominance of hematite
- HIRM curve provides information about the absolute concentration of high coercivity minerals, has similar characteristics to NRM, susceptibility, ARM, and IRM.
- IRM acquisition curves show different behaviour above and below 35 cm. In the uppermost 35 cm the medium-coercivity component, consistent with biogenic magnetite, is accounting for more than 84% of the magnetic signal. Below 35 cm depth, the medium coercivity component has higher dispersion, which indicates that the magnetite is either not biogenic or that the magnetite crystals have undergone some kind of alteration and the hematite contributions increase with depth.
- FORCs (figure 40) have a distinct narrow horizontal central ridge that extends from near Bc = 0 to maximum values at ~30–40 mT, with negligible magnetostatic interactions (vertical axis). This ridge is prominent only in the uppermost 34 cm of the core. Below this depth only the superparamagnetic component is visible.

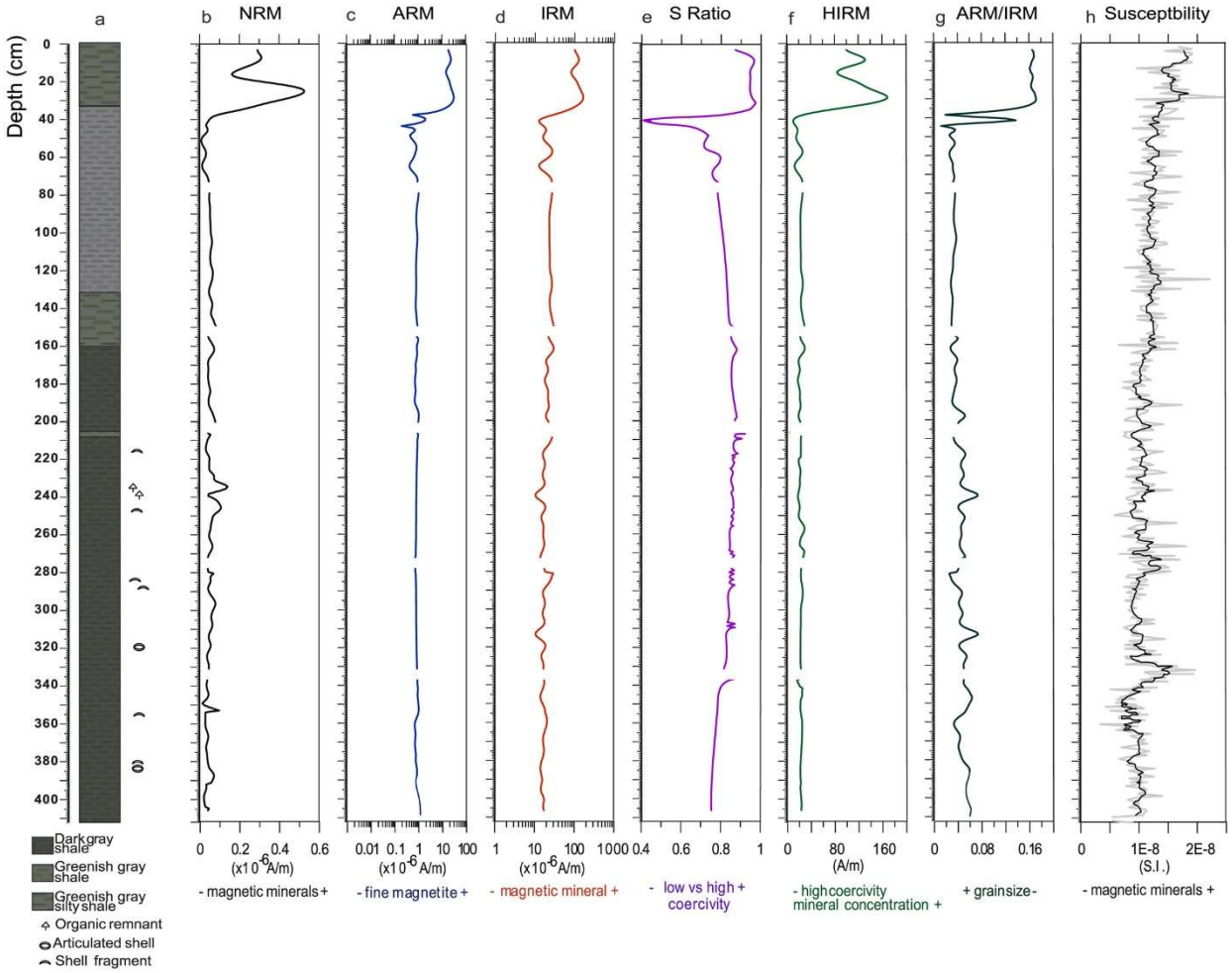


**Fig. 39: Magnetic properties of Mamanguá 9 showing important high values at the top of the core (first 35 cm) and below this depth a substancially homogeneous signal.**

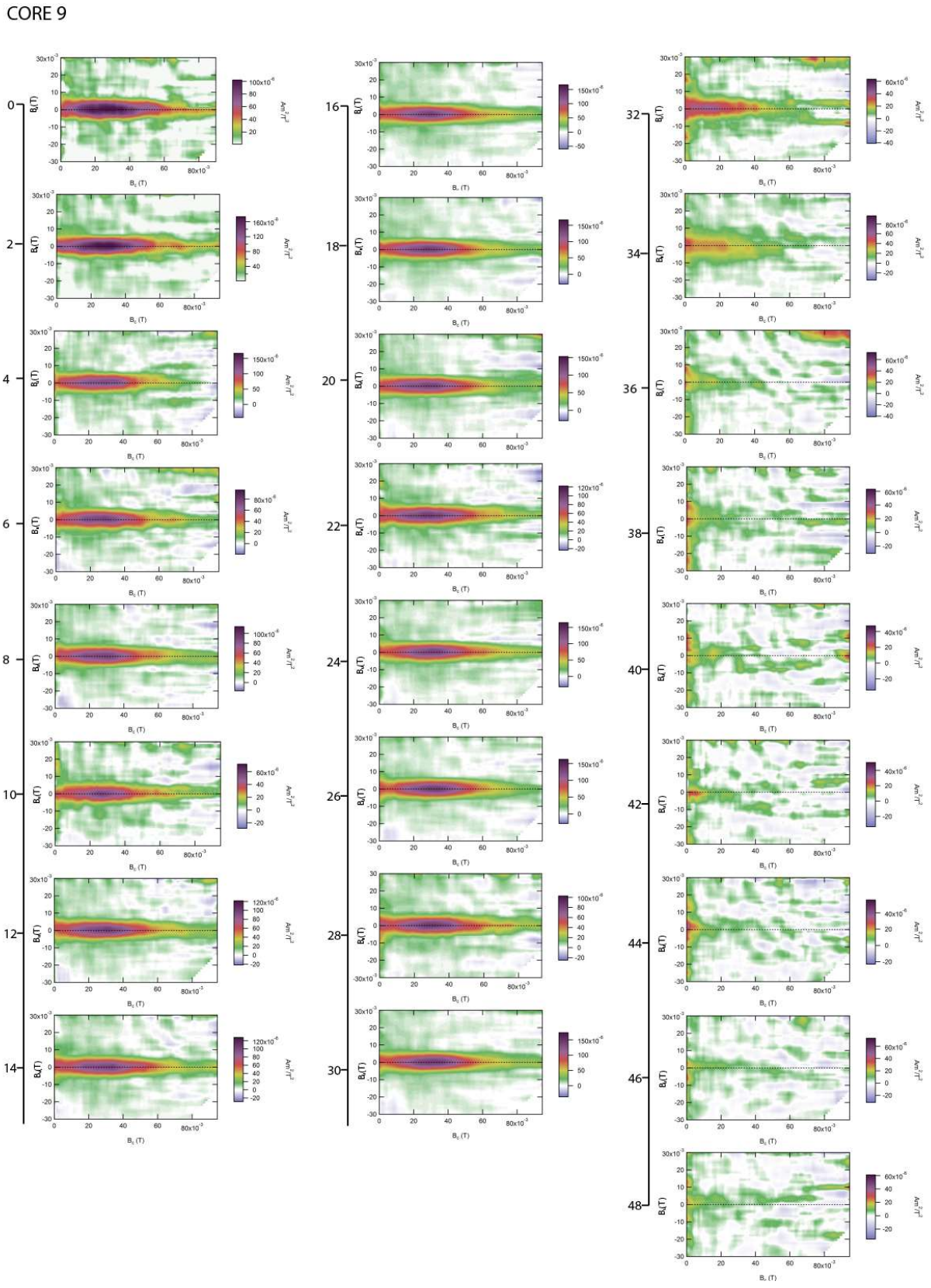


**Fig. 40: FORCs results for Mamanguá core 9. (Rodelli et al.; 2019)**

### *6.4.Discussion*

Environmental magnetic variations and FORCs measurements indicate that the uppermost 32 cm of sediment of the Core 9M from Mamanguá Ría are rich in biogenic magnetite, produced in situ by MTB, mixed with a small proportion of detrital magnetite and hematite coming from weathering of local granites and from pedogenesis (RODELLI et al., 2019). The high biogenic magnetite content present in the uppermost 32 cm of the core indicates that the site represents a favourable environment for MTB production.

Sedimentation rate, detrital magnetic mineral abundance, mineralogy, sediment density, porosity, and grain size did not change significantly during the deposition, so the external supply of key nutrients, such as Fe, is likely to have been relatively constant throughout the studied sediment. The DO content is quite stable for the first 30 cm, decreases gradually between 30 and 50 cm, and falls drastically between 50 and 60 cm. The signal of MTB starts to decrease around 30 cm, where the sample still presents a quite distinct biogenic signal and disappears below 35 cm. Oxygen content is one of the main factors that control the presence of MTB. The abrupt transition between relatively well oxygenated and oxygen depleted sediment is marked by MTB disappearance. MTB magnetite production and preservation is mainly limited by dissolved oxygen contents in the water column and pore waters (ROBERTS et al., 2011; MAO et al., 2014).

Mineralogical data for this core indicate a stable and moderately high total clay content (between 30 and 40% of the total mineralogical composition) throughout the core. There is no appreciable link between the presence of the MTB and the clay content, but it is clear that the environment here presented is really favourable for MTB production as magnetic properties indicate that about 84% of the magnetic signal within the uppermost 30 cm of sediment is due to biogenic magnetite produced in situ by MTB. If we suppose that the clay content in the sediment is at a favourable level and stable throughout the core, the limiting environmental factors for MTB production in this environment would be others, such as pore water oxygen content. Lithological indicators (mineralogy, grain size, and sediment density) and sedimentation rate are essentially constant along the core, which means that variations in the concentration and characteristics of biogenic magnetite depend mostly on pore water chemistry.

### *6.5.Conclusions*

We presented a favourable environment for MTB from the Mamanguá Ría, Brazil, as demonstrated by the high presence of MTB in the surface sediments. The environmental conditions at this site are very stable; sediment supply does not change significantly throughout

the studied core, so that sediment composition and relative nutrient abundances are likely to have been almost constant. Dissolved oxygen content measured in pore waters within the studied sediments is the main factor controlling the presence or absence of living MTB. The abrupt transition between relatively well oxygenated and oxygen depleted sediment is marked by the disappearance of magnetite producing MTB, and by magnetosomes dissolution.

The data presented show that the Mamangua riá is an environment favourable for the MTB, which are highly abundant within the uppermost 32 cm of the sediment. Mineralogical data indicate homogeneous and moderately high total clay content (between 30% and 40% of the total mineralogical composition) throughout the core. There is no appreciable link between the presence of MTB and the clay content, however, since the clay content is high, it might not be a limiting factor in this environment. Therefore, the limiting environmental factors for MTB production are others at this site, such as pore water oxygen content (RODELLI et al. 2019).

# 7 - FINAL CONSIDERATIONS AND CONCLUSIONS

During this PhD work, samples of marine sediments were analysed with XRPD to characterize the mineralogical assemblages with focus on paleoceanographic reconstructions and characterization of the environment in which MTB thrive. As MTB have a potential use as paleoceanographic and paleoenvironmental proxies, understanding the processes that link MTB to their living environments is fundamental to constrain their ecology and therefore define the best use for them as environmental proxy indicators. Since the MTB live within the sediments, it is probable that the sediment composition would have an influence on the ecology of these organisms; characterizing the mineralogical composition of marine sediments in which MTB were found could clarify such relationship, if present. The use of mineralogical assemblages as a tool to reconstruct past and present environmental settings is a very useful tool and has a great potential if used with the appropriate care, we combined the search for a correlations between MTB and mineral compositions with the use of the variations in sedimentary minerals to reconstruct present and past environments.

The two case studies discussed in chapter 4 and 5 of this work are examples where the variation in mineralogical composition of marine sediments reflected important environmental changes, and thus it has been used to reconstruct the evolution of these conditions through time. The mineralogical characterization of the sedimentary mineral assemblage is a versatile tool, which can be used in the most different settings. In particular, we presented a lagoonal-estuarine environment with anthropic interference at 100yr scale and an abyssal setting with climate induced modifications at the 100kyr scale. Both these environments were successfully reconstructed through the characterization of the sedimentary mineral assemblage in a multidisciplinary approach.

In Cananeia we observed a recent marine sediment record in a lagoonal-estuarine environment, and reconstructed the anthropically induced environmental modifications through the sedimentary mineral assemblage. In core U1511B-16R from the TAP we presented the first record of the MECO in an abyssal setting and evidence for deep water acidification during this event.

The mineralogical assemblages are a very sensitive paleoenvironmental proxy, which has to be used with utmost care, in an interdisciplinary multiproxy approach. For this reason, in this work we have complemented the mineralogical data with geochemical, magnetic, and elemental, data. Besides, statistical analyses, especially HAC, are very helpful for identifying variations throughout a core and identify sections with similar characteristics. HAC is important especially

for selecting the samples for more detailed analyses, as it indicates the most representative sample of each cluster.

To understand the importance of the sediment composition, especially clay minerals, in the ecology of MTB, we compared the mineralogical variations throughout each of the three cores presented in the case studies of this work with the presence (or absence) of MTB indicated by magnetic properties. The presence of living and magnetite producing MTB in Cananeia is very low and limited to a very short interval at around 5 cm depth, implying that the living conditions at this site are not favourable. The clay content throughout the core is quite low (between 16 and 25% of the total mineral assemblage), with the highest value in the short interval in which the MTB were found. This suggests that clay can be important for the presence of MTB in this context, however more specific and detailed analyses are necessary to confirm this hypothesis. On the other hand we presented data from the Saco do Mamanguá setting, where MTB are clearly thriving and therefore the environmental conditions for their survival are optimal. In this context, MTB have a strong signal within the uppermost 30 cm of sediment. Below this depth the DO content starts to decrease, and the MTB production and magnetosomes preservation as well. In this setting, the mineralogical variations throughout the sediment core are minimal and the clay content is relatively high, with about 30-40% of the total. If we assume that the clay content is optimal for the survival of the MTB the limiting factor for their production in this settings are others (DO, for example).

In the TAP setting we observed a correlation between the clay composition of the sediment and the presence of the MTB during the MECO interval. When the biogenic silica flux to the sediment decreases and clay minerals increase, then higher MTB production is recorded. The correlation between MS (linked to the presence of MTB in this setting) and Mn might indicate Mn-doping of the MTB, as already observed in laboratory experiments. If this hypothesis is confirmed, then this will be the first record of naturally occurring Mn-doped magnetosomes.

The data produced in this study show that MTB presence seems to be tied to higher levels of clay minerals, as already suggested by Savian et al. (2014). This is especially clear in the TAP, and in Cananeia. The situation is different in Mamanguá, where the mineralogy is rather steady throughout the core. However, in this environment the concentration of clay mineral is rather high, about 30-40% of the total, so in these conditions the oxygen levels seem to be more important for the survival of MTB than the mineralogical composition of the sediment.

Although the data obtained seem to indicate a preference of MTB for sediments with higher clay content, the results are still not conclusive. The main problems in demonstrating the importance of the sediment composition for the ecology of MTB encountered during this PhD

work are related directly to the nature of MTB, which represent a polyphyletic group, and thus the term *"magnetotactic bacterium"* does not have a taxonomic significance. MTB are ubiquitous in aquatic environments, and recently a number of extremophile MTB have been described and include halophilic, alkaliphilic, cryophilic, and thermophilic taxa (BAZYLINSKI and LEFÈVRE, 2013; ABREU et al., 2016; ABREU, 2018). This implies that it is not possible to relate the general term MTB to a specific taxon or mode of life. Although in all our case studies the presence of MTB is concomitant with an increase in the clay mineral fraction, or with sediments with high clay content, we were unable to characterize the MTB species for each study. Even if MTB seem to prefer to live in clay-rich sediments, the variables influencing their survival are many and a more extensive study should be conducted, including many factors alongside the mineralogical composition of the environment, first of all the taxonomic classification of the studied bacteria, which has not been possible to do in this study. A more extensive study will require the selection of well-defined MTB communities in collaboration with biologists to get accurate taxonomic and corresponding life mode constraints.

# 8 -REFERENCES

ABREU, F.; ACOSTA-AVALOS, D. Biology and physics of magnetotactic bacteria. *Metagenomics-Basics, Methods and Applications*. IntechOpen, 2018.

ALMEIDA, F. F. O cr_aton do sao francisco e suas faixas marginais de dobramentos.*Congresso Brasileiro de Geologia.* 1976. v. 29.

ALPHANDÉRY, E. Applications of magnetosomes synthesized by magnetotactic bacteria in medicine. *Frontiers in bioengineering and biotechnology*, Frontiers, v. 2, p. 5, 2014.

ANAGNOSTOU, E. et al. Changing atmospheric co 2 concentration was the primary driver of early cenozoic climate. *Nature*, Nature Publishing Group, v. 533, n. 7603, p. 380-384, 2016.

BALACHANDRAN, U.; EROR, N. Raman spectra of titanium dioxide. *Journal of Solid State Chemistry*, Academic Press, v. 42, n. 3, p. 276-282, 1982.

BALZER, W. On the distribution of iron and manganese at the sediment/water interface: thermodynamic versus kinetic control. *Geochimica et Cosmochimica Acta*, Elsevier, v. 46, n. 7, p. 1153-1161, 1982.

BAZYLINSKI, D. A.; FRANKEL, R. B. Magnetosome formation in prokaryotes. *Nature Reviews Microbiology,* Nature Publishing Group, v. 2, n. 3, p. 217 -230, 2004.

BAZYLINSKI, D. A. et al. Controlled biomineralization of magnetite ($Fe_3O_4$) and greigite ($Fe_3S_4$) in a magnetotactic bacterium. *Appl. Environ. Microbiol*., Am Soc Microbiol, v. 61, n. 9, p. 3232-3239, 1995.

BAZYLINSKI, D. A.; LEFÈVRE, C. T. Magnetotactic bacteria from extreme environments. *Life*, Multidisciplinary Digital Publishing Institute, v. 3, n. 2, p. 295-307,2013.

BAZYLINSKI, D. A.; SCHUBBE, S. Controlled biomineralization by and applications of magnetotactic bacteria. *Advances in applied microbiology*, Elsevier, v. 62, p. 21-62, 2007.

BAZYLINSKI, D. A.; WILLIAMS, T. J. Ecophysiology of magnetotactic bacteria. *Magnetoreception and magnetosomes in bacteria.* Springer, 2006. p. 37-75.

BAZYLIZINKI, D. A. et al. $Fe_3O_4$ and $Fe_3S_4$ in a bacterium. *Nature*, Springer, v. 366, n. 6452,. 218-218, 1993.

BENITES, M. et al. Shallow gas occurrence in a Brazilian ría (saco do mamanguá, Rio de Janeiro) inferred from high-resolution seismic data. *Continental Shelf Research, Elsevier*,v. 108, p. 89 -96, 2015.

BERBEL, G. B.; FAVARO, D. I.; BRAGA, E. S. Impact of harbour, industry and sewage on the phosphorus geochemistry of a subtropical estuary in Brazil. *Marine pollution bulletin*, Elsevier, v. 93, n. 1-2, p. 44 -52, 2015.

BÉRGAMO, A. L. Características da hidrografía, circulação e transporte de sal: Barra de Cananéia, Sul do mar de Cananéia e Barra do Trapandé. Tese (Doutorado) Universidade de São Paulo, 2000.

BERNARDES, R. A.; YAMAGUTI, N. Estrutura e dinâmica da ictiofauna do saco de mamanguá (Paraty-RJ). 1996.

BERNARDINI, S. et al. Raman spectra of natural manganese oxides. *Journal of Raman Spectroscopy*, Wiley Online Library, v. 50, n. 6, p. 873 -888, 2019.

BERNER, R. A. Sedimentary pyrite formation: an update. *Geochimica et cosmochimica Acta*, Elsevier, v. 48, n. 4, p. 605 -615, 1984.

BEZDEK, J.; EHRLICH, R. Numerical methods for fuzzy clustering. *Comput. Geosci*, v. 10, p. 191 -203, 1984.

BIJL, P. K. et al. Transient middle eocene atmospheric co2 and temperature variations. *Science*, American Association for the Advancement of Science, v. 330, n. 6005, p. 819 -821, 2010.

BISCAYE, P. E. Mineralogy and sedimentation of recent deep-sea clay in the Atlantic ocean and adjacent seas and oceans. *Geological Society of America Bulletin*, Geological Society of America, v. 76, n. 7, p. 803 -832, 1965.

BLAKEMORE, R. Magnetotactic bacteria. *Science,* American Association for the Advancement of Science, v. 190, n. 4212, p. 377 -379, 1975.

BLOEMENDAL, J. et al. Rock magnetism of late neogene and pleistocene deep-sea sediments: Relationship to sediment source, diagenetic processes, and sediment lithology. *Journal of Geophysical Research: Solid Earth*, Wiley Online Library, v. 97, n. B4, p. 4361 -4375, 1992.

BOHATY, S. M.; ZACHOS, J. C. Significant southern ocean warming event in the late middle eocene. *Geology*, Geological Society of America, v. 31, n. 11, p. 1017 -1020, 2003.

BOHATY, S. M. et al. Coupled greenhouse warming and deep-sea acidi_cation in the middle eocene. *Paleoceanography*, Wiley Online Library, v. 24, n. 2, 2009.

BONETTI FILHO, J.; MIRANDA, L. B. d. Estimativa da descarga de água doce no sistema estuarino-lagunar de cananéia-Iguapé. *Revista Brasileira de Oceanografia*, SciELO Brasil, v. 45, n. 1-2, p. 89 -94, 1997.

BRAGA, E. S. et al. Eutrophication and bacterial pollution caused by industrial and domestic wastes at the baixada santista estuarine system -Brazil. *Marine Pollution Bulletin*, Elsevier, v. 40, n. 2, p. 165 -173, 2000.

CALVERT, S.; PEDERSEN, T. Geochemistry of recent oxic and anoxic marine sediments: implications for the geological record. *Marine geology*, Elsevier, v. 113, n. 1-2, p. 67 -88, 1993.

CALVERT, S.; PEDERSEN, T. Sedimentary geochemistry of manganese; implications for the environment of formation of manganiferous black shales. *Economic Geology,* Society of Economic Geologists, v. 91, n. 1, p. 36 -47, 1996.

CALVERT, S. et al. On the organic carbon maximum on the continental slope of the eastern arabian sea. *Journal of Marine Research*, Sears Foundation for Marine Research, v. 53, n. 2, p. 269 -296, 1995.

CANFIELD, D. E.; THAMDRUP, B. Towards a consistent classfication scheme for geochemical environments, or, why we wish the term ‘suboxic’ would go away. *Geobiology*, Wiley Online Library, v. 7, n. 4, p. 385 -392, 2009.

CASTAING, P.; GUILCHER, A. Geomorphology and sedimentology of rias. *Developments in sedimentology*.Elsevier, 1995. v. 53, p. 69 -111.

CHALMIN, E.; FARGES, F.; BROWN, G. E. A pre-edge analysis of mn k-edge xanes spectra to help determine the speciation of manganese in minerals and glasses. *Contributions to Mineralogy and Petrology*, Springer, v. 157, n. 1, p. 111 -126, 2009.

CHAMLEY, H. North atlantic clay sedimentation and paleoenvironment since the late jurassic. Deep Drilling Results in the Atlantic Ocean: continental margins and paleoenvironment, Wiley Online Library, v. 3, p. 342 -361, 1979.

CHAMLEY, H. Clay formation through weathering. *Clay sedimentology*. Springer, 1989. p. 21-50.

CHAMLEY, H. *Clay sedimentology*. Springer Science & Business Media, 2013.

CHANG, L. et al. Coupled microbial bloom and oxygenation decline recorded by magnetofossils during the palaeocene -eocene thermal maximum. *Nature communications*, Nature Publishing Group, v. 9, n. 1, p. 1 -9, 2018.

CHANG, L. et al. Giant magnetofossils and hyperthermal events. *Earth and Planetary Science Letters*, Elsevier, v. 351, p. 258 -269, 2012.

CHANG, L. et al. Low-temperature magnetic properties of pelagic carbonates: Oxidation of biogenic magnetite and identification of magnetosome chains. *Journal of Geophysical Research:* Solid Earth, Wiley Online Library, v. 118, n. 12, p. 6049 -6065, 2013.

CHUKANOV, N. V. Ir spectra of minerals and reference samples data. *Infrared spectra of mineral species*. Springer, 2014. p. 21 -1701.

CHUNG, F. H. Quantitative interpretation of x-ray diffraction patterns of mixtures. matrix-ushing method for quantitative multicomponent analysis. *Journal of Applied Crystallography,* International Union of Crystallography, v. 7, n. 6, p. 519 -525, 1974.

CORNAGGIA, F. et al. Diversions of the ribeira river flow and their influence on sediment supply in the Cananeia-Iguapé estuarine-lagoonal system (SE Brazil). *Frontiers in Earth Science*, Frontiers, v. 6, p. 25, 2018.

CRAMWINCKEL, M. J. et al. Synchronous tropical and polar temperature evolution in the eocene. *Nature*, Nature Publishing Group, v. 559, n. 7714, p. 382 -386, 2018.

CRAMWINCKEL, M. J. et al. Surface-circulation change in the southern ocean across the middle eocene climatic optimum: inferences from dinoagellate cysts and biomarker paleothermometry.

DAVIS, B. et al. Wellsite mineralogical data acquisition; understanding results from multiple analytical sources. SOCIETY OF PETROLEUM ENGINEERS. SPE European Formation Damage Conference and Exhibition. 2015.

DAY, R.; FULLER, M.; SCHMIDT, V. Hysteresis properties of titanomagnetites: grain-size and compositional dependence. *Physics of the Earth and planetary interiors*, Elsevier, v. 13, n. 4, p. 260 -267, 1977.

DEKKERS, M. et al. Fuzzy c-means cluster analysis of early diagenetic effects on natural remanent magnetisation acquisition in a 1.1 myr piston core from the central Mediterranean. *Physics of the Earth and Planetary Interiors*, Elsevier, v. 85, p. 155 -171, 1994.

DELONG, E. F.; FRANKEL, R. B.; BAZYLINSKI, D. A. Multiple evolutionary origins of magnetotaxis in bacteria. *Science*, American Association for the Advancement of Science, v. 259, n. 5096, p. 803 -806, 1993.

DELONG, E. F.; FRANKS, D. G.; ALLDREDGE, A. L. Phylogenetic diversity of aggregate-attached vs. free-living marine bacterial assemblages. *Limnology and Oceanography*, Wiley Online Library, v. 38, n. 5, p. 924 -934, 1993.

DILLON, M.; BLEIL, U. Rock magnetic signatures in diagenetically altered sediments from the niger deep-sea fan. *Journal of Geophysical Research: Solid Earth*, Wiley Online Library, v. 111, n. B3, 2006.

DOWNS, R. T.; HALL-WALLACE, M. *The american mineralogist crystal structure database*. American Mineralogist, Mineralogical Society of America, v. 88, n. 1, p. 247 -250, 2003.

DUNLOP, D. J.; OZDEMIR, O. *Rock magnetism: fundamentals and frontiers*. Cambridge university press, 2001. v. 3.

EDGAR, K. et al. New biostratigraphic, magnetostratigraphic and isotopic insights into the middle eocene climatic optimum in low latitudes. *Palaeogeography, Palaeoclimatology, Palaeoecology*, Elsevier, v. 297, n. 3-4, p. 670 -682, 2010.

EGLI, R. Characterization of individual rock magnetic components by analysis of remanence curves. 3. bacterial magnetite and natural processes in lakes. *Physics and Chemistry of the Earth*, Parts A/B/C, Elsevier, v. 29, n. 13-14, p. 869 -884, 2004.

EGLI, R. et al. Detection of noninteracting single domain particles using first-order reversal curve diagrams. Geochemistry, Geophysics, Geosystems, Wiley Online Library, v. 11, n. 1, 2010.

ESLINGER, E.; PEVEAR, D. R. Clay minerals for petroleum geologists and engineers , 1988.

EVANS, M.; HELLER, F. Environmental magnetism: principles and applications of enviromagnetics. Elsevier, 2003.

FAIVRE, D.; SCHULER, D. Magnetotactic bacteria and magnetosomes. *Chemical Reviews*, v. 108, n. 11.

FAIVRE, D.; SCHULER, D. Magnetotactic bacteria and magnetosomes. *Chemical Reviews*, ACS Publications, v. 108, n. 11, p. 4875 -4898, 2008.

FAN, C. et al. The mineralogical characterization of argentian cryptomelane from xiangguang mn -ag deposit, north china. *Journal of Mineralogical and Petrological Sciences*, Japan Association of Mineralogical Sciences, v. 110, n. 5, p. 214 -223, 2015.

FARIA, D. L. A. de; L_OPES, F. N. Heated goethite and natural hematite: can raman spectroscopy be used to di_erentiate them? *Vibrational Spectroscopy*, Elsevier, v. 45, n. 2, p. 117 -121, 2007.

FIGUEIRA, R. C. L. Inventory of artifcial radionuclides in seawater and marine sediments from southern coast of Brazil. 2000.

FILHO, J. B.; MIRANDA, L. B. d. Estimativa da descarga de água doce no sistema estuarino-lagunar de Cananeia-Iguapé. *Revista Brasileira de Oceanografia*, SciELO Brasil, v. 45, n. 1-2, p. 89 -94, 1997.

FRANK, U.; NOWACZYK, N. R. Mineral magnetic properties of artificial samples systematically mixed from haematite and magnetite. *Geophysical Journal International*, Blackwell Publishing Ltd Oxford, UK, v. 175, n. 2, p. 449 -461, 2008.

GAINA, C. et al. The tectonic history of the tasman sea: a puzzle with 13 pieces. *Journal of Geophysical Research: Solid Earth*, Wiley Online Library, v. 103, n. B6, p. 12413 -12433, 1998.

GALAZZO, F. B. et al. The middle eocene climatic optimum (meco): A multiproxy record of paleoceanographic changes in the southeast atlantic (odp site 1263, walvis ridge). *Paleoceanography*, Wiley Online Library, v. 29, n. 12, p. 1143 -1161, 2014.

GARMING, J.; BLEIL, U.; RIEDINGER, N. Alteration of magnetic mineralogy at the sulfate -methane transition: analysis of sediments from the argentine continental slope. *Physics of the Earth and Planetary Interiors*, Elsevier, v. 151, n. 3-4, p. 290 -308, 2005.

GEISSMAN, J. Environmental magnetism: principles and applications of enviromagnetics. *Eos, Transactions American Geophysical Union*, Wiley Online Library, v. 85, n. 20, p. 202 -202, 2004.

GEOBRAS FUNDAÇÕES. *Complexo valo grande, mar pequeno, rio ribeira de Iguapé*. Relatório Geobras. S/A, Engenharia e Fundações para o Serviço do Vale do Ribeira do Departamento de Águas e Energia Elétrica, SP, v. 2, 1966.

GIORGIONI, M. et al. Carbon cycle instability and orbital forcing during the middle eocene climatic optimum. *Scientific Reports*, Nature Publishing Group, v. 9, n. 1, p. 1 -10, 2019.

GIORGIONI, M. et al. Environmental and climatic response during the middle eocene climatic optimum in the western tethys (baskil section, turkey). *AGU Fall Meeting 2019*

GORBY, Y. A.; BEVERIDGE, T. J.; BLAKEMORE, R. P. Characterization of the bacterial magnetosome membrane. *Journal of Bacteriology*, Am Soc Microbiol, v. 170, n. 2, p. 834 -841, 1988.

GRASSHOFF, K.; EHRHARDT, M.; KREMLING, K. Methods of seawater analysis. Verlag chemie gmbh. Weinheim. *Phys. Chem. Lett*, v. 55, n. 2014, p. 1953, 1983.

GRAY, J. S.; WU, R. S.-s.; OR, Y. Y. E_ects of hypoxia and organic enrichment on the coastal marine environment. *Marine ecology progress series*, v. 238, p. 249 -279, 2002.

GRIFFIN, J. J.; WINDOM, H.; GOLDBERG, E. D. The distribution of clay minerals in the world ocean. *Deep Sea Research and Oceanographic Abstracts*. Elsevier. 1968. v. 15, n. 4, p. 433 -459.

HALASZ, I. et al. Real-time in situ powder x-ray di_raction monitoring of mechanochemical synthesis of pharmaceutical cocrystals. *Angewandte Chemie International Edition*, Wiley Online Library, v. 52, n. 44, p. 11538 -11541, 2013.

HARASKO, G. et al. Determination of the concentration of magnetotactic bactéria by means of susceptibility measurements. *Japanese journal of applied physics*, IOP Publishing, v. 32, n. 1R, p. 252, 1993.

HARRISON, R. J.; FEINBERG, J. M. Forcinel: An improved algorithm for calculating first-order reversal curve distributions using locally weighted regression smoothing. *Geochemistry, Geophysics, Geosystems*, Wiley Online Library, v. 9, n. 5, 2008.

HASSAN, M. B. et al. Presence of biogenic magnetite in ferromanganese nodules. *Environmental Microbiology Reports*, Wiley Online Library.

HESLOP, D.; MCINTOSH, G.; DEKKERS, M. Using time-and temperature-dependent preisach models to investigate the limitations of modelling isothermal remanent magnetization acquisition curves with cumulative log gaussian functions. *Geophysical Journal International*, Blackwell Publishing Ltd Oxford, UK, v. 157, n. 1, p. 55 -63, 2004.

HESLOP, D.; ROBERTS, A. P.; CHANG, L. Characterizing magnetofossils from first-order reversal curve (forc) central ridge signatures. *Geochemistry, Geophysics, Geosystems*, Wiley Online Library, v. 15, n. 6, p. 2170 -2179, 2014.

HESSE, Paul P. "Evidence for bacterial palaeoecological origin of mineral magnetic cycles in oxic and sub-oxic Tasman Sea sediments." *Marine Geology, v.*117, n.1-4 p. 1-17, 1994.

HILLIER, S. et al. Role of quantitative mineralogical analysis in the investigation of sites contaminated by chromite ore processing residue. *Science of the Total Environment*, Elsevier, v. 308, n. 1-3, p. 195 -210, 2003.

IACOVIELLO, F. et al. Evolution with depth from detrital to authigenic smectite in sediments from and-2a drill core (mcmurdo sound, antarctica). *Clay Minerals*, De Gruyter, v. 47, n. 4, p. 481 -498, 2012.

ILIEV, M.; HADJIEV, V.; LITVINCHUK, A. Raman and infrared spectra of brookite (TiO2): experiment and theory. Vibrational Spectroscopy, Elsevier, v. 64, p. 148 -152, 2013.

INGLIS, G. N. et al. Descent toward the icehouse: Eocene sea surface cooling inferred from gdgt distributions. Paleoceanography, Wiley Online Library, v. 30, n. 7, p. 1000 -1020, 2015.

ITALIANI, D. M.; MAHIQUES, M. M. O registro geológico da atividade antropogênica na região do valo grande, estado de São Paulo, Brasil. *Quaternary and Environmental Geosciences*, v. 5, n. 2, 2014.

JOGLER, C.; SCHULER, D. Genomics, genetics, and cell biology of magnetosome formation. *Annual review of microbiology*, Annual Reviews, v. 63, p. 501 -521, 2009.

JOVANE, L. et al. Prismatic magnetite magnetosomes from cultivated magnetovibrio blakemorei strain mv-1: a magnetic fingerprint in marine sediments? *Environmental Microbiology Reports*, Wiley Online Library, v. 4, n. 6, p. 664 -668, 2012.

JOVANE, L. et al. The middle eocene climatic optimum event in the contessa highway section, umbrian apennines, italy. *Geological Society of America Bulletin*, Geological Society of America, v. 119, n. 3-4, p. 413 -427, 2007.

JOVANE, L. et al. Magnetic methods and the timing of geological processes. *Geological Society, London, Special Publications*, Geological Society of London, v. 373, n. 1, p. 1 -12, 2013.

JOVANE, L. et al. Astronomical calibration of the middle eocene contessa highway section (Gubbio, Italy). *Earth and Planetary Science Letters*, Elsevier, v. 298, n. 1-2, p. 77 -88, 2010.

KEIM, C. N.; LINS, U.; FARINA, M. Manganese in biogenic magnetite crystals from magnetotactic bacteria. *FEMS microbiology letters*, Blackwell Publishing Ltd Oxford, UK, v. 292, n. 2, p. 250 -253, 2009.

KING, J. W.; CHANNELL, J. E. Sedimentary magnetism, environmental magnetism, and magnetostratigraphy. *Reviews of Geophysics*, Wiley Online Library, v. 29, n. S1, p. 358 -370, 1991.

KIRSCHVINK, J. The least-squares line and plane and the analysis of palaeomagnetic data. Geophysical Journal International, Oxford University Press, v. 62, n. 3, p. 699 -718, 1980.

KOMEILI, A. et al. Magnetosomes are cell membrane invaginations organized by the actin-like protein mamk. *Science*, American Association for the Advancement of Science, v. 311, n. 5758, p. 242 -245, 2006.

KOPP, R. E.; KIRSCHVINK, J. L. The identification and biogeochemical interpretation of fossil magnetotactic bacteria. *Earth-Science Reviews*, Elsevier, v. 86, n. 1-4, p. 42 -61, 2008.

LANGMUIR, D. Aqueous environmental. *Geochemistry Prentice Hall*, NJ, 1997.

LARRASOANA, J. C. et al. Magnetotactic bacterial response to antarctic dust supply during the palaeocene -eocene thermal maximum. *Earth and Planetary Science Letters*, Elsevier, v. 333, p. 122 -133, 2012.

LEFÉVRE, C. T.; BAZYLINSKI, D. A. Extremophilic magnetotactic bacteria. *Polyextremophiles.*Springer, 2013. p. 581 -595.

LEFÉVRE, C. T.; FRANKEL, R. B.; BAZYLINSKI, D. A. *Magnetotaxis in prokaryotes*. eLS, Wiley Online Library, 2001.

LIN, W.; PAN, Y. ; BAZYLINSKI, D. A. *Diversity and ecology of and biomineralization by magnetotactic bacteria.* Environmental microbiology reports, v. 9, n. 4, p. 345-356, 2017.

LOWENSTAM, H. A. Minerals formed by organisms. *Science,* American Association for the Advancement of Science, v. 211, n. 4487, p. 1126 -1131, 1981.

MAHIQUES, M. M. d. et al. Anthropogenic inuences in a lagoonal environment: a multiproxy approach at the valo grande mouth, Cananéia-Iguapé system (SE Brazil). *Brazilian Journal of Oceanography*, SciELO Brasil, v. 57, n. 4, p. 325 -337, 2009.

MAHIQUES, M. M. de et al. 150 years of anthropogenic metal input in a biosphere reserve: the case study of the Cananéia-Iguapé coastal system, southeastern Brazil. *Environmental earth sciences*, Springer, v. 68, n. 4, p. 1073 -1087, 2013.

MANDERNACK, K. W.; POST, J.; TEBO, B. M. Manganese mineral formation by bacterial spores of the marine bacillus, strain sg-1: evidence for the direct oxidation of Mn (ii) to Mn (iv). Geochimica et Cosmochimica Acta, Elsevier, v. 59, n. 21, p. 4393 -4408, 1995.

MAO, X. et al. Magnetotaxis and acquisition of detrital remanent magnetization by magnetotactic bacteria in natural sediment: _rst experimental results and theory. *Geochemistry, Geophysics, Geosystems*, Wiley Online Library, v. 15, n. 1, p. 255 -283, 2014.

MARINOV, I. et al. Impact of oceanic circulation on biological carbon storage in the ocean and atmospheric pco2. Global Biogeochemical Cycles, Wiley Online Library, v. 22, n. 3, 2008.

MARVEL, K.; BONFILS, C. Identifying external inuences on global precipitation. *Proceedings of the National Academy of Sciences*, National Acad Sciences, v. 110, n. 48, p. 19301 -19306, 2013.

MATHURIYA, A. S. Magnetotactic bacteria: nanodrivers of the future. *Critical reviews in biotechnology*, Taylor & Francis, v. 36, n. 5, p. 788 -802, 2016.

MATSUNAGA, T.; OKAMURA, Y. Genes and proteins involved in bacterial magnetic particle formation. *Trends in microbiology*, Elsevier, v. 11, n. 11, p. 536 -541, 2003.

MATSUNAGA, T.; TADOKORO, F.; NAKAMURA, N. Mass culture of magnetic bacteria and their application to ow type immunoassays. *IEEE transactions on magnetics*, IEEE, v. 26, n. 5, p. 1557 -1559, 1990.

MATTHIES, M.; BICKERT, T.; PAUL, A. Last glacial 13 c distribution and deep-sea circulation in the atlantic ocean: a model-data comparison. *The South Atlantic in the Late Quaternary.* Springer, 2003. p. 695 -722.

MOEBIUS, I.; FRIEDRICH, O.; SCHER, H. D. Changes in southern ocean bottom water environments associated with the middle eocene climatic optimum (MECO). *Palaeogeography, palaeoclimatology, palaeoecology*, Elsevier, v. 405, p. 16 -27, 2014.

NELSON, C. S.; COOKE, P. J. History of oceanic front development in the new zealand sector of the southern ocean during the cenozoic: a synthesis. *New Zealand Journal of geology and geophysics*, Taylor & Francis, v. 44, n. 4, p. 535 -553, 2001.

NEVES, P. A. et al. Radioanalytical assessment of sedimentation rates in Guajara bay (Amazon estuary, N Brazil): a study with unsupported $^{210}$Pb and $^{137}$Cs modeling. *Journal of radioanalytical and nuclear Chemistry*, Springer, v. 299, n. 1, p. 407 -414, 2014.

OZIMA, M.; LARSON, E. Low-and high-temperature oxidation of titanomagnetite in relation to irreversible changes in the magnetic properties of submarine basalts. *Journal of Geophysical Research*, Wiley Online Library, v. 75, n. 5, p. 1003 -1017, 1970.

PETERSEN, N.; DOBENECK, T. von; VALI, H. Fossil bacterial magnetite in deep-sea sediments from the south atlantic ocean. *Nature*, Springer, v. 320, n. 6063, p. 611 -615, 1986.

PETERSEN, N.; WEISS, D. G.; VALI, H. Magnetic bacteria in lake sediments. *Geomagnetism and palaeomagnetism.* Springer, 1989. p. 231 -241.

PÓSFAI, M.; KASAMA, T.; DUNIN-BORKOWSKI, R. E. Characterization of bacterial magnetic nanostructures using high-resolution transmission electron microscopy and off-axis electron holography. *Magnetoreception and magnetosomes in bacteria*. Springer, 2006. p. 197 -225.

POSTEC, A. et al. Magnetotactic bacteria in microcosms originating from the french mediterranean coast subjected to oil industry activities. *Microbial ecology*, Springer, v. 63, n. 1, p. 1 -11, 2012.

PROZOROV, T. et al. Manganese incorporation into the magnetosome magnetite: magnetic signature of doping. *European Journal of Mineralogy*, E. Schweizerbart'sche Verlagsbuchhandlung Science Publishers, v. 26, n. 4, p. 457 -471, 2014.

RAJAN, H. et al. Building the american mineralogist crystal structure database: a recipe for construction of a small internet database. SPECIAL PAPERS-GEOLOGICAL SOCIETY OF AMERICA, Boulder, Colorado; Geological Society of America; 1999, v. 397,p. 73, 2006.

RASMUSSEN, Edie M. "Clustering algorithms." *Information retrieval: data structures & algorithms* 419 (1992): 442.

RATEEV, M. et al. The distribution of clay minerals in the oceans. *Sedimentology*, Wiley Online Library, v. 13, n. 1-2, p. 21 -43, 1969.

REGO, E. S. et al. Mineralogical evidence for warm and dry climatic conditions in the neo-Tethys (eastern turkey) during the middle eocene. *Palaeogeography, palaeoclimatology, palaeoecology*, Elsevier, v. 501, p. 45 -57, 2018.

REITNER, J. et al. Methane-derived carbonate build-ups and associated microbial communities at cold seeps on the lower crimean shelf (black sea). *Facies*, Springer, v. 51, n. 1-4, p. 66 -79, 2005.

RICCOMINI, C. Padrão de fraturamentos do maciço alcalino de Cananeia, estado de São Paulo: relações com a tectônica mesozoica do sudeste do Brasil. *Revista Brasileira de Geociências*, v. 25, n. 2, p. 79 -84, 1995.

RICCOMINI, C. . Padrão de fraturamentos do maciço alcalino de Cananeia, estado de São Paulo: relações com a tectônica mesozoico-cenozoica do sudeste do Brasil. *Revista Brasileira de Geociências*, v. 25, n. 2, p. 79 -84, 2017.

ROBBINS, J. A.; EDGINGTON, D. N. Determination of recent sedimentation rates in lake michigan using 210Pb and 137Cs. *Geochimica et Cosmochimica acta*, Elsevier, v. 39, n. 3, p. 285 -304, 1975.

ROBERT, C.; CHAMLEY, H. Paleoenvironmental signi_cance of clay mineral associations at the cretaceous-tertiary passage. *Palaeogeography, Palaeoclimatology, Palaeoecology*, Elsevier, v. 79, n. 3-4, p. 205 -219, 1990.

ROBERTS, A. P. et al. Resolving the origin of pseudo-single domain magnetic behavior. *Journal of Geophysical Research: Solid Earth*, Wiley Online Library, v. 122, n. 12, p. 9534 - 9558, 2017.

ROBERTS, A. P. et al. Searching for single domain magnetite in the pseudo-single domain sedimentary haystack: Implications of biogenic magnetite preservation for sediment magnetism and relative paleointensity determinations. *Journal of Geophysical Research: Solid Earth*, Wiley Online Library, v. 117, n. B8, 2012.

ROBERTS, A. P. et al. Magnetotactic bacterial abundance in pelagic marine environments is limited by organic carbon ux and availability of dissolved iron. *Earth and Planetary Science Letters*, Elsevier, v. 310, n. 3-4, p. 441 -452, 2011.

ROBERTS, A. P.; PIKE, C. R.; VEROSUB, K. L. First-order reversal curve diagrams: A new tool for characterizing the magnetic properties of natural samples. *Journal of Geophysical Research: Solid Earth*, Wiley Online Library, v. 105, n. B12, p. 28461 -28475, 2000.

ROBOTTI, N. The discovery of X-ray diffraction. *Rendiconti Lincei*, Springer, v. 24, n. 1, p. 7 -18, 2013.

RODELLI, D. et al. Diagenetic fate of biogenic soft and hard magnetite in chemically stratified sedimentary environments of Mamanguá ría, Brazil. *Journal of Geophysical Research: Solid Earth*, Wiley Online Library, v. 124, n. 3, p. 2313 -2330, 2019.

RODELLI, D. et al. High-resolution integrated magnetobiostratigraphy of a new middle eocene section from the neotethys (elazig basin, eastern turkey). *GSA Bulletin*, GeoScienceWorld, v. 130, n. 1-2, p. 193 -207, 2018.

ROHL, U. et al. Sea level and astronomically induced environmental changes in middle and late eocene sediments from the east tasman plateau. *Washington DC American Geophysical Union Geophysical Monograph Series*, v. 151, p. 127 -151, 2004.

ROY, S. Genetic diversity of manganese deposition in the terrestrial geological record. *Special Publications,* Geological Society of London, v. 119, n. 1, p. 5 -27, 1997.

SAKAGUCHI, T.; ARAKAKI, A.; MATSUNAGA, T. Desulfovibrio magneticus sp. nov., a novel sulfate-reducing bacterium that produces intracellular single-domain-sized magnetite particles. *International journal of systematic and evolutionary microbiology*, Microbiology Society, v. 52, n. 1, p. 215 -221, 2002.

SAVIAN, J. F. et al. Enhanced primary productivity and magnetotactic bacterial production in response to middle eocene warming in the neo-tethys ocean. *Palaeogeography, Palaeoclimatology, Palaeoecology*, Elsevier, v. 414, p. 32 -45, 2014.

SAVIAN, J. F. et al. Environmental magnetic implications of magnetofossil occurrence during the middle eocene climatic optimum (MECO) in pelagic sediments from the equatorial indian ocean. *Palaeogeography, palaeoclimatology, palaeoecology*, Elsevier, v. 441, p. 212 -222, 2016.

SCHAEFFER-NOVELLI, Y. et al.. The Cananeia lagoon estuarine system, São Paulo, Brazil. Estuaries, Springer, v. 13, n. 2, p. 193 -203, 1990.

SCHULER, D.; BAEUERLEIN, E. Dynamics of iron uptake and $Fe_3O_4$ biomineralization during aerobic and microaerobic growth of magnetospirillum gryphiswaldense. *Journal of bacteriology*, Am Soc Microbiol, v. 180, n. 1, p. 159 -162, 1998.

SCHUMANN, D. et al. Gigantism in unique biogenic magnetite at the paleocene–eocene thermal maximum. *Proceedings of the National Academy of Sciences*, National Acad Sciences, v. 105, n. 46, p. 17648 -17653, 2008.

SHARMA, G. P.; BALOMAJUMDER, C. Preliminary isolation report of aerobic magnetotactic bacteria in a modi_ed nutrient medium. *Recent Research in Science and Technology*, v. 3, n. 11, 2011.

SINGER, A. The paleoclimatic interpretation of clay minerals in sediments|a review. *Earth-Science Reviews*, Elsevier, v. 21, n. 4, p. 251 -293, 1984.

SLUIJS, A. et al. A middle eocene carbon cycle conundrum. *Nature Geoscience*, Nature Publishing Group, v. 6, n. 6, p. 429 -434, 2013.

SMITH, C. R.; DEMOPOULOS, A. W. The deep pacific ocean floor. *Ecosystems of the World*, p. 179 -218, 2003.

SOUZA, L. A. P. de; TESSLER, M. G.; GALLI, V. L. O gráben de Cananeia. *Revista Brasileira de Geociências*, v. 26, n. 3, p. 139 -150, 2017.

SPERA, A. M. Registro de variaçõoes ambientais dos últimos 3000 anos da Região da Ria do Mamanguá, Rio de Janeiro, utilizando marcadores orgânicos moleculares. Tese (Doutorado), Universidade de Sâo Paulo, 2012.

SPINELLI, F. P.; GOMES, C. de B. A ocorrência alcalina de Cananeia, litoral sul do estado de São Paulo: química mineral. *Geologia USP*. Série Científica, v. 9, n. 1, p. 1 -13, 2009.

SPRING, S. et al. Dominating role of an unusual magnetotactic bacterium in the microaerobic zone of a freshwater sediment. *Appl. Environ. Microbiol*., Am Soc Microbiol, v. 59, n. 8, p. 2397 -2403, 1993.

SUGUIO, K. et al. Upper pleistocene deposits of the comprida island (São Paulo state) dated by thermoluminescence method. Anais da Academia Brasileira de Ciências, SciELO Brasil, v. 75, n. 1, p. 91 -96, 2003.

SUTHERLAND, R. Basement geology and tectonic development of the greater New Zealand region: an interpretation from regional magnetic data. *Tectonophysics*, Elsevier, v. 308, n. 3, p. 341 -362, 1999.

SUTHERLAND, R. et al. *Site U1511*. 2019.

TANAKA, M. et al. Highest levels of Cu, Mn and Co doped into nanomagnetic magnetosomes through optimized biomineralisation. *Journal of Materials Chemistry*, Royal Society of Chemistry, v. 22, n. 24, p. 11919 -11921, 2012.

TEIXEIRA, C. L. et al. Caracterização do sedimento superficial de enseadas da baía da ilha Grande-RJ, com enfase na distribuição espacial de metais. Niteroi, 2009.

TELEGINSKI, A. Aspectos históricos e fundiarios no vale do ribeira e sua influência no desenvolvimento econômico da região. *III Simposio de Ecossistemas da Costa Brasileira*, v. 1, p. 104 -106, 1993.

TRÉGUER, P.; CORRE, P. Manuel d'analyse des sels nutritifs dans l'eau de mer. Laboratoire d'Oceanographie Chimique, Université de Bretagne Occidentale, Brest, v. 110, 1975.

VASILIEV, I. et al. Putative greigite magnetofossils from the Pliocene epoch, *Nat. Geosci*, 2008.

VEROSUB, K. L.; ROBERTS, A. P. Environmental magnetism: Past, present, and future. *Journal of Geophysical Research: Solid Earth*, Wiley Online Library, v. 100, n. B2, p. 2175 -2192, 1995.

WARNAAR, J. et al. Orbitally forced climate changes in the tasman sector during the middle eocene. *Palaeogeography, Palaeoclimatology, Palaeoecology*, Elsevier, v. 280, n. 3-4, p. 361 -370, 2009.

WEEKS, R. et al. Improvements in long-core measurement techniques: applications in palaeomagnetism and palaeoceanography. *Geophysical Journal International*, Blackwell Publishing Ltd Oxford, UK, v. 114, n. 3, p. 651 -662, 1993.

WELTJE, G. J.; TJALLINGII, R. Calibration of xrf core scanners for quantitative geochemical logging of sediment cores: Theory and application. *Earth and Planetary Science Letters*, Elsevier, v. 274, n. 3-4, p. 423 -438, 2008.

XUAN, C.; CHANNELL, J. E. Upmag: Matlab software for viewing and processing U-channel or other pass-through paleomagnetic data. *Geochemistry, Geophysics, Geosystems*, Wiley Online Library, v. 10, n. 10, 2009.

YAMAZAKI, T. Magnetostatic interactions in deep-sea sediments inferred from first-order reversal curve diagrams: Implications for relative paleointensity normalization. *Geochemistry, Geophysics, Geosystems*, Wiley Online Library, v. 9, n. 2, 2008.

YAMAZAKI, T.; KAWAHATA, H. Organic carbon ux controls the morphology of magnetofossils in marine sediments. *Geology*, Geological Society of America, v. 26, n. 12, p. 1064 -1066, 1998.

YAMAZAKI, T.; SHIMONO, T. Abundant bacterial magnetite occurrence in oxic red clay. *Geology*, Geological Society of America, v. 41, n. 11, p. 1191 -1194, 2013.

YAN, L. et al. Magnetotactic bacteria, magnetosomes and their application. *Microbiological research*, Elsevier, v. 167, n. 9, p. 507 -519, 2012.

ZACHOS, J. C.; DICKENS, G. R.; ZEEBE, R. E. An early cenozoic perspective on greenhouse warming and carbon-cycle dynamics. *Nature*, Nature Publishing Group, v. 451, n. 7176, p. 279 -283, 2008.

ZIMMERMAN, H. B.; HB, Z. Clay mineral stratigraphy and distribution in the South Atlantic ocean. 1977.